

WL-TR-94-3050

MEASURES OF MERIT FOR MULTIVARIABLE
FLIGHT CONTROL



AD-A279 143



MARK R. ANDERSON
ABBAS EMAMI-NAEINI
JAMES H. VINCENT

SYSTEMS CONTROL TECHNOLOGY, INC.
100 EXPLORATION
SUITE 2005
LEXINGTON PARK MD 20653

FEBRUARY 1991

FINAL REPORT FOR 09/01/90-02/01/91

APPROVED FOR PUBLIC RELEASE; DISTRIBUTION IS UNLIMITED.

DTIC
SELECTE
MAY 12 1994
S B D

11308 94-14088



94 5 10 042

FLIGHT DYNAMICS DIRECTORATE
WRIGHT LABORATORY
AIR FORCE SYSTEMS COMMAND
WRIGHT PATTERSON AFB OH 45433-7562

REPRODUCTION PROHIBITED

NOTICE

When Government drawings, specifications, or other data are used for any purpose other than in connection with a definitely Government-related procurement, the United States Government incurs no responsibility or any obligation whatsoever. The fact that the government may have formulated or in any way supplied the said drawings, specifications, or other data, is not to be regarded by implication, or otherwise in any manner construed, as licensing the holder, or any other person or corporation; or as conveying any rights or permission to manufacture, use, or sell any patented invention that may in any way be related thereto.

This report is releasable to the National Technical Information Service (NTIS). At NTIS, it will be available to the general public, including foreign nations.

This technical report has been reviewed and is approved for publication.



JOHN A. BOWLUS
Chief, Control Analysis Section



FRANK R. SWORTZEL
Chief, Control Dynamics Branch



DAVID P. LEMASTER
Chief, Flight Control Division

If your address has changed, if you wish to be removed from our mailing list, or if the addressee is no longer employed by your organization please notify WL/FIGC, WPAFB, OH 45433-7562 to help us maintain a current mailing list.

Copies of this report should not be returned unless return is required by security considerations, contractual obligations, or notice on a specific document.

FEB 1991

FINAL

09/01/90--02/01/91

MEASURES OF MERIT FOR MULTIVARIABLE FLIGHT CONTROL

C F33615-90-C-3611
PE 65
PR 3005
TA 40
WU 81

MARK R. ANDERSON
ABBAS EMAMI-NAEINI
JAMES H. VINCENT

SYSTEMS CONTROL TECHNOLOGY, INC.
100 EXPLORATION
SUITE 2005
LEXINGTON PARK MD 20653

FLIGHT DYNAMICS DIRECTORATE
WRIGHT LABORATORY
AIR FORCE SYSTEMS COMMAND
WRIGHT PATTERSON AFB OH 45433-7562

WL-TR-94-3050

THIS IS A SMALL BUSINESS INNOVATION RESEARCH REPORT, PHASE 1

APPROVED FOR PUBLIC RELEASE; DISTRIBUTION IS UNLIMITED.

13. ABSTRACT
The purpose of this research is to develop new measures of merit specifically for multivariable aircraft flight control systems. This report provides a theoretical development of the measures of merit based on "modern" multivariable control analysis methods. The analysis techniques used to form the new criteria draw from recent control theory research in Hankel singular values, matrix singular values, and the so-called "structured" singular values. The proposed measures of merit are computed for a high-fidelity linear model of the F-16 aircraft at one cruise flight condition. The results of this investigation demonstrate the usefulness, computational methods, and numerical values expected from the new measures. It is hoped that this research will provide the foundation for compilation of multivariable flight control system evaluation results such that the Air Force and aircraft manufacturers can directly compare the performance of different designs.

14. SUBJECT TERMS
FLIGHT CONTROL, FLYING QUALITIES, MULTIVARIABLE SYSTEMS

116

17. SECURITY CLASSIFICATION OF REPORT
UNCLASSIFIED

18. SECURITY CLASSIFICATION OF THIS PAGE
UNCLASSIFIED

UNCLASSIFIED

UL

Forward

This report represents the first phase of a Small Business Innovative Research (SBIR) program intended to identify new measures of merit for the evaluation of multivariable aircraft (multi-loop) flight control systems. The research reported was sponsored by the Flight Dynamics Laboratory of the Wright Research and Development Center (WRDC) under contract F33615-90-C-3611. The work was performed at the Systems Control Technology, Inc. (SCT) offices in Palo Alto, CA and Lexington Park, MD. The WRDC project engineer was Capt. Randy L. Robinson of the Control Dynamics Branch.

The authors would like to thank Ms. Barbara Stanka of SCT, Lexington Park, and Dr. Horst Salzwedel of SCT, Palo Alto, for their assistance in preparation of the F-16 aircraft linear model used to generate the example results given in this report.

| Accession For | |
|--------------------|-------------------------------------|
| NTIS GRA&I | <input checked="" type="checkbox"/> |
| DTC TAB | <input type="checkbox"/> |
| Unannounced | <input type="checkbox"/> |
| Justification | |
| By _____ | |
| Distribution/How | |
| Availability Codes | |
| Dist | Avail and/or Special |
| A-1 | |

Table of Contents

| | | |
|--------|---|------|
| 1. | Introduction | 1-1 |
| 1.1. | Phase I Program Overview | 1-3 |
| 1.2. | Report Summary | 1-5 |
| 2. | Aircraft Model and Control Task Selection..... | 2-1 |
| 2.1 | F-16 Aircraft Model | 2-1 |
| 2.2 | Control Task Description | 2-2 |
| 3. | Review of Multivariable Control System Analysis Methods..... | 3-1 |
| 3.1 | Linear Model Descriptions | 3-1 |
| 3.2 | Matrix Singular Values | 3-2 |
| 3.3 | Hankel Singular Values and the 2-Norm | 3-2 |
| 3.4 | Structured Singular Values | 3-4 |
| 4. | Measures of Merit for Flight Control Systems..... | 4-1 |
| 4.1. | Nominal Stability Measures | 4-1 |
| 4.1.1. | Mode Classification..... | 4-3 |
| 4.2. | Robust Stability Measures | 4-7 |
| 4.2.1. | Multi-loop Stability Margins..... | 4-8 |
| 4.2.2. | Open-loop Bandwidth..... | 4-12 |
| 4.2.3. | Departure Susceptibility..... | 4-14 |
| 4.3. | Nominal Performance Measures | 4-28 |
| 4.3.1. | Effective Order..... | 4-28 |
| 4.3.2. | Equivalent System Error..... | 4-29 |
| 4.3.3. | Turbulence Response..... | 4-36 |
| 4.3.4. | Response Decoupling..... | 4-39 |
| 4.4. | Robust Performance Measures | 4-42 |
| 4.4.1 | The Standard Uncertainty Set..... | 4-43 |
| 5. | Measure of Merit Results for the F-16 Aircraft..... | 5-1 |
| 5.1. | Nominal Stability Measures | 5-1 |
| 5.1.1. | Mode Classification..... | 5-1 |
| 5.2. | Robust Stability Measures | 5-2 |
| 5.2.1. | Multi-loop Stability Margins..... | 5-3 |
| 5.2.2. | Open-loop Bandwidth..... | 5-11 |
| 5.2.3. | Departure Susceptibility..... | 5-11 |
| 5.3. | Nominal Performance Measures | 5-19 |

| | | |
|--------|---------------------------------------|------|
| 5.3.1. | Effective Order..... | 5-19 |
| 5.3.2. | Equivalent System Error..... | 5-20 |
| 5.3.3. | Turbulence Response..... | 5-25 |
| 5.3.4. | Response Decoupling..... | 5-29 |
| 5.4. | Robust Performance Measures | 5-31 |
| 5.4.1. | Robustness of Effective Order..... | 5-33 |
| 5.4.2. | Robustness of Equiv. System Error.... | 5-34 |
| 5.4.3. | Turbulence Response Robustness..... | 5-41 |
| 5.4.4. | Response Decoupling Robustness..... | 5-41 |
| 6. | Conclusions | 6-1 |
| 7. | Recommendations for Phase II..... | 7-1 |
| 8. | References | 8-1 |

List of Figures

| | | |
|-------------|---|------|
| Figure 2.1 | F-16 Closed-loop System..... | 2-3 |
| Figure 4.1 | Weisman's Departure Criterion..... | 4-16 |
| Figure 4.2 | Sample Stability Map from Stengel and Berry..... | 4-17 |
| Figure 4.3 | Block Diagram for Departure Analysis..... | 4-19 |
| Figure 4.4 | DP for Space Shuttle Example..... | 4-24 |
| Figure 4.5 | DP Compared to Stengel's Result..... | 4-25 |
| Figure 4.6 | Expected Departure Parameter Behavior..... | 4-26 |
| Figure 4.7 | Added Dynamics Specification..... | 4-34 |
| Figure 4.8 | Development of Equivalent System Error Bound..... | 4-37 |
| Figure 5.1 | Block Diagram for Input Complimentary Sensitivity Function..... | 5-4 |
| Figure 5.2 | Input Complimentary Sensitivity Function Singular Value..... | 5-5 |
| Figure 5.3 | Block Diagram for Input Sensitivity Function..... | 5-6 |
| Figure 5.4 | Input Sensitivity Function Singular Values..... | 5-7 |
| Figure 5.5 | Block Diagram for Output Complimentary Sensitivity Function..... | 5-9 |
| Figure 5.6 | Output Complimentary Sensitivity Function Singular Values..... | 5-10 |
| Figure 5.7 | Block Diagram for Output Sensitivity Function..... | 5-12 |
| Figure 5.8 | Output Sensitivity Function Singular Values..... | 5-13 |
| Figure 5.9a | Block Diagram for Computing Departure Parameter... | 5-14 |
| Figure 5.9b | Airframe Block Diagram for Computing Departure Parameter..... | 5-15 |
| Figure 5.10 | Closed-Loop Departure Parameter Sturctured Singular Values..... | 5-17 |
| Figure 5.11 | Open-Loop Departure Parameter Structured Singular Values..... | 5-18 |
| Figure 5.12 | Nominal Longitudinal Equivalent System Comparison. | 5-23 |
| Figure 5.13 | Nominal Longitudinal Equivalent System Error..... | 5-24 |
| Figure 5.14 | Nominal Lateral-Directional Equivalent System Comparison..... | 5-26 |
| Figure 5.14 | (con't)..... | 5-27 |
| Figure 5.15 | Nominal Lateral-Directional Equivalent System | |

| | | |
|-------------|--|------|
| | Error..... | 5-28 |
| Figure 5.16 | Nominal Response Decoupling..... | 5-30 |
| Figure 5.17 | Worse cas Output Structured Singular Values..... | 5-32 |
| Figure 5.18 | Phase Perturbed Longitudinal Equivalent System Comparison..... | 5-36 |
| Figure 5.19 | Phase Perturbed Longitudinal Equivalent System Error..... | 5-37 |
| Figure 5.20 | Phase Perturbed Lateral-Directional Equivalent System Comparison..... | 5-38 |
| Figure 5.20 | (con't)..... | 5-39 |
| Figure 5.21 | Phase Perturbed Lateral-Directional Equivalent System Error..... | 5-40 |
| Figure 5.22 | Phase Perturbed Response Decoupling..... | 5-42 |

List of Tables

| | | |
|-----------|---|------|
| Table 4.1 | MIL-F-87242 Gain and Phase Margin Specification | 4-8 |
| Table 4.2 | Space Shuttle Stability Derivatives | 4-22 |
| Table 4.3 | Space Shuttle Uncertainty System | 4-23 |
| Table 4.4 | Lingitudinal Equivalent System Model Structures . . . | 4-30 |
| Table 4.5 | Lateral-Directional Equivalent system Model Structures | 4-31 |
| Table 4.6 | Linearized Aircraft Equations with Non-zero Roll Rate | 4-41 |
| Table 5.1 | Nominal Equivalent System Transfer Functions | 5-22 |
| Table 5.2 | Phase Perturbed Equivalent System Transfer Functions | 5-35 |

1. Introduction

The objective of this research is to initiate the study of new evaluation measures of merit specifically for multivariable flight control systems. A flight control system is usually considered a multivariable system if more than one control effector (control surface, for example) or more than one feedback variable is used to control the aircraft motion. With this multivariable system definition, almost all aircraft flying today can be considered to have a multivariable flight control system. However, most older aircraft control systems have been designed such that interaction among each control effector and feedback variable pair is minimized. Each feedback loop becomes independent and can be designed and tested separately from the others.

Many of the recently developed aircraft have very sophisticated control systems consisting of many different control effectors and feedback variables. To optimize performance, the control and feedback variable are no longer separated but may actually be designed to interact - as in the case of an integrated control system. Centralized flight control systems are now being considered which combine many other subsystems, such as an engine or rotor controller, with the primary flight control system. An example is the control system designed for the B-1 aircraft which combines the primary flight control system with a structural control system designed to reduce vibration in the cockpit. Another example is the use of thrust vectoring as a means of producing additional pitch, roll, or yaw control effectiveness.

New aircraft are also being designed with an increased emphasis on low radar signature airframe shapes. The B-2 bomber and the F-117A are recent examples. The low observability design requirements have resulted in rather unconventional airframe shapes which may degrade inherent

stability of the design. A sophisticated, multivariable control system has undoubtedly been used to improve the stability and maneuverability of these stealth aircraft.

A future need for multivariable flight control systems is the area of aircraft flow control. Various boundary layer flow control devices, such as small movable chin fins or surface blowing devices, are being considered to improve aircraft maneuverability, especially at high angles of attack. Additional flow control effectors will require a multivariable control system to function in concert with the primary control surfaces of the aircraft.

To assess the effectiveness of any flight control system design, criteria must be developed such that a minimum acceptable performance can be specified. For military aircraft, the flying qualities^[1] (MIL-STD-1797) and flight control system specifications^[2] (MIL-F-87242) serve as the principal flight control related performance specifications. These military specifications have been formed after compilation of many years of investigations and flight test experience.

The current versions of the specifications, to a large extent, are applicable only to aircraft with single-loop control systems. Although the current specifications have been used successfully with many multivariable flight control systems, this success is due to the fact the control systems have been designed such that individual control loops can be isolated and evaluated separately.

It has been only recently that analysis methods which can be used for true multivariable control system evaluation have matured to the point where they may be utilized to assess actual aircraft flight control systems. Research in the last ten years has resulted in many new analytical tools for the evaluation (and design) of multivariable control systems. Most important has been the research on the use of matrix norms, such as the matrix singular value, as a method to combine the characteristics of many control signals into

one parameter which can be studied. Instead of evaluating each control loop individually, all of the control loops are evaluated at once. Thus, the analysis method can assess the operation of the multivariable control system wherein all of the control loops are interacting simultaneously.

1.1. Phase I Program Overview

This report documents the results obtained during Phase I work of a Small Business Innovative Research (SBIR) contract. The objective of the research was to demonstrate the feasibility of the developing new measures of merit specifically for multivariable flight control systems. In addition, the results of the Phase I work is intended to provide a foundation through which Phase II development of the research can follow.

The Phase I work was divided into several tasks. Task 1 was to select a control task and aircraft for study. An existing linear model of the F-16 aircraft, actuators, sensors and control system was used. Unfortunately, time was not allotted in Phase I for a complete validation of this model. Therefore, no specific conclusions should be drawn from the research results reported herein regarding the performance of the actual F-16 aircraft. For the purposes of this initial study, the model represents a typical modern, multivariable flight control system.

The purpose of Task 2 was to identify and define the new measures of merit. Several sources of pertinent literature were used to identify the measures of merit. Specifically, recent technical papers regarding multivariable control system evaluation and design techniques were used along with papers describing recent successful multivariable flight control system applications. Whenever possible, new measures of merit were developed to address areas which are already included in the current military flying qualities and flight control system specifications. The idea was to form new

measures of merit which were, at least in spirit, multivariable generalizations of established single-loop criteria for flight control system evaluations. For example, a new measure of merit is proposed for computing the multivariable system bandwidth. Bandwidth usually defines the expected maximum frequency of good tracking and disturbance rejection behavior. The calculations required to compute the multivariable system bandwidth are very different from the bandwidth criteria specified in MIL-STD-1797. The results obtained from the new bandwidth criteria should not be compared directly to the criteria. However, both the MIL-STD-1797 bandwidth criteria and the new multivariable bandwidth measure of merit are intended to quantify some concept of system bandwidth.

The proposed new measures of merit were not intended to replace any of the current applicable specifications, but should be considered as an additional evaluation test specifically designed for multivariable systems. The measures were also chosen such that they do not favor one design approach over another. The intent is to provide a basis for comparison of multivariable flight control system performance without regard to how the system was designed or implemented.

Task 3 consisted of constructing analysis diagrams suitable for describing each new measure. An example of each measure is then computed using the linear model of the F-16 aircraft. Comparisons are made to any existing specification or evaluation criteria which has a similar intent. These comparisons are made to instill confidence in the new measures of merit and are not meant to reflect on the performance of the F-16 aircraft model or the adequacy of the existing criteria used for the comparison.

Eight new measures of merit were defined in this research: mode classification and nominal stability, multi-loop stability margins, open-loop bandwidth, departure susceptibility, effective response order, equivalent system

error, turbulence response, and response decoupling. The technical feasibility of the proposed new measures was demonstrated by application of the measures to a linear model of the F-16 aircraft. The results of the F-16 model analysis reveal that each of the new measures can be computed for a realistic multivariable flight control system.

1.2. Report Summary

The first task of this research was to select a control task and aircraft for study. A high-order linear model of the F-16 aircraft was chosen for this study. The description of the model is given in Section 2 of this report.

The purpose of Task 2 was to identify the new measures of merit. Section 3 of the report reviews some of the theoretical definitions and nomenclature needed to describe the new measures. Section 4 describes each proposed evaluation measure and, when possible, expected results are reported from available literature and experience.

Task 3 consisted of constructing analysis diagrams suitable for specifying each new measure. An example of each measure is then computed using a linear model of the F-16 aircraft. The results of Task 3 are documented in Section 5 of this report. Conclusions obtained from this research are given in Section 6 while recommendations for Phase II are noted in Section 7. Technical references are listed in Section 8.

2. Aircraft Model and Control Task Selection

A high-fidelity model of the F-16 C/D aircraft was chosen for this study primarily because a nonlinear simulation of the aircraft has already been developed by Systems Control Technology, Inc. personnel for a separate contract (F33657-85-C-0027). The F-16 C/D simulation model was initially used to verify the implementation of the digital flight control system. The simulation is based on the Block 15 aerodynamic characteristics^[3] (angle-of-attack < 29 deg, altitude < 60000 ft, $0.2 < \text{Mach} < 2.0$) and the Block 25 digital control laws.^[4]

2.1 F-16 Aircraft Model

A linear model defined at 20,000 ft altitude and Mach 0.8 was used for the Phase I work. The linear model of the aircraft has ten states: axial velocity, lateral velocity, vertical velocity, pitch rate, roll rate, yaw rate, roll Euler angle, pitch Euler angle, yaw Euler angle, and altitude. The eigenvalues of the bare airframe are shown in Table 2.1. As indicated by the list of eigenvalues, the F-16 C/D model for the selected flight condition has an aperiodic instability with a time-to-double amplitude of 6.6 seconds.

Table 2.1 Open-Loop Airframe Eigenvalues

| Eigenvalue | Mode Classification |
|--------------|---------------------|
| 0.0 | heading |
| 0.0 | altitude |
| -0.0132 | spiral |
| 0.105 | phugoid |
| -0.114 | phugoid |
| -0.991+j1.41 | short period |
| -0.991-j1.41 | short period |
| -2.78 | roll |
| -0.410+j3.97 | dutch roll |
| -0.410-j3.97 | dutch roll |

A block diagram of the complete control system, as modeled, is given in Figure 2.1. The digital control laws were first transformed to an analog equivalent so that all of the subsequent analysis could be carried out in the continuous time domain. First order lag approximations of the digital sample-and-hold functions were utilized assuming a sample rate of 64 Hz. The sensor and actuator models included 5 states and 10 states, respectively. The primary control system has 17 states. The Dryden turbulence model was used to model turbulence in the axial, lateral, and vertical velocity components. The turbulence model has five states. The complete closed-loop system has 53 states.

2.2 Control Task Description

The F-16 multi-role fighter is considered a Class IV aircraft by the current flying qualities specification. The flight condition considered in this analysis is a nonterminal flight phase wherein rapid maneuvering, precision tracking, and precise flight-path control may be required. Therefore, Category A flight phases are considered representative. Category A flight phases directly applicable to this investigation are: air-to-air combat (CO), reconnaissance (RC), in-flight refueling (receiver) (RR), and close formation flying (FF).

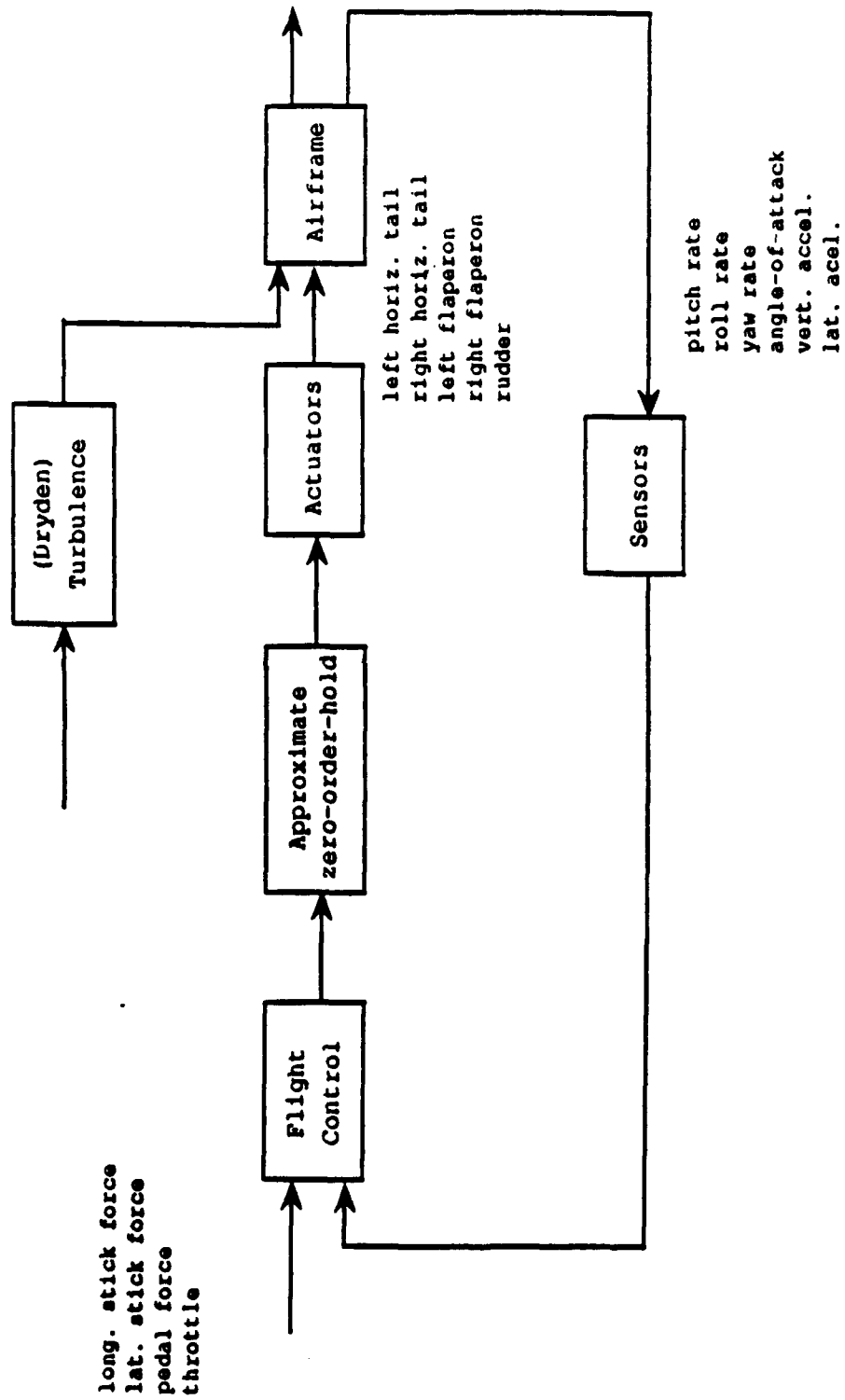


Figure 2.1 F-16 Closed-loop System

3. Review of Multivariable Control System Analysis Methods

This section is intended to introduce the terminology which will be used in subsequent theoretical development. The material to be covered is not new, but it is recent enough to warrant a brief review. References are cited, where appropriate, wherein further information can be found concerning these concepts.

3.1 Linear Model Descriptions

A continuous linear model will have the assumed form,

$$\begin{aligned}\dot{x}(t) &= Ax(t) + Bu(t) \\ y(t) &= Cx(t) + Du(t)\end{aligned}\quad (3.1)$$

where $x(t)$ represents a vector of system state, $u(t)$ represents a vector of system inputs, and $y(t)$ is a vector of system outputs. The overstrike dot denotes differentiation, i.e. $\dot{x}(t) = dx(t)/dt$.

The transfer function matrix of the continuous time linear model is obtained from the Laplace transform of the continuous state space model. The transfer function matrix for the continuous model will be denoted $G(s)$, and is defined by,

$$y(s) = G(s)u(s) = [C(sI-A)^{-1}B + D]u(s) \quad (3.2)$$

Frequency response of the individual elements of the transfer function matrix are obtained by replacing 's' with 'j ω ' for selected frequency ω values. Traditional Bode magnitude and phase curves can then be obtained for each transfer function element.

3.2 Matrix Singular Values

The size of a matrix can be quantified by its norm. One can think of the matrix norm as the maximum gain of the matrix. In most recent multivariable control research, the spectral norm has been used to measure the size of a matrix. The spectral norm of a matrix is also the maximum singular value of a matrix, denoted $\bar{\sigma}[A]$ and can be computed by,

$$\bar{\sigma}[A] = \sqrt{\lambda_{\max}(A^*A)} \quad (3.3)$$

where $\lambda_{\max}(A^*A)$ is the maximum eigenvalue of A^*A . Algorithms for computing singular values are readily available in commercial computer-aided engineering packages such as Ctrl-C[®].

Singular values have many applications in control system analysis primarily because of the convenience it provides in measuring the size of a transfer function matrix. Typically, the maximum and minimum singular values of the transfer function matrix are plotted against frequency, like Bode plots.^[5] For a continuous model, $\bar{\sigma}[G(j\omega_i)]$ is plotted for selected frequency points ω_i .

3.3 Hankel Singular Values and the 2-Norm

The Hankel singular values of a linear system are closely related to the controllability and observability properties of the system. If the linear, continuous, state-space model is stable, the controllability grammian P is defined by,

$$P = \int_0^{\infty} \exp(At)BB^*\exp(A^*t) dt \quad (3.4)$$

while the observability grammian Q is,

$$Q = \int_0^{\infty} \exp(A^*t) C^* C \exp(At) dt \quad (3.5)$$

It can be shown that the grammians also satisfy the following Lyapunov equations,

$$AP + PA^* + BB^* = 0 \quad (3.6)$$

and,

$$A^*Q + QA + C^*C = 0 \quad (3.7)$$

The Hankel singular values of the system G(s) are then,

$$h_i[G(s)] = \sqrt{\lambda_i(PQ)} \quad (3.8)$$

where, by convention, $h_i \geq h_{i+1}$. [6]

The 2-Norm of a linear system is also obtained from the controllability and observability grammians. [7] The 2-norm is typically denoted by $\|G(s)\|_2$ and is,

$$\|G(s)\|_2^2 = \text{trace}[CPC^T] = \text{trace}[B^TQB] \quad (3.9)$$

where the trace operator stands for the sum of the diagonal elements. The 2-norm essentially measures the rms response value if the system is excited by white noise. This property is evident by noting that,

$$\|G(s)\|_2^2 = \frac{1}{2\pi} \int_{-\infty}^{\infty} \text{trace}[G^*(j\omega)G(j\omega)] d\omega \quad (3.10)$$

The expression above is the same as computing the rms response of a transfer function matrix if the noise process had an identity spectral density matrix. It also should be noted that the direct feedthrough term of the transfer function matrix (i.e. the D matrix in (3.1)) must be zero for the 2-norm to be finite.

3.4 Structured Singular Values

The structured singular value has been defined to measure the robustness properties of linear, multivariable control systems. [8-10] The robustness measure determines whether the system remains stable for a given set of perturbations to the nominal model. Performance robustness tests are also possible wherein the system is checked against performance requirements (and remains stable) for a given set of perturbations to the nominal model.

The robustness measure is intimately tied to the definitions of the perturbations which are to be investigated. Typically the perturbations are described by a block diagonal matrix $\Delta = \text{diag}(\Delta_1, \dots, \Delta_n)$. The individual Δ_i blocks may be either scalars or matrices and can be complex in some cases.

The structured singular value of a complex matrix M, denoted $\mu(M)$, is defined by,

$$\frac{1}{\mu(M)} = \min_{\Delta} \bar{\sigma}[\Delta] \quad \{ \det(I - \Delta M) = 0 \} \quad (3.11)$$

The value of $1/\mu(M)$ determines the size of the smallest "destabilizing" Δ which satisfies $\det(I - \Delta M) = 0$. Also, $1/\mu(M(s_0))$ measures the size of the "worst case" or smallest perturbation Δ which moves a closed-loop pole to s_0 .

Computation of the structured singular value continues to be an area of concentrated research. However, the Frobenius norm scaling technique has proven to be a reliable

alternative to exact computation of the structured singular value. Algorithms which utilize the Frobenius norm scaling technique are now widely available. Therefore, it is reasonable to assume that a measure of merit based on a structured singular value computation will be acceptable by industry.

The Frobenius norm scaling technique makes use of the fact that,

$$\mu(M) \leq \min_D \bar{\sigma}[DMD^{-1}] \quad (3.12)$$

where D is a diagonal scaling matrix which is formed such that each block in Δ is scaled by the associated diagonal element in D. The equation above indicates that the scaling matrix D must be found which minimizes $\bar{\sigma}[DMD^{-1}]$. The Frobenius norm scaling technique typically uses Osborne's method of finding a scaling matrix D which minimizes the Frobenius norm, $\|DMD^{-1}\|_F$.^[11] The resulting D matrix is then used to compute $\bar{\sigma}[DMD^{-1}]$ as an (upper bound) approximation to $\mu(M)$.

An approximation to the structured singular value is also available for the special case when the model perturbation Δ is strictly real.^[12] For this special case, the structured singular value will be denoted $\mu_R(M)$ and is approximated by,

$$\mu_R(M) \equiv \max_{\Phi} \min_D \rho\left[-\frac{1}{2}(DMD^{-1}\Phi + \Phi D^{-1}M^*D)\right] \quad (3.13)$$

where ρ is the spectral radius and Φ is a permutation matrix with the same form as D but with either a +1 or -1 on the diagonal elements. The approximation involves searching for the permutation matrix which maximizes $\mu_R(M)$ and therefore

predicts the sign (\pm) of the worst case real perturbations in Δ .

4. Measures of Merit for Flight Control Systems

In flight control system evaluation and analysis, one is typically concerned with the criteria developed to test nominal stability, nominal performance, robust stability and robust performance. Nominal stability and performance measures are used to define stability and performance properties of the flight control system at the nominal design conditions. Robust stability and performance measures deal with how model uncertainty influences stability and performance. The remainder of this section serves to introduce the new multivariable measures of merit.

4.1. Nominal Stability Measures

Nominal stability has been indirectly specified in the military flying qualities specifications by requirements regarding the location of dominant characteristics roots. For example, damping and natural frequencies are specified for the short period, phugoid, and dutch roll modes. In addition, time-to-double amplitudes are specified for the spiral mode.

The flight control or stability augmentation system may introduce additional modes into the actual response of the aircraft as commanded by the pilot. With control system complexity increasing in an effort to maximize performance, the order of the control system itself may be quite large.

The current aircraft flying qualities specification takes into account these additional control system modes by utilizing the definition of an equivalent system. An equivalent system is simply a low-order equivalent representation of the actual high-order response. The equivalent system model includes a pure time delay as an approximation of the effect of higher-order dynamics. Assuming an appropriate equivalent system can be found, the

parameters of the equivalent model are then used to assess flying qualities. The equivalent system method works quite well in measuring response characteristics but the roots of the equivalent system model are not necessarily a good indicator of nominal stability. For example, if the recommended method of matching frequency response characteristics is used to develop the equivalent system model, it is possible that an unstable mode is approximately (but not completely) cancelled by a non-minimum phase zero and therefore will not appear in the low-order equivalent system model. As a result, nominal stability should only be measured on the highest fidelity model available.

The V/STOL aircraft flying qualities handles the nominal stability assessment problem for hovering V/STOL aircraft by specifying stability for all modes of the characteristic equations as opposed to an approximation made by equivalent systems modeling.^[13] The specification requires that all aperiodic roots of the longitudinal and lateral-directional characteristic equation should be stable for Level I rating. Oscillatory modes of frequency greater than 0.5 rad/sec should also be stable, but oscillatory modes of frequency less than or equal to 0.5 rad/sec can be unstable provided the damping ratio is less than -0.1.

The nominal stability specification for V/STOL aircraft provides a good model for new specifications concerning conventional aircraft. Nominal stability requirements for all of the modes represented in the highest possible fidelity linear model should be specified. The aircraft flying qualities specification allows for an unstable spiral mode; as long as the time-to-double amplitude is greater than 12 sec (Cat. A and C). Therefore, all unstable modes of the high-order, closed-loop aircraft model should have an equivalent time-to-double amplitude of greater than 12 sec.

This nominal stability requirement can be evaluated by computing the eigenvalues of the entire, closed-loop model of the aircraft. The complete model should include both

longitudinal and lateral-directional dynamics, and the complete operational control system. It is possible that the closed-loop model may have up to one hundred states, but it is very important that all possible dynamic modes be represented. The closed-loop eigenvalues should then be sorted to determine any which have a positive (unstable) real part. The time-to-double amplitude of the unstable modes should then be computed and shown to be greater than 12 sec. The time-to-double amplitude (t_{2d}) can be computed for each unstable aperiodic mode from the equation,

$$t_{2d} = \frac{\ln 2}{p} \quad (4.1)$$

where p is the unstable root. For unstable oscillatory modes, the time-to-double amplitude is given by,

$$t_{2d} = \frac{\ln 2}{\zeta \omega_n} \quad (4.2)$$

where ζ is the damping ratio and ω_n is the natural frequency of the unstable mode. [14]

4.1.1. Mode Classification

The fact that the control system is multivariable does not change its characteristic roots; however, it becomes more difficult to classify the modes according to the traditional bare-airframe rigid-body modes. Mode classification is also complicated by the fact that the stability augmentation system may introduce many extra modes which may or may not influence the response of the aircraft to pilot stick inputs. For these reasons, a mode classification procedure is proposed to aid in measuring nominal stability of the dominant modes of the longitudinal and lateral-directional axes.

With a model represented in modal form, the input-output residues are readily available.^[15] The magnitude of each residue reflects the contribution of that mode to the input-output response. A residue with zero magnitude indicates that the mode is uncontrollable, unobservable, or both. Assuming the continuous system has real, distinct eigenvalues, the modal decomposition of the full order state matrix is,

$$AM = MA \quad (4.3)$$

where $\Lambda = \text{diag}(\lambda_1, \lambda_2, \dots, \lambda_n)$, M is a real matrix of eigenvectors, and λ_i are the (real) eigenvalues. A similar decomposition is possible for systems with complex eigenvalues.

The system can be transformed to modal form by defining a new state vector q as, $x = Mq$, and then the linear model can be written as,

$$\begin{aligned} \dot{q}(t) &= \Lambda q(t) + B_m u(t) \\ y(t) &= C_m q(t) + Du(t) \end{aligned} \quad (4.4)$$

where $\Lambda = M^{-1}AM$, $C_m = CM$ and $B_m = M^{-1}B$. The continuous model transfer function matrix is obtained by using the Laplace transform and solving for $y(s)$,

$$y(s) = [C_m(sI - \Lambda)^{-1}B_m + D]u(s) \quad (4.5)$$

Because Λ is diagonal, the system transfer function matrix can also be written as,

$$y(s) = \left[\sum_{i=1}^n \frac{R_i}{s/\lambda_i - 1} + D \right] u(s) \quad (4.6)$$

R_i is the residue matrix for the i th mode, computed from,

$$R_i = \frac{c_{mi}b_{mi}}{\lambda_i} \quad (4.7)$$

where c_{mi} is the i th column of C_m and b_{mi} is the i th row of B_m .

It should be clear that if R_i is very small for some given mode, the mode does not contribute significantly to the response of the system. The maximum matrix singular value of the residue matrix will be used to measure the size of residue matrix. Therefore, all modes with residue matrices such that,

$$\bar{\sigma}[R_i] > \kappa \quad (4.8)$$

can be considered as contributors to the response of the system.

Equation (4.8) illustrates that the value of κ determines which modes are considered contributors to the response of interest. Consequently, κ should be chosen as some small number so that only those modes with large residue magnitudes are classified. Although κ ultimately depends on the units of the response variables, a value of $\kappa = 0.00001$ was chosen for this study.

The aircraft military flying qualities specification requires that the phugoid mode of the aircraft should be stable and have a damping ratio greater than 0.04. Consequently, it should seem reasonable to specify that all longitudinal axis modes should be stable. To determine the longitudinal axis modes, the mode classification procedure defined above will be used, with the longitudinal control force input (lb) and responses of pitch rate q (rad/sec) and vertical acceleration (g's).

As stated earlier, the aircraft flying qualities specification allows for an unstable spiral mode as long as the time to double is greater than 12 sec. Therefore, we

will measure lateral-directional axis nominal stability by requiring that all lateral-directional axis modes have a time to double greater than 12 sec. The lateral-directional axis modes are to be determined by the classification of modes procedure with lateral stick and directional pedal force (lb) input. Responses of interest are roll attitude (deg) and sideslip (deg).

4.2. Robust Stability Measures

The purpose of this section is to review the concepts related to stability robustness. Stability robustness is the property whereby the system remains stable in spite of the existence of various sources of uncertainty (modeling errors). Model uncertainty may be due to a number of sources including the ones mentioned in the military flight control specifications:

- a. Mathematical modeling and errors in defining the nominal system model and the plant;
- b. Variations in dynamic characteristics caused by changes in environmental conditions, manufacturing tolerances, aging, wear, noncritical material failures, and off-nominal power supplies;
- c. Maintenance induced errors in calibration, installation, and adjustment;
- d. Errors due to modeling of airframe structural dynamics/inertial coupling between axes and frequency dependency of stability derivatives;
- e. Digitization effects due to digital control implementation (phase shift due to sampling).

This research will consider three measures of stability robustness. The first measure is a multi-loop equivalent of the traditional single-loop stability margins which are specified in the flight control system specifications. The second measure, open-loop bandwidth, stems largely from flight control design concepts which rely on the importance of bandwidth to gain and phase margin definition, tracking performance and disturbance rejection. The last stability robustness measure is a measure of the susceptibility of an aircraft to depart from controlled flight. The departure susceptibility metric is based on measuring the robustness of the control system to variations in aerodynamic stability

derivatives which are known to dominate aircraft departure warning, susceptibility, and severity.

4.2.1. Multi-loop Stability Margins

It has been standard practice in control engineering to represent model uncertainty in two distinctive types: loop gain uncertainty and phase uncertainty. The standard single-loop gain margin is a measure of the amount of tolerance of the system to only loop gain uncertainty such that the system remains stable. The phase margin is a measure of the tolerance of the system to only phase lag or delay, i.e. loop phase uncertainty such that the system remains stable.

The military flight control system specification uses gain and phase margins to assess stability robustness. A typical form of the phase and gain margins required to pass the military specifications is shown in Table 4.1. The phase and gain margins include both positive and negative entries corresponding to gain amplification or attenuation and phase advance or phase delay uncertainty.

Table 4.1 MIL-F-87242 Gain and Phase Margin Specification

| Mode Frequency f_m , Hz | GM (dB) | PM (deg) |
|--|-----------|----------|
| $f_m < 0.06$ | ± 4.5 | ± 30 |
| $0.06 < f_m < \text{first aeroelastic mode}$ | ± 6.0 | ± 45 |
| $f_m > \text{first aeroelastic mode}$ | ± 8.0 | ± 60 |

The military specification requires computation of a gain and phase margin for each feedback loop. The loop in question is tested while all other loops are closed at their nominal gain values. It has been pointed out by many

researchers that this type of one-loop-at-a-time uncertainty representation is not realistic for a multi-loop system. It is possible for a lightly damped system to have acceptable single-loop gain and phase margins yet very small simultaneous gain and phase variations could drive the system unstable. A more realistic measure of system robustness should allow simultaneous perturbations in all the feedback loops.

The stability margin of a system can be assessed by examining the Nyquist plot and determining its closest approach to the -1 point. To aid in this analysis, Smith introduced a vector margin which was defined to be the distance to the -1 point from the closest approach of the Nyquist plot.^[16] For a multi-loop system, the Nyquist Stability Criterion still applies except that the stability is related to the closeness of the determinant $\det[I+G(s)]$ to the -1 point.

Using a multivariable version of the Nyquist Stability Criterion, a non-unique (estimate) of the multi-loop gain margin is,^[17]

$$GM_1 = \frac{1}{1 \pm \alpha} \quad (4.9)$$

where,

$$\alpha \equiv \min_{\omega \geq 0} \frac{1}{\sigma[S(j\omega)]} \quad (4.10)$$

The parameter α is essentially the magnitude of the vector distance from a multivariable Nyquist plot generalization to the -1 point.

The transfer function matrix $S(j\omega)$ is the system sensitivity function, typically defined as,

$$S(s) = [I + G(s)]^{-1} \quad (4.11)$$

where $G(s)$ is the open-loop system return ratio matrix. The open-loop return ratio matrix is essentially all of the feedback system components placed in series from the loop breaking point. In contrast to the single-loop stability margins described previously, the return ratio matrix is obtained by opening all of the feedback loops at the same time.

Note also that the multi-loop margin can be defined for any loop breaking point in the feedback system. Typically, loop stability margins are defined at the interface between the control system and the actuators, or the "input" to the controlled system and the "output" of the system which is the interface between the sensors and the control system.

The multi-loop phase margin PM_1 , computed using the system sensitivity function, is given by,

$$PM_1 = \cos^{-1}\left(1 - \frac{\alpha^2}{2}\right) \quad (4.12)$$

Another multi-loop stability margin can be defined using the equivalent of an inverse Nyquist plot. The gain margin GM_2 is then defined, [18]

$$GM_2 = 1 \pm \beta \quad (4.13)$$

where

$$\beta = \min_{\omega \geq 0} \frac{1}{\sigma[T(j\omega)]} \quad (4.14)$$

and $T(s) = G(s)[I + G(s)]^{-1}$ is the complimentary sensitivity function. The multi-loop phase margin PM_2 is,

$$PM_2 = \cos^{-1}\left(1 - \frac{\beta^2}{2}\right) \quad (4.15)$$

The multi-loop stability margin estimates obtained using the system sensitivity functions may be conservative. In other words, these methods may predict stability margins which are much smaller than the actual margins. To alleviate some of the conservatism, it is possible to combine the results of the two methods to improve the estimated stability margins. [19] Accordingly, a positive gain margin GM_{pos} is defined by,

$$GM_{pos} = \max\left(\frac{1}{1-\alpha}, 1+\beta\right) \quad (4.16)$$

and a negative gain margin as,

$$GM_{neg} = \min\left(\frac{1}{1+\alpha}, 1-\beta\right) \quad (4.17)$$

The final gain margin estimate, which will be denoted by GM , will be obtained by combining GM_{pos} and GM_{neg} to form a "symmetric" (\pm) answer,

$$GM \equiv \pm 20 \log(\min(GM_{pos}, 1/GM_{neg})) \quad (4.18)$$

and the final phase margin estimate is,

$$PM \equiv \pm \max(PM_1, PM_2) \quad (4.19)$$

Conservatism also results from the relative scaling of the system where the loop is broken. This means that depending on the units of the signals, different estimates of GM and PM may result using these singular value relations. At this point, it is necessary to either include an explicit definition of signal units in the definition of multi-loop stability margin requirements, or to propose an automatic scaling algorithm which is reliable and readily available.

The Frobenius norm scaling technique discussed in Section 3 has been successfully used to reduce the effect of scaling in the definitions of α and β . Results shown in Section 5 for the F-16 aircraft will consider the effect of unit scaling in more detail.

4.2.2. Open-loop Bandwidth

It is particularly appealing to measure stability robustness using the open-loop vehicle response bandwidth because of the relationship between open-loop bandwidth and traditional single-loop gain and phase margin definitions. For example, the current flying qualities specification includes a requirement on open-loop bandwidth of the pitch axis transfer function in the short-term pitch axis requirements, Para. 4.2.1.2, Part D. This bandwidth requirement is intended to define the maximum frequency at which closed-loop tracking can take place without threatening stability. The system bandwidth, in this case, is defined as the highest frequency at which the phase margin is at least 45 deg and the gain margin is at least 6 dB. The gain and phase margin values are consistent with the stability margins specified in the military flight control system specification.

Generalizations of the open-loop bandwidth for a single-loop system to multivariable system definitions have not been very successful. For example, some researchers have proposed the use of singular value plots to define open-loop bandwidth frequencies. Doyle and Stein^[5] have defined "...the bandwidth of G , i.e., for ω such that $\bar{\sigma}[G(j\omega)] \ll 1$." On the other hand, Safonov, Chiang, and Flashner,^[20] note that "Loosely speaking, the bandwidth ω_B of a control system is the frequency range where the loop transfer function is 'big', i.e. $\underline{\sigma}[G(j\omega)] \gg 1$ for all $\omega < \omega_B$." Most researchers seem to agree that the open-loop bandwidth should be defined somewhere between where $\underline{\sigma}[G(j\omega)] \gg 1$ and $\bar{\sigma}[G(j\omega)] \ll 1$. The

problem is complicated by the fact that the units of $G(j\omega)$ can affect the singular value computations such that a different bandwidth can be computed for different signal units.

To even further complicate the definition of bandwidth, there exist flight control systems wherein the loop gain does not cross unity magnitude at all. This situation occurs when the control system is not providing stability augmentation but merely an augmentation of the aircraft responses. A specific example is when a pitch damper is used simply to modify short-period damping and not necessarily to provide good tracking capabilities.

The bandwidth of the multivariable system will be defined, for this research, as the lesser of the frequencies at which the multi-loop gain margin and the multi-loop phase margin are determined. This definition is a direct analogy of the pitch-axis bandwidth criterion currently included in the aircraft flying qualities specification. The stability margin definition also avoids the limitations of the maximum or minimum singular value gain crossover frequency definitions. Bandwidth in terms of stability margins also does not require an open-loop gain crossover frequency and is therefore applicable to simple response augmentation systems (pitch and yaw dampers) as well as more sophisticated tracking systems. Finally, if a reliable scaling algorithm is used for multi-loop stability margin computation, the issue of signal units is, at least, minimized.

To define the requirements for bandwidth, the pitch axis requirements for the aircraft flying qualities will be used as a start. The recommended bandwidth for a Level I rating in the pitch axis is a minimum of 6.5 rad/sec and a maximum of 11 rad/sec (with no assumed time delay). These values are also consistent with a recent evaluation of the multi-loop stability margins of the lateral-directional flight control system of the X-29.^[21] The multi-loop stability margins for the X-29 were defined from frequencies between 4.3 to 9.8

rad/sec for a variety of flight conditions. The recommended bandwidth should be compared to the lesser of the frequencies at which the multi-loop gain margin and the multi-loop phase margin are determined, in the frequency range of 0.06 Hz to the first aeroelastic mode frequency.

4.2.3. Departure Susceptibility

Early efforts to evaluate aircraft spin susceptibility were based on design criteria for satisfactory spin recovery, should a spin condition be encountered. [22] By government suggestion, research since 1970 has focused on predicting and evaluating an aircraft's resistance to departure. [23] Therefore, much of the more recent developments in analytic measures for departure susceptibility have been based on groundwork formed in the 1970's. [24]

Investigation of the relationships between the post-stall behavior and aircraft stability derivatives revealed a strong relationships between departure susceptibility and certain lateral-directional derivatives; namely, the weathercock stability derivative $C_{n\beta}$ and the dihedral effect $C_{l\beta}$. Bihrie, for example, plotted $C_{l\beta}$ against $C_{n\beta}$ to yield regions in which the aircraft is predicted to be susceptible to roll reversal or departure. [25]

Using $C_{n\beta}$ and $C_{l\beta}$, along with the yawing and roll moment derivatives to lateral control deflection, $C_{n\delta a}$ and $C_{l\delta a}$, Weissman developed a departure susceptibility criteria by combining the stability derivatives to relate specific transfer function numerators and denominator coefficients. [26] The variables of interest are,

$$C_{n\beta, \text{dyn}} = C_{n\beta} \cos \alpha - \left(\frac{I_z}{I_x} \right) C_{l\beta} \sin \alpha \quad (4.20)$$

and the Lateral Control Departure Parameter (LCDP), defined as,

$$\text{LCDP} = C_{n\beta} - C_{l\beta} \left(\frac{C_{n\delta a}}{C_{l\delta a}} \right) \quad (4.21)$$

Weissman plotted $C_{n\beta, \text{dyn}}$ against LCDP and defined three regions which correspond to a high departure susceptibility. A sample plot of Weissman's departure criteria is shown in Figure 4.1. From Figure 4.1, one can see that Weissman was also able to predict the type of departure in the defined regions.

The effects of non-zero sideslip angles were first investigated using root locus plots of the lateral-directional mode poles for changing sideslip. [27,28] Stengel investigated the effect of combined non-zero roll-rate with a non-zero sideslip angle using this technique. [29] Along with Berry, he then made use of stability maps by plotting (and classifying) regions of instability for all of the airplane modes with various combinations of non-zero aircraft states. [30] A sample stability map of the type reported by Stengel and Berry is shown in Figure 4.2.

Pelikan has reported a modification to the traditional definition of $C_{n\beta, \text{dyn}}$ which uses a non-zero sideslip explicitly. [31] His departure parameter, called $C_{n\beta, \text{apparent}}$, also includes the effects of various control inputs. The definition of $C_{n\beta, \text{apparent}}$ is,

$$C_{n\beta, \text{apparent}} = C_{n\beta, \text{dyn}} + \sum_i \frac{u_i}{\beta_0} (C_{nui} \cos \alpha - \frac{I_z'}{I_x} C_{lui} \sin \alpha) \quad (4.22)$$

where u_i is the deflection of the i th control surface.

Many of the analytical methods described above are based on establishing regions of departure stability and instability. Starting from a known stable flight condition, an alternative departure resistance criteria would consider some measure of how close the aircraft is to an unstable departure condition. Such a measure could be defined by

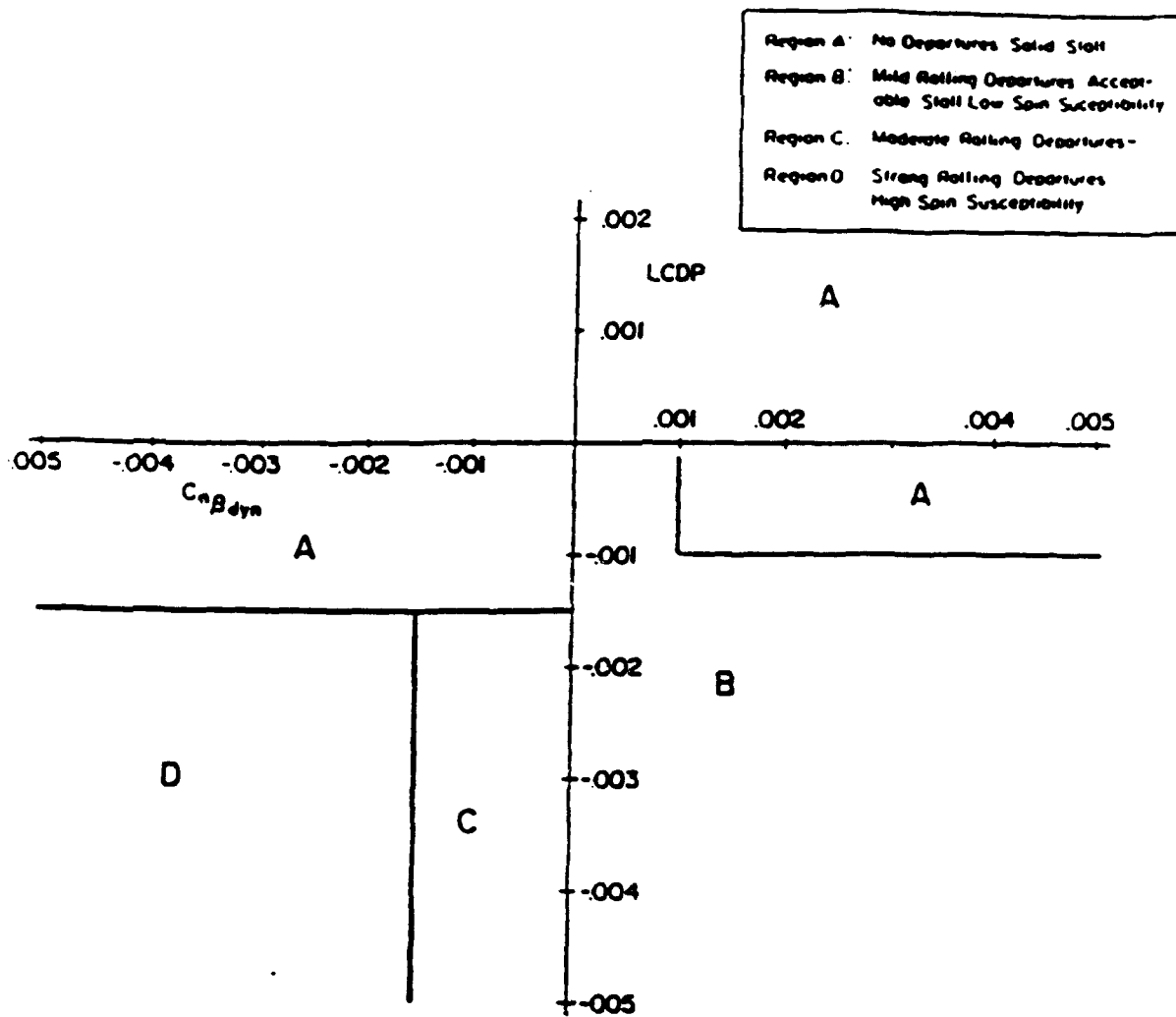


Figure 4.1 Weissman's Departure Criterion

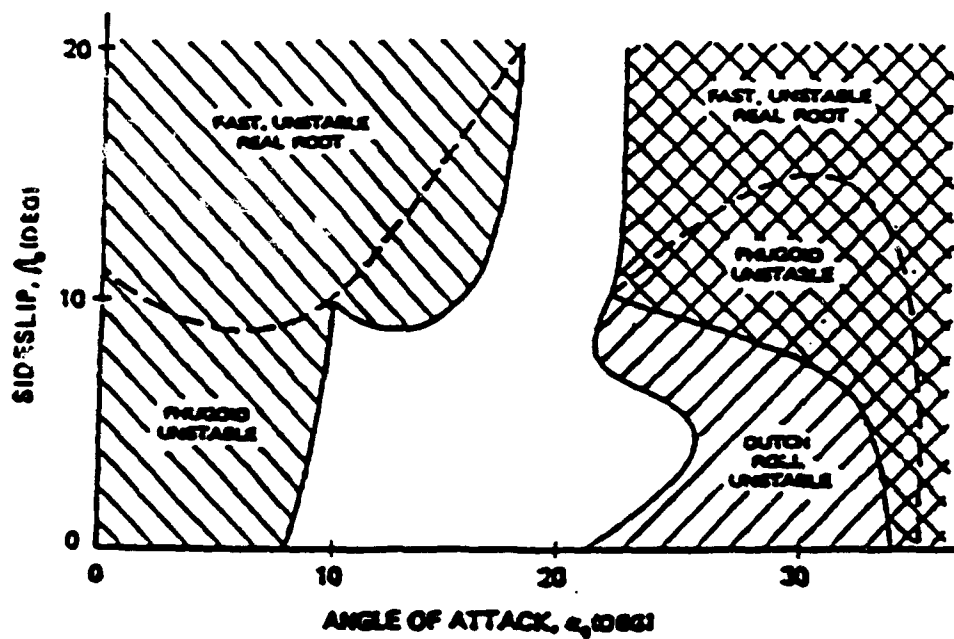


Figure 4.2 Sample Stability Map from Stengel and Berry

considering the dynamic effects of extreme maneuvering as an uncertainty in the nominally stable aircraft dynamics. The measure would relate the amount of uncertainty allowable before a departure stability condition is violated. A departure resistant aircraft would then be one which tolerates a large amount of uncertainty while a departure prone aircraft would be one which tolerates very little uncertainty because it is already very near an instability boundary.

Structured singular values have recently been considered for departure analysis by measuring the effect of uncertainty in some of the key airframe stability derivatives.^[32] The uncertainty matrix Δ will therefore represent a diagonal matrix of uncertain stability derivatives. For stability analysis, one must consider how the eigenvalues of the vehicle state matrix are effected by the uncertainty from Δ . Equivalently, one is interested in the eigenvalues of the uncertain linear system,

$$\dot{x} = (A - B\Delta C)x \quad (4.23)$$

where, $\Delta = \text{diag}\{\delta_i\}$ is diagonal matrix of stability derivative uncertainties. The matrices B and C are defined such that the stability derivative uncertainties are added to the vehicle state matrix in the appropriate location. The feedback system which results is shown in Figure 4.3, where $M(s) = C(sI - A)^{-1}B$. The relevant departure parameter DP is defined by the largest structured singular value over positive frequencies,

$$DP = \max_{\omega \geq 0} \mu(M(j\omega)) \quad (4.24)$$

and the corresponding stability condition becomes,

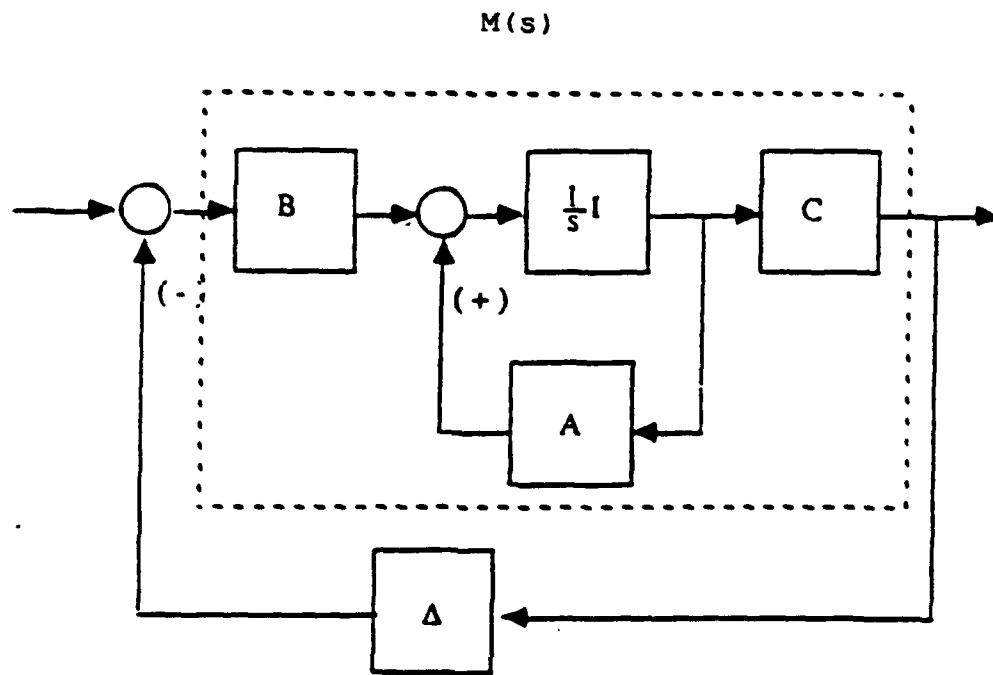


Figure 4.3 Block Diagram for Departure Analysis

$$\max_i |\delta_i| < 1/DP \quad (4.25)$$

The expression above shows that if DP is small, the aircraft is predicted to be departure resistant because it can tolerate large amounts of uncertainty before the stability condition is violated. Conversely, if DP is large, the stability condition can be violated for small uncertainties and the aircraft is not departure resistant.

The primary advantage of the structured singular value formulation is that perturbations in any number of stability derivatives can be studied by appropriate definitions of the Δ matrix. Also, the structured singular value departure methodology can be readily adapted to include the aircraft control system. Until now, only Pelikan's $C_n\beta$, apparent parameter considered the effect of the control system. Mathematically, the aircraft control system becomes imbedded in the definition of $M(s)$; i.e., $M(s)$ is made up of airframe states and control system states. Consequently, open-loop (bare airframe) as well as closed-loop departure parameters can be defined.

As an example, Stengel investigated the effect of simultaneously perturbing the derivatives N_β and L_β on the stability of a fourth-order lateral-directional model of the Space Shuttle Orbiter.^[33] Stengel predicted stability boundaries by "varying the aerodynamic derivatives, computing the eigenvalues, and cross-plotting to define regions of stability and instability as functions of the derivatives." Similarly, the structured singular value technique can be used to determine, from one calculation, the nearest instability boundary from the (stable) nominal point.

Stengel considered a fourth-order airframe described by,

$$\frac{d}{dt} \begin{pmatrix} r \\ \beta \\ p \\ \phi \end{pmatrix} = \begin{pmatrix} N_r & N_\beta & N_p & 0 \\ Y_r & Y_\beta & 0 & Y_\phi \\ N_r & N_\beta & N_p & 0 \\ 0 & 0 & 1 & 0 \end{pmatrix} \begin{pmatrix} r \\ \beta \\ p \\ \phi \end{pmatrix} \quad (4.26)$$

The stability derivatives describing the Space Shuttle Orbiter at $M = 1.5$, $\alpha = 6.6^\circ$ are listed in Table 4.2. The definition of $M(s)$ for the simultaneous perturbations δN_β and δL_β is shown in Table 4.3. Note that the Δ matrix is defined to normalize the perturbations in each derivative by the nominal derivative value so that an allowable perturbation error percentage is predicted.

Figure 4.4 shows the inverse of the structured singular values for the Space Shuttle, example. The minimum of the curve defines $1/DP = 0.26$, or $DP = 3.85$. Therefore, the stability derivatives N_β and L_β can be simultaneously perturbed by 26% before instability can occur. The value of DP also defines the following stability requirement,

$$\max \left(\frac{|\delta N_\beta|}{|N_\beta|}, \frac{|\delta L_\beta|}{|L_\beta|} \right) < \frac{1}{DP} = 0.26 \quad (4.27)$$

In terms of the actual dimensional stability derivatives, the equivalent stability condition above bounds the allowable absolute variation of the derivatives,

$$0.44 < N_\beta \text{ (1/sec}^2\text{)} < 0.74 \quad (4.29)$$

and,

$$-6.30 < L_\beta \text{ (1/sec)} < -3.71 \quad (4.30)$$

This result is compared to Stengel's result in Figure 4.5. Note in Figure 4.5 that the departure parameter DP defines a square which, in turn, determines the distance to the nearest instability boundary.

To utilize the new departure parameter DP as an indicator of departure susceptibility, one must plot DP against angle-of-attack. Figure 4.6 depicts the expected behavior of the departure parameter. It is expected that as

Table 4.2 Space Shuttle Stability Derivatives

| Derivatives | Value |
|-------------|------------------------------|
| N_r | -0.117 (1/sec) |
| N_β | 0.587 (1/sec ²) |
| N_p | 0.053 (1/sec) |
| Y_r | -1.0 |
| Y_β | -0.090 (1/sec) |
| Y_ϕ | 0.023 (1/sec) |
| L_r | 0.203 (1/sec) |
| L_β | -5.003 (1/sec ²) |
| L_p | -0.490 (1/sec) |

Table 4.3 Space Shuttle Uncertainty System

$$x^T = [r \ \beta \ p \ \phi]$$

$$A = \begin{bmatrix} N_r N_\beta N_p & 0 \\ Y_r Y_\beta & 0 & Y_\phi \\ L_r L_\beta L_p & 0 \\ 0 & 0 & 1 & 0 \end{bmatrix}$$

$$B = \begin{bmatrix} N_\beta & C \\ 0 & 0 \\ 0 & L_\beta \\ 0 & 0 \end{bmatrix}$$

$$C = \begin{bmatrix} 0 & 1 & 0 & 0 \\ 0 & 1 & 0 & 0 \end{bmatrix}$$

$$\Delta = \begin{bmatrix} \frac{\delta N_\beta}{N_\beta} & 0 \\ 0 & \frac{\delta L_\beta}{L_\beta} \end{bmatrix}$$

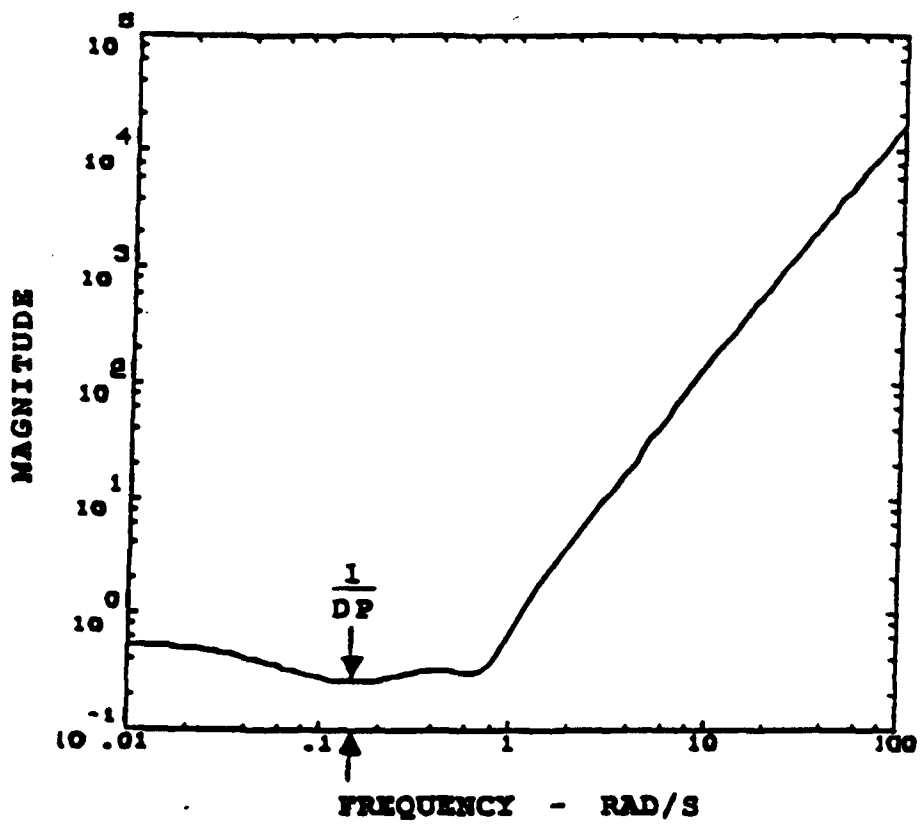


Figure 4.4 DP for Space Shuttle Example

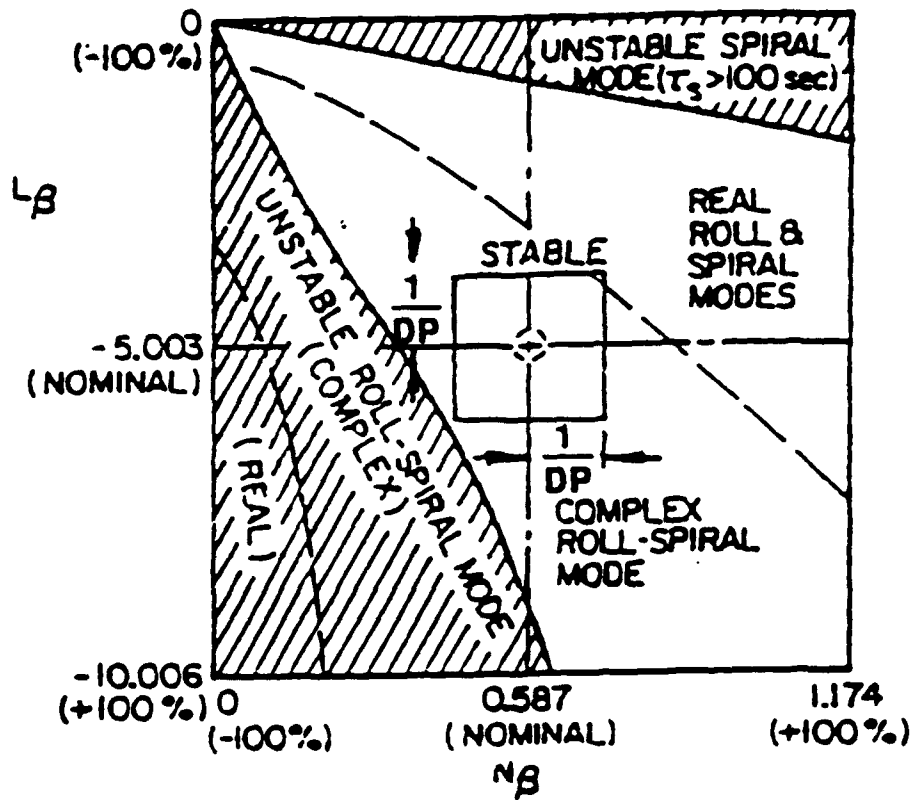


Figure 4.5 DP Compared to Stengel's Result

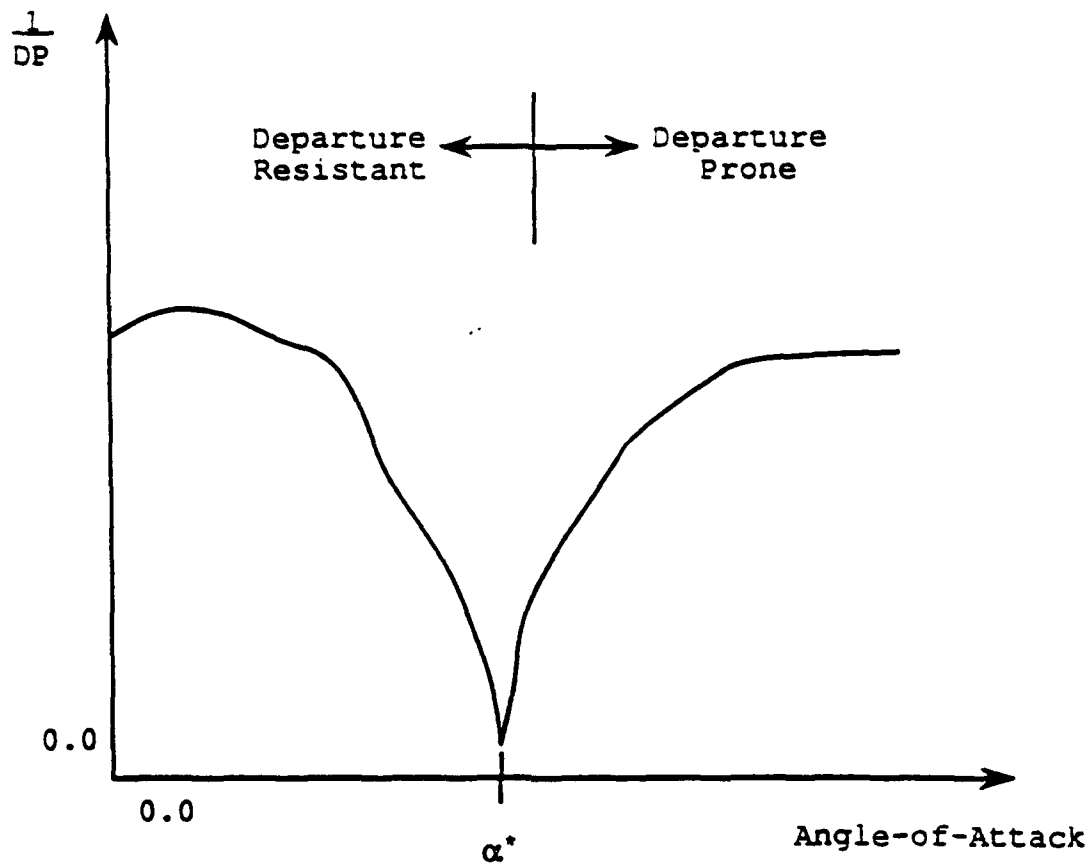


Figure 4.6 Expected Departure Parameter Behavior

angle-of-attack is increased, $1/DP$ will be reduced until ultimately it will come very close to zero. For all angles-of-attack less than where $1/DP \approx 0$, the aircraft will be considered departure resistant. For all angles-of-attack greater than the point where $1/DP \approx 0$, the aircraft will be considered departure prone.

Johnston has defined several open-loop airframe dimensional stability derivatives which have been shown to dominate aircraft departure warning, susceptibility, and severity.^[34] These derivatives are: $N_{\delta A}$ or $N_{\delta DH}$, M_{β} , L_{β} , L_{α} , L_p , N_{β} , N_{α} , and M_{β} . Any number or grouping of these key derivatives might be considered in developing the uncertainty structure in Δ needed to predict departure susceptibility reliably. The appropriate selection of key derivatives will no doubt be a fruitful area of new research. For this research effort, however, we will define the uncertainty matrix Δ as,

$$\Delta = \begin{pmatrix} \frac{\delta N_{\beta}}{|N_{\beta}|} & 0 \\ 0 & \frac{\delta L_{\beta}}{|L_{\beta}|} \end{pmatrix} \quad (4.31)$$

The selection of δN_{β} and δL_{β} in the uncertainty description is prompted by the use of $C_{n\beta}$ and $C_{l\beta}$ in the definitions of both $C_{n\beta, dyn}$ and LCDP.

4.3. Nominal Performance Measures

Nominal performance has been traditionally evaluated using the military flying qualities and flight control system specifications. The flying qualities specifications deal primarily with response of the aircraft from pilot inputs. The flight control system specification considers the performance of auto-pilot modes and also defines stability requirements.

Typically, specification compliance testing consists of some type of analysis conducted from a particular input to only one output. However, there are a few areas wherein a multivariable measure may more accurately measure the nominal performance of the aircraft. This section introduces four areas in which multivariable measures can be used to evaluate flight control systems. The four chosen areas are actually generalizations of single-loop measures that are included in the military specifications.

4.3.1. *Effective Order*

The current aircraft flying qualities specification, MIL-STD-1797 and the proposed V/STOL specification MIL-F-83300, [35] require the use of low order equivalent systems to compute certain modal parameters for flying qualities evaluation. This requirement was motivated by the fact that little correlation was found between "dominant response" parameters, extracted directly from high-order models, and flying qualities ratings.

There are many procedures available in the literature for extracting reduced order models of dynamic systems. Each of these methods have some characteristics of a high order model as input and a linear low order equivalent system as output. Generally, the particular method(s) used is left to the choice of the individual contractor and the procuring agency. Some of the methods mentioned in the military standard are:

- matching frequency responses of high order linearized models
- matching frequency responses extracted from flight time histories using a Fast Fourier algorithm
- matching frequency responses generated by stick cycling in flight
- using a maximum likelihood technique to match flight time history data

The acceptable forms for equivalent system models are listed in Tables 4.4 and 4.5.^[36] The order of the desired response is dictated by specification of the structure of the equivalent system models. In fact, it has been found that pilot opinion ratings can be degraded when the response of the closed-loop aircraft system are not of the same order as the equivalent system model forms.^[37] As a consequence, the effective order of a higher order system is of critical importance.

The relative magnitude of the Hankel singular values can be used to measure the effective order of the system.^[15] For example, if the Hankel singular values are sorted in descending order and the magnitude of the 'r' Hankel singular value was much greater than the magnitude of the 'r+1' Hankel singular value, the effective system order is 'r'. In other words, the full order system can be well represented by a system of order 'r'. Therefore, for the desired fourth order equivalent system models shown in Tables 4.4 and 4.5, if the Hankel singular values are sorted in ascending order, the fourth Hankel singular value should be much larger than the fifth.

4.3.2. *Equivalent System Error*

In the determination of equivalent systems for flying qualities studies, some measure must be used to assess the quality of the equivalent system match. The military flying

Table 4.4 Longitudinal Equivalent System Model Structures

| Longitudinal Axis Models | Reference |
|--|--------------|
| $\frac{\dot{\theta}}{\delta_{10n}} = \frac{K_{\theta}(s + 1/\tau_{\theta 2})e^{-\tau_{\theta} s}}{s^2 + 2\zeta_{sp}\omega_{sp}s + \omega_{sp}^2}$ | AIAA 77-1122 |
| $\frac{\theta}{\delta_{10n}} = \frac{K_{\theta}(s + 1/\tau_{\theta 1})(s + 1/\tau_{\theta 2})e^{-\tau_{\theta} s}}{(s^2 + 2\zeta_p\omega_p s + \omega_p^2)(s^2 + 2\zeta_{sp}\omega_{sp}s + \omega_{sp}^2)}$ | MIL-STD-1797 |
| $\frac{\dot{\theta}}{\delta_{10n}} = \frac{K_{\theta}s(s + 1/\tau_{\theta 1})(s + 1/\tau_{\theta 2})e^{-\tau_{\theta} s}}{(s^2 + 2\zeta_p\omega_p s + \omega_p^2)(s^2 + 2\zeta_{sp}\omega_{sp}s + \omega_{sp}^2)}$ | |
| <p>and simultaneously,</p> | |
| $\frac{n_z'}{\delta_{10n}} = \frac{K_{ns}(s + 1/\tau_{n 1})e^{-\tau_n s}}{(s^2 + 2\zeta_p\omega_p s + \omega_p^2)(s^2 + 2\zeta_{sp}\omega_{sp}s + \omega_{sp}^2)}$ | MIL-STD-1797 |

Table 4.5 Lateral-Directional Equivalent System Model Structures

| Lateral-Directional Axis Models | Reference |
|---|--------------|
| $\frac{\dot{\phi}}{\delta_{lat}} = \frac{K_{\dot{\phi}} e^{-\tau_{\phi} s}}{s + 1/\tau_R}$ | AIAA 77-1122 |
| $\frac{\beta}{\delta_{ped}} = \frac{K_{\beta} e^{-\tau_{\beta} s}}{s^2 + 2\zeta_{dr}\omega_{drs} + \omega_{dr}^2}$ | MIL-STD-1797 |
| $\frac{\phi}{\delta_{lat}} = \frac{K_{\phi}(s^2 + 2\zeta_{\phi}\omega_{\phi}s + \omega_{\phi}^2)e^{-\tau_{\phi} s}}{(s + 1/\tau_S)(s + 1/\tau_R)(s^2 + 2\zeta_{dr}\omega_{drs} + \omega_{dr}^2)}$ | |
| and simultaneously, | |
| $\frac{\beta}{\delta_{lat}} = \frac{K_{\beta}(s + 1/\tau_{\beta 1})(s + 1/\tau_{\beta 2})(s + 1/\tau_{\beta 3})e^{-\tau_{\beta} s}}{(s + 1/\tau_S)(s + 1/\tau_R)(s^2 + 2\zeta_{dr}\omega_{drs} + \omega_{dr}^2)}$ | MIL-STD-1797 |
| $\frac{\phi}{\delta_{lat}} = \frac{K_{\phi}(s^2 + 2\zeta_{\phi}\omega_{\phi}s + \omega_{\phi}^2)e^{-\tau_{\phi} s}}{(s + 1/\tau_S)(s + 1/\tau_R)(s^2 + 2\zeta_{dr}\omega_{drs} + \omega_{dr}^2)}$ | |
| and simultaneously, | |
| $\frac{\beta}{\delta_{ped}} = \frac{(A_3 s^3 + A_2 s^2 + A_1 s + A_0)e^{-\tau_{\beta} s}}{(s + 1/\tau_S)(s + 1/\tau_R)(s^2 + 2\zeta_{dr}\omega_{drs} + \omega_{dr}^2)}$ | MIL-STD-1797 |

qualities specification recommends the use of the following mismatch function,

$$J = \frac{20}{n} \sum_{\omega_1}^{\omega_2} [(\text{gain}_{\text{HOS}} - \text{gain}_{\text{LOS}})^2 + 0.02(\text{phase}_{\text{HOS}} - \text{phase}_{\text{LOS}})^2] \quad (4.32)$$

where 'gain' and 'phase' represent the gain and phase of the frequency response to be matched and HOS refers to the original high-order model and LOS refers to the low-order equivalent system model. The matching function is to be evaluated at twenty frequency points in the range from ω_1 to ω_2 .

The mismatch function above attempts to measure the error in the frequency response gain and phase. To generalize this idea, we will consider a measure of the transfer function error between the original high-order model and that of the low-order equivalent system model. Matrix singular values will then be used to indicate the size of the error. Expressed mathematically, the equivalent system error will be,

$$\bar{\sigma}[G_{\text{HOS}}(j\omega) - G_{\text{LOS}}(j\omega)] < e(\omega) \quad (4.33)$$

where $G_{\text{HOS}}(j\omega)$ is the transfer function matrix of the high-order model and $G_{\text{LOS}}(j\omega)$ is the transfer function matrix of the low-order equivalent system model. The frequency dependent function $e(\omega)$ will specify the allowable equivalent system error.

A suitable definition for $e(\omega)$ can be obtained from the current military flying qualities specification requirement on the "added dynamics" which frequently result from additional control system modes and can degrade pilot opinion ratings. [38] The requirement was obtained by examining pilot rating differences between pairs of in-flight simulated responses which included various dynamic modes added to low-

order equivalent models. The low-order equivalent models each reflected Level I flying qualities. Additional modes which caused a change in pilot rating of one unit (Cooper-Harper scale) were used to define an envelope of maximum unnoticeable added dynamics.

The "added dynamics" includes any dynamics in the vehicle closed-loop response which are not represented in the equivalent system dynamics. Therefore, the added dynamics specification limits the deviation of the actual closed-loop response from the low-order equivalent system. The added dynamics specification consists of upper and lower magnitude and phase bounds which are depicted in Figure 4.6. The response of the added dynamics alone should lie inside the envelopes pictured in Figure 4.6.

The upper and lower magnitude bounds of the added dynamics requirement are frequency dependent functions. The upper bound, which will be referred to as $m_u(\omega)$ is defined by,

$$m_u(\omega) = \left| \frac{3.16s^2 + 31.61s + 22.79}{s^2 + 27.14s + 1.84} \right|_{s=j\omega} \quad (4.34)$$

while the lower bound, $m_l(\omega)$, is expressed by,

$$m_l(\omega) = \left| \frac{0.095s^2 + 9.92s + 2.15}{s^2 + 11.6s + 4.95} \right|_{s=j\omega} \quad (4.35)$$

It is interesting to note that these functions are most restrictive near the probable crossover frequency of the pilot/vehicle system.

The added dynamics magnitude envelopes are meant to form the following inequality,

$$m_l(\omega) |g_{LOS}(j\omega)| \leq |g_{HOS}(j\omega)| \leq m_u(\omega) |g_{LOS}(j\omega)| \quad (4.36)$$

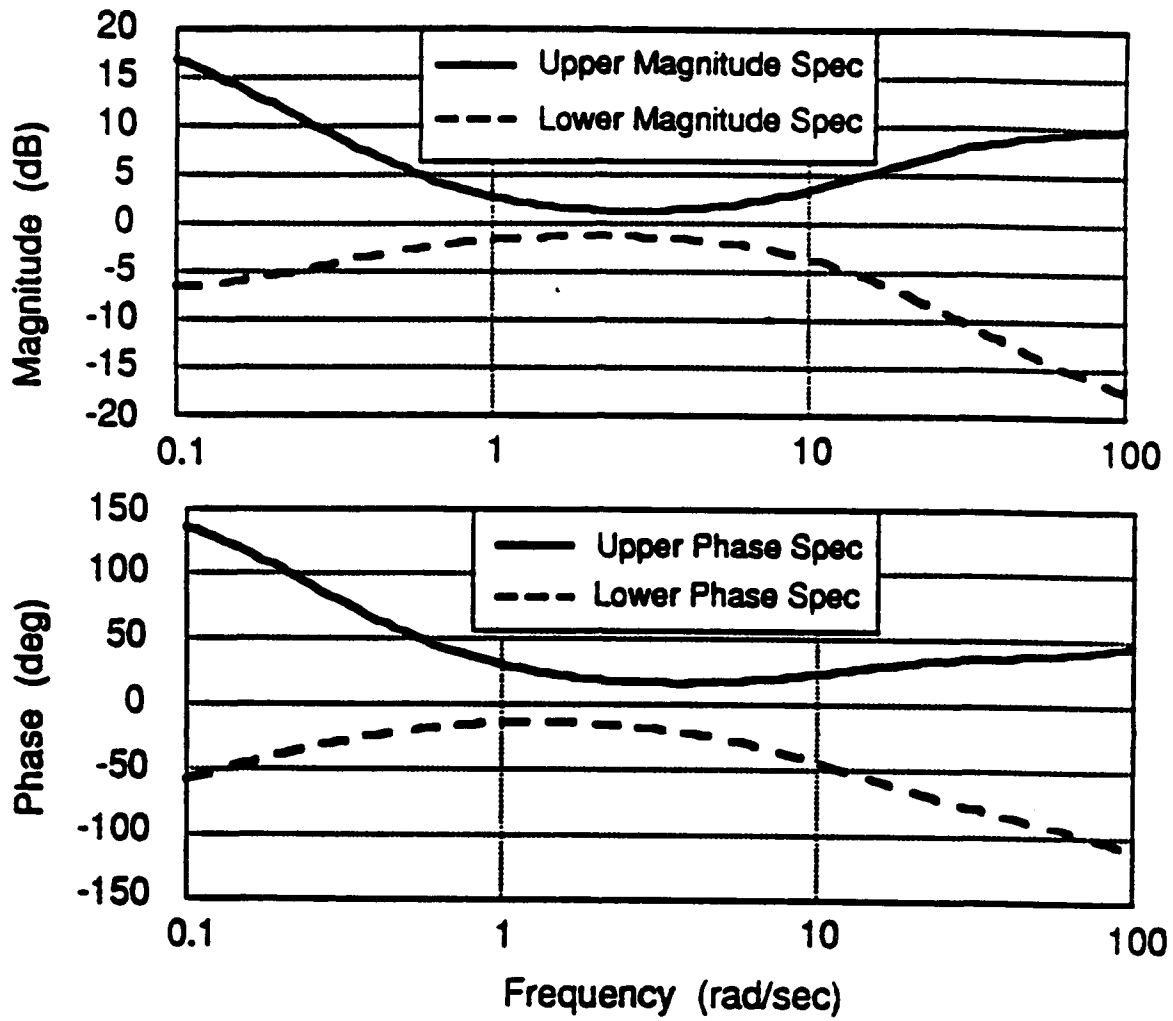


Figure 4.7 Added Dynamics Specification

where $g_{HOS}(j\omega)$ is the high-order transfer function frequency response and $g_{LOS}(j\omega)$ is the low-order equivalent system frequency response. To generalize this inequality to the multivariable case, the maximum singular value will be used to measure the size of the transfer function matrices such that,

$$m_1(\omega) \bar{\sigma}[G_{LOS}(j\omega)] \leq \bar{\sigma}[G_{HOS}(j\omega)] \leq m_u(\omega) \bar{\sigma}[G_{LOS}(j\omega)] \quad (4.37)$$

By adding and subtracting $G_{LOS}(j\omega)$ from $G_{HOS}(j\omega)$, the left side of the inequality becomes,

$$m_1(\omega) \bar{\sigma}[G_{LOS}(j\omega)] \leq \bar{\sigma}[G_{LOS}(j\omega) - (G_{LOS}(j\omega) - G_{HOS}(j\omega))] \quad (4.38)$$

If $\bar{\sigma}[G_{LOS}(j\omega)] > \bar{\sigma}[G_{LOS}(j\omega) - G_{HOS}(j\omega)]$, the following inequality insures (4.38),

$$\bar{\sigma}[G_{LOS}(j\omega) - G_{HOS}(j\omega)] \leq (1 - m_1(\omega)) \bar{\sigma}[G_{LOS}(j\omega)] \quad (4.39)$$

By a similar development, the upper bound will be met if,

$$\bar{\sigma}[G_{HOS}(j\omega) - G_{LOS}(j\omega)] \leq (m_u(\omega) - 1) \bar{\sigma}[G_{LOS}(j\omega)] \quad (4.40)$$

As a result, an effective measure of equivalent system error for multivariable flight control systems is,

$$\frac{\bar{\sigma}[G_{HOS}(j\omega) - G_{LOS}(j\omega)]}{\bar{\sigma}[G_{LOS}(j\omega)]} \leq e(\omega) \quad (4.41)$$

where $e(\omega)$ is chosen such that,

$$e(\omega) \leq m_u(\omega) - 1 \quad \text{and} \quad e(\omega) \leq 1 - m_1(\omega) \quad (4.42)$$

The frequency dependent functions $m_u(\omega)-1$ and $1-m_1(\omega)$ are plotted in Figure 4.7. This figure was used to choose a suitable $e(\omega)$, which is,

$$e(\omega) = \left| \frac{s^2 + 4.1s + 4.4}{1.17s^2 + 29.63s + 7.33} \right|_{s=j\omega} \quad (4.43)$$

4.3.3. Turbulence Response

A measure of merit for the turbulence response of the vehicle can be defined to assess ride quality of the aircraft in turbulence. To provide a measure of merit for aircraft turbulence response, one might consider specifying the shape of the aircraft response spectral density. The power spectral density of some scalar response 'y' of the aircraft, denoted $\Phi_y(\omega)$, to turbulence inputs is given by,

$$\Phi_y(\omega) = |f(j\omega)|^2 \Phi_t(\omega) \quad (4.44)$$

where $\Phi_t(\omega)$ is the power spectral density of the turbulence input and $f(s)$ is the transfer function from the turbulence input to the aircraft response of interest. The spectral densities of turbulence, in both the Dryden and von Karman form, are specified in the military flying qualities specification.

Unfortunately, a measure of merit based on the shape of the response spectral density may be too restrictive. As an alternative, the root-mean-square (rms) of the cockpit acceleration response to turbulence should provide an adequate measure of turbulence response. The rms value σ_y is given by,

$$\sigma_y^2 = \frac{1}{2\pi} \int_{-\infty}^{\infty} |f(j\omega)|^2 \Phi_t(\omega) d\omega \quad (4.45)$$

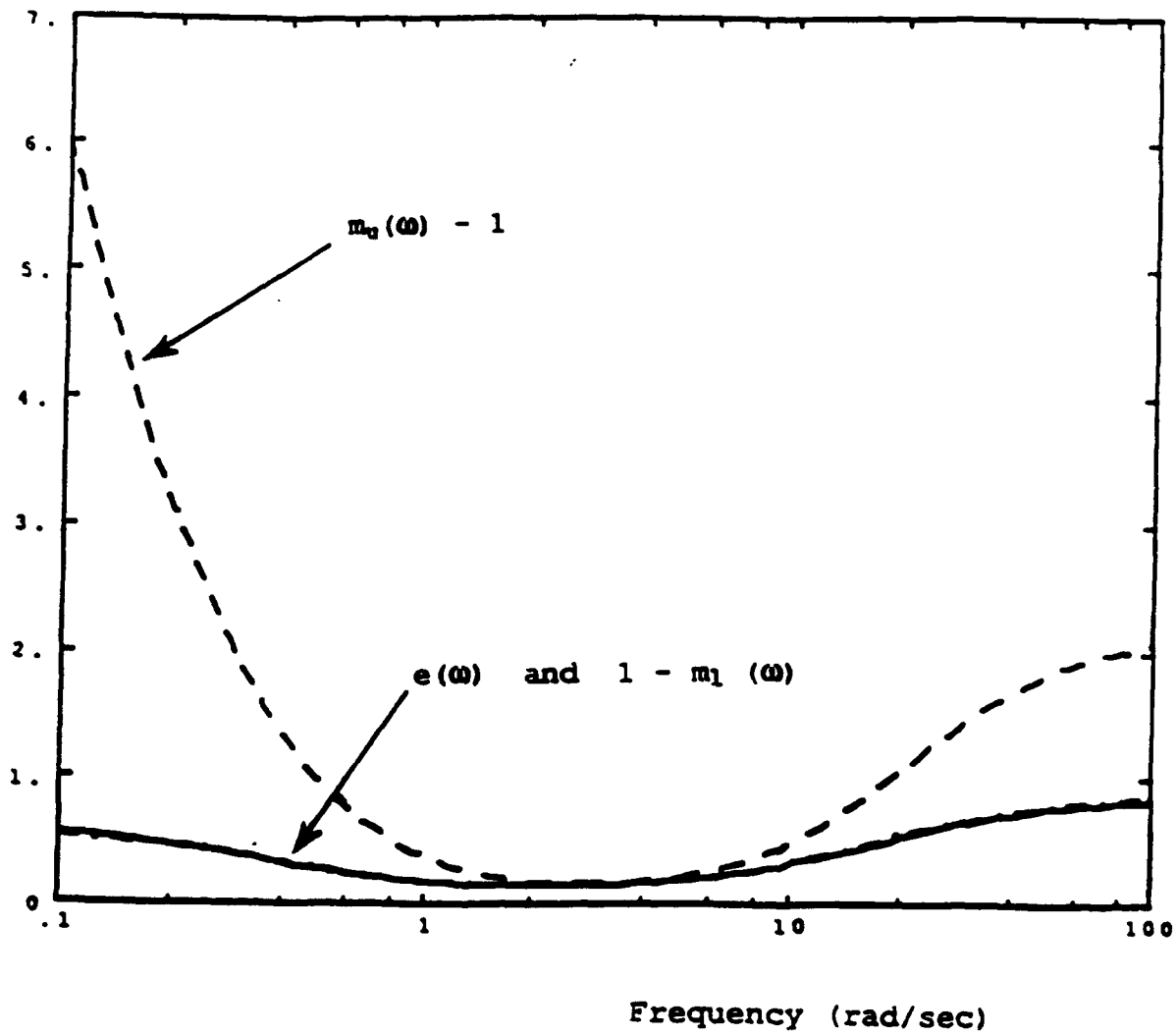


Figure 4.8 Development of Equivalent System Error Bound

Typically, the rms value of the aircraft response in one axis can be specified for turbulence in the same axis. For multivariable flight control systems, it is possible that the longitudinal and lateral-directional axes are coupled in some manner. When the two axes are coupled, the effect of simultaneous turbulence should be considered. When more than one response variable is of interest, the rms response variables are most easily determined using the state space equations,

$$\begin{aligned}\dot{x}(t) &= Ax(t) + Bw(t) \\ y(t) &= Cx(t)\end{aligned}\tag{4.46}$$

where $w(t)$ is assumed to be white noise with intensity $e[w(t)w^T(\tau)] = Q\delta(t-\tau)$. It is assumed that a state space representation of the turbulence spectral density has been augmented with the aircraft state equations in order to form (4.46). The rms values of the output vector are found as the diagonal elements of the matrix CXC^T where X (the state covariance) is obtained from,

$$AX + XA^T + BQB^T = 0\tag{4.47}$$

The 2-norm of the system is the trace of the matrix CXC^T and, therefore, it represents the sum of the squares of the rms values. The 2-norm of the aircraft excited by turbulence input will become the measure of turbulence response. Obviously, a smaller 2-norm value will indicate a greater degree of turbulence rejection.

To measure ride quality, the responses of interest are generally the vertical and lateral accelerations at the pilot station. The turbulence input should include, at least, turbulence in both the vertical velocity and side velocity directions. The matrix Q usually contains the rms intensity of the turbulence inputs, i.e., $Q = \text{diag}[\sigma_{wg}^2, \sigma_{vg}^2]$. But in

order to standardize the results of the linear analysis, unit intensities should be considered, $Q = \text{diag}[1, 1]$.

Requirements for turbulence response 2-norm will be established using the F-16 model. However, there is some guidance available from the flight control system specifications with regard to acceptable comfort levels. The background guide to MIL-F-9490D specifies a ride requirement limit of $\pm 0.1g$, zero to peak, for all single frequency vibrations below 22 Hz.^[39] The equivalent rms value of a 0.1 zero-to-peak sinusoid is 0.07 g's. As a result, for a system including both vertical and horizontal axis accelerations, the 2-norm of the system should be less than $\sqrt{2}$ times the expected rms value. For a 0.07 g acceleration in both axes, the expected 2-norm value is 0.10 g's. Normalizing this result by turbulence intensity of 5 ft/sec yields an expected 2-norm value of 0.02 (g/ft/sec).

For nominally unstable systems, the Lyapunov equation does not have a bounded solution. However, some indication of the response to turbulence can be obtained by numerically integrating the transfer function matrix frequency response to obtain an approximation of the 2-norm. The approximation is,

$$\|G(s)\|_2^2 \cong \frac{1}{\pi} \int_{\omega_1}^{\omega_2} \text{trace}[G^*(j\omega)G(j\omega)] d\omega \quad (4.48)$$

where the frequency range of integration is from ω_1 to ω_2 (rad/s). The transfer function matrix is defined by $G(s) = C(sI-A)^{-1}B$.

4.3.4. Response Decoupling

The most important aircraft cross-axis coupling problem occurs when the aircraft is rolling. When the aircraft is rolling, objectionable transients in pitch rate, roll rate, and lateral acceleration may occur. The military

specifications include many different criteria aimed at measuring this coupling behavior. The flying qualities specifications of interest are: Para. 4.8.1 Cross-Axis Coupling in Roll Maneuvers and Para. 4.5.4 Lateral Acceleration at the Pilot Stations. The applicable flight control system specification is Para. 3.1.2.4.2 Lateral Acceleration Limits, Rolling. Each of these requirements are designed to limit the allowable amount of cross-axis coupling when the aircraft is rolling.

Clearly, several responses are of interest in assessment of cross-axis coupling. The size of these responses should be the measure of merit. Therefore, it is recommended that the size of these cross-axis responses be measured using singular values. A limit on the size of these responses will limit the magnitude of their response in a rolling maneuver. As a result, the measure of cross-axis coupling will be,

$$\max_{\omega \geq 0} \bar{\sigma}[G(j\omega)] < v \quad (4.49)$$

where $G(s)$ is the transfer function matrix from the lateral stick force (lb) to the cross-axis variables of interest: pitch rate (rad/s), yaw rate (rad/s), and side acceleration (g's). The parameter v will be determined using the F-16 model.

Note that the aircraft state equations must be modified for this assessment because the aircraft should be rolling at some constant rate p_0 (rad/sec). The linearized equations of motion, in the body-axis, must be modified by the underlined terms shown in Table 4.6 to reflect the non-zero roll rate.

The effect of a non-zero roll rate on the linearized airframe stability has been considered before by Stengel.^[30] Stengel showed that the short-period and Dutch roll modes typically decrease in damping and increase in natural frequency, for increasing body-axis roll rate. When computing the proposed cross-axis coupling measure, the

Table 4.6 Linearized Aircraft Equations with Non-zero Roll Rate

$$m (\dot{u} + W_1 q) = -mg \theta \cos \theta_1 + F_{AX} + F_{TX}$$

$$m (\dot{v} + U_1 r - W_1 p - P_1 w) = mg \phi \cos \theta_1 + F_{AY} + F_{TY}$$

$$m (\dot{w} - U_1 q + P_1 v) = F_{AZ} + F_{TZ}$$

$$I_{xx} \dot{p} - I_{xz} \dot{r} - I_{xz} P_1 q = L_A + L_T$$

$$I_{yy} \dot{q} + (I_{xx} - I_{zz}) P_1 r - 2I_{xz} P_1 p = M_A + M_T$$

$$I_{zz} \dot{r} - I_{xz} \dot{p} + (I_{yy} - I_{xx}) P_1 q = N_A + N_T$$

maximum achievable roll rate should be used for the given flight condition.

4.4. Robust Performance Measures

The variation in performance due to model uncertainty defines the performance robustness of the closed-loop system. There are very few robust performance requirements directly relevant to aircraft flight control system assessment. Consequently, the measures of performance robustness considered herein constitute one of the few new research efforts aimed at quantifying the effect of model uncertainty on the performance of multivariable flight control systems.

There are at least two ways in which robust performance of a system can be measured. The first would be to compute the sensitivity of a particular performance parameter to model uncertainty. The measure, in this case, would be some ratio of the change in performance divided by the change in model parameters. The sensitivity approach has the distinct appeal of being somewhat analytical in that an analytical expression must be formed to describe the sensitivities of interest. As a result, valuable insight might be obtained in the development of the sensitivity expressions which may ultimately lead to a better understanding of which model uncertainty sources lead to the largest changes in aircraft performance.

As an example, the matrix Lyapunov equation has been used to propose nominal performance measures for effective system order and for turbulence response. It has been shown that the sensitivity of the Lyapunov solution to a parameter p is given by, [40]

$$A \frac{\partial X}{\partial p} + \frac{\partial X}{\partial p} A^T + \left(\frac{\partial A}{\partial p} X + X \frac{\partial A^T}{\partial p} + \frac{\partial B}{\partial p} Q B^T + B Q \frac{\partial B^T}{\partial p} \right) = 0 \quad (4.50)$$

With the partials $\partial A/\partial p$ and $\partial B/\partial p$ defined, the above equation can be used to solve for $\partial X/\partial p$, which is the sensitivity of the Lyapunov equation solution to the parameter variation p .

While the sensitivity approach is by far the most intellectually appealing, it suffers from the fact that very little research has been conducted in this area. As a result, only a few of the proposed nominal performance measures have a direct analytical solution describing the sensitivity of the solution to parameter variations. Furthermore, verification of the predicted performance robustness would be very difficult to conduct in practice, especially given the highly nonlinear model structure of some airplanes.

The second approach is to actually vary the aircraft model dynamics by some standardized method and retest the nominal performance measures. This approach is equivalent to evaluating the performance sensitivity numerically. The numerical perturbation approach also offers a straightforward verification process wherein the model dynamics or high-fidelity simulation dynamics are perturbed and well defined performance metrics are retested. In order to implement such an approach, a standard uncertainty set must be defined. The standard uncertainty set proposed for this research is defined in the next section.

4.4.1. *The Standard Uncertainty Set*

It is expected that the manufacturer of the airplane will consider uncertainty modeling specific to the airplane as an integral part of the development of the airplane. Therefore, the standard uncertainty set, which will be used to measure the performance robustness of a variety of aircraft, should not contain specific uncertainties which might favor one particular aircraft or control system type over another. For this reason, the standard uncertainty set defined for this research will only include gain and phase uncertainty at pre-determined levels.

The magnitude of the gain and phase uncertainty levels might be expressed in either absolute values or as a percentage of the specified minimum multi-loop gain and phase margins. Obviously, the standard uncertainty set for performance robustness testing cannot be larger in magnitude than the recommended stability margins.

For gain uncertainty, the standard uncertainty set will consist of a gain perturbation of ± 1.5 dB introduced into each feedback loop. A perturbation of ± 1.5 dB represents 1/4th of the military specification single-loop stability margin of ± 6 dB and yields approximately $\pm 19\%$ variation in loop gain.

The feedback loops should also be perturbed in the worst case direction. The "direction" for gain variations means whether $+1.5$ dB or -1.5 dB is added to the loop gain. The sign of the worst case direction can be found using the real approximation to the structured singular value (see Section 3.4). At the bandwidth frequency, the permutation matrix Φ which maximizes the structured singular value reveals the worst case directions of the standard gain uncertainty set. [41]

Pure phase uncertainty is difficult to implement into state space models and it is therefore difficult to analyze and verify the effect of pure phase uncertainty in linear models. As an alternative, the standard phase uncertainty set will consist of a transport or time delay introduced into each feedback path. The pure time delay is modeled by the transfer function $e^{-\tau s}$ where τ is the effective time delay in seconds. The time delay τ will be defined for the phase uncertainty set as the delay which introduces 10 degrees of phase loss at the bandwidth frequency. A phase loss of 10 degrees is approximately 1/5th of the recommended single-loop phase margin. Therefore, the standard phase uncertainty time delay is,

$$\tau = \frac{10\pi}{180\omega_{BW}} \quad (4.51)$$

where ω_{BW} is the multi-loop bandwidth in rad/sec and τ is the time delay in seconds.

A Pade' approximation of the pure time delay will be utilized for analysis of continuous time models. The first-order Pade' approximation is, [42]

$$e^{-\tau s} \cong \frac{1 - \tau s/2}{1 + \tau s/2} \quad (4.52)$$

With the preceding definitions of the standard uncertainty set, performance robustness measurement will commence by perturbing the aircraft system dynamics by the amounts defined in the standard uncertainty set. Each of the nominal performance measures are then computed using the perturbed aircraft system dynamics. The computed measures using the perturbed system dynamics are the measures of performance robustness.

5. Measure of Merit Results for the F-16 Aircraft

In this section, the proposed new measures of merit are computed for the F-16 aircraft model. While the results are only applicable to one flight condition, they are representative of the numerical values and computational requirements of the new measures. The results of the application to the F-16 also reveal areas where the measures need to be refined, based on a comparison of the results to the expected characteristics described in Section 4.

5.1. Nominal Stability Measures

To test nominal closed-loop stability, the eigenvalues of the complete closed-loop system were first computed. The complete closed-loop system has 53 eigenvalues ranging in equivalent natural frequency from 0.0 to 351.0 rad/sec. Only one eigenvalue was found to be unstable. The unstable mode is a real eigenvalue located at +0.02 rad/s. The time-to-double amplitude for this mode is 34.7 seconds. It was recommended in Section 4.1, based on current specifications, that all closed-loop eigenvalues have an equivalent time-to-double of greater than 12 seconds. Therefore, the F-16 model meets this measure of merit.

5.1.1. Mode Classification

The proposed new nominal stability measure requires classification of each of the characteristics roots of the closed-loop system. Once the modes have been classified, the stability or instability of each mode is tested. The mode classification was carried out using the modal residue method described in Section 4.1.1.

Of the 53 closed-loop eigenvalues, 15 were classified as longitudinal modes. All of the longitudinal modes were found to be stable except that the unstable mode located at +0.02

rad/s was classified as a longitudinal mode. It is believed that the unstable mode results because the control system has failed to stabilize the open-loop unstable phugoid mode of the airplane. The open-loop airframe eigenvalues were listed in Table 2.1 where it was noted that the phugoid mode consisted of two real eigenvalues located at +0.1 and -0.01 rad/s. The time-to-double amplitude for the open-loop unstable phugoid root is 6.6 seconds. As a result, the control system has increased the time-to-double for this mode from 6.6 to 34.7 seconds, but the mode has not been stabilized. Consequently, the F-16 model does not meet the recommended requirement of all stable longitudinal modes.

Twenty-one eigenvalues were classified as lateral-directional modes. All of the classified lateral-directional modes were found to be stable. Thus, the recommended 12 second or greater time-to-double amplitude requirement for lateral-directional modes has been met for this F-16 model.

It is interesting to note that only 36 of the total 53 eigenvalues were classified as longitudinal or lateral-directional. Therefore, there are 17 eigenvalues which do not appear to contribute to the longitudinal or lateral-directional motion of the aircraft, as commanded by the pilot. Five of these states stem from the turbulence model, which is not excited by pilot inputs. It is possible that the other unclassified modes stem from parts of the control system which are not in use at this particular flight condition.

5.2. Robust Stability Measures

The stability robustness measures are intended to quantify the effect of model uncertainty on the stability of the aircraft. It has already been shown in the previous section that the nominal closed-loop system is unstable. As a result, these stability robustness measures must be

interpreted as the amount of tolerable uncertainty before an additional closed-loop eigenvalue becomes unstable.

5.2.1. Multi-loop Stability Margins

Multi-loop stability margins were computed at both the input to the actuator model (output of the control system) and the output of the sensor model (input to the control system within the feedback loop). The block diagram manipulations required to form the appropriate sensitivity functions were completed using SCT's the graphical modeling tool Model-C™.

Figure 5.1 shows a Model-C™ diagram with an uncertainty block inserted at the actuator input in the closed-loop system diagram. The uncertainty block serves as a placeholder such that the response from the input of the uncertainty block to the output of the block is the same as the complementary sensitivity function.

Figure 5.2 shows a plot of the inverse of the maximum complimentary sensitivity function singular value as a function of frequency. From this figure, one can see that $\beta = 0.902$ at 5.3 rad/s for this configuration.

The equivalent Model-C™ diagram to compute α from the system sensitivity function is shown in Figure 5.3. A plot of the inverse of the maximum sensitivity function singular value is shown in Figure 5.4. The minimum value shown in Figure 5.4 reveals that $\alpha = 0.57$ at 12.3 rad/s. As a comparison; a recent study of the X-29 lateral directional flight control system resulted in a value of $\alpha = 0.67$ at 7.9 rad/s.[21] This value of α was also obtained at the input node of the control system and a similar flight condition ($M = 0.7$, 30,000 ft altitude).

The multi-loop gain and phase margins, at the actuator input, are computed from α and β obtained above.

$$GM_{pos} = \max\left(\frac{1}{1-\alpha}, 1+\beta\right) = \max(1.9, 2.3) = 2.3 \quad (5.1)$$

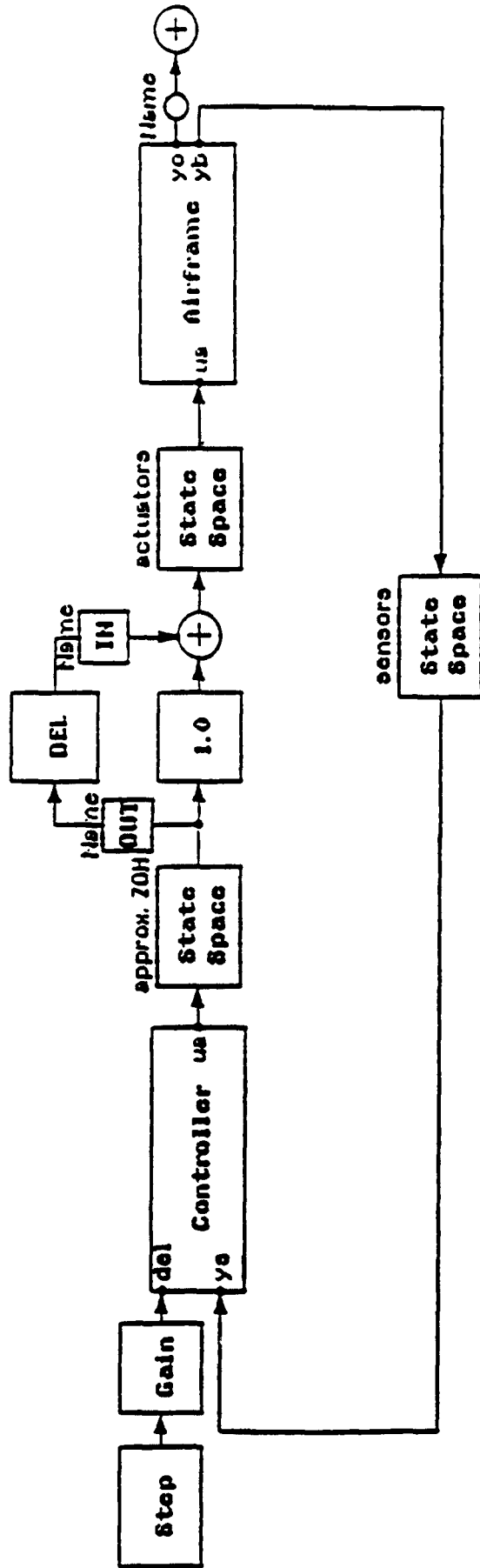


Figure 5.1 Block Diagram for Input Complimentary Sensitivity Function

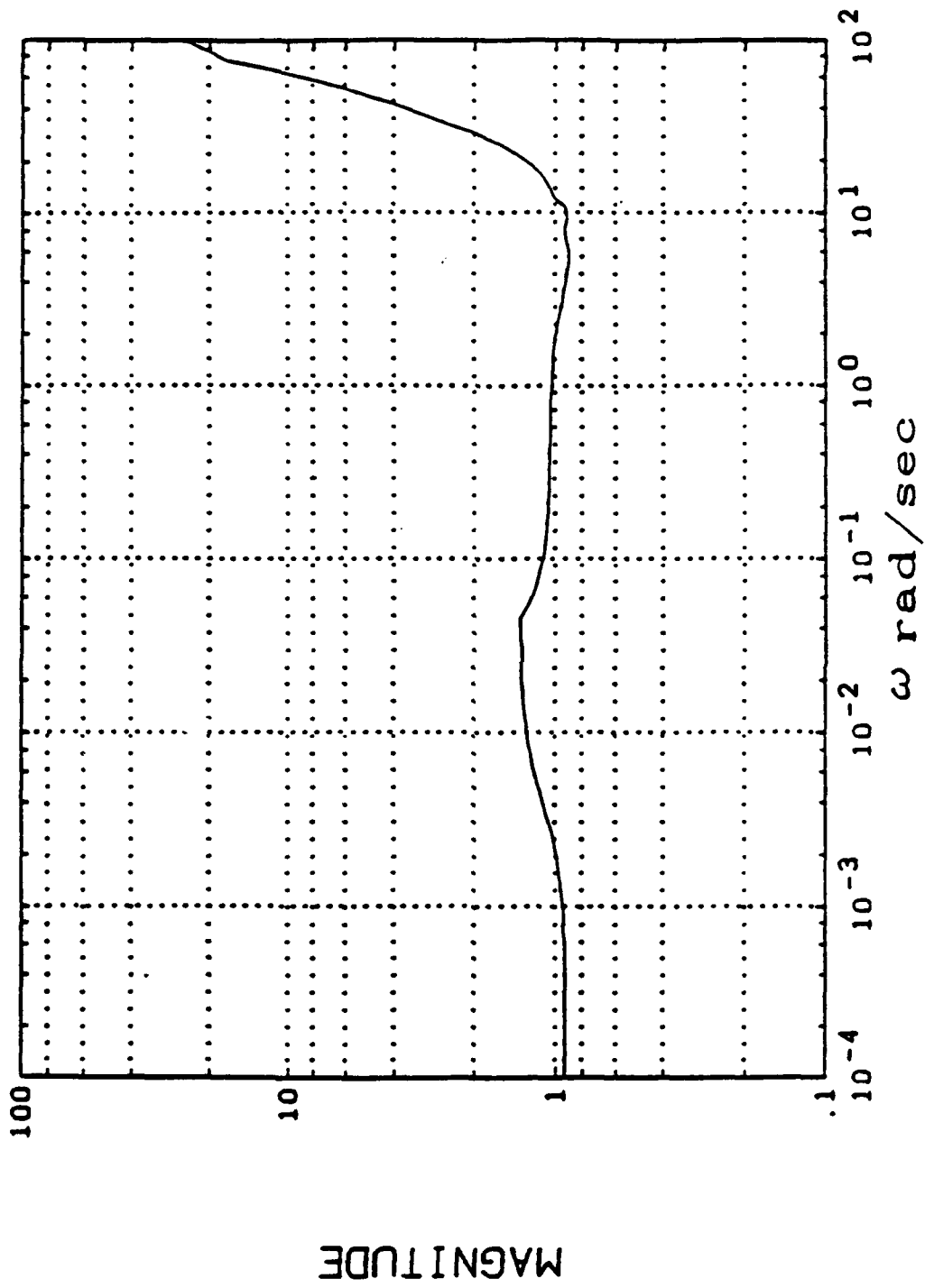


Figure 5.2 Input Complimentary Sensitivity Function Singular Values

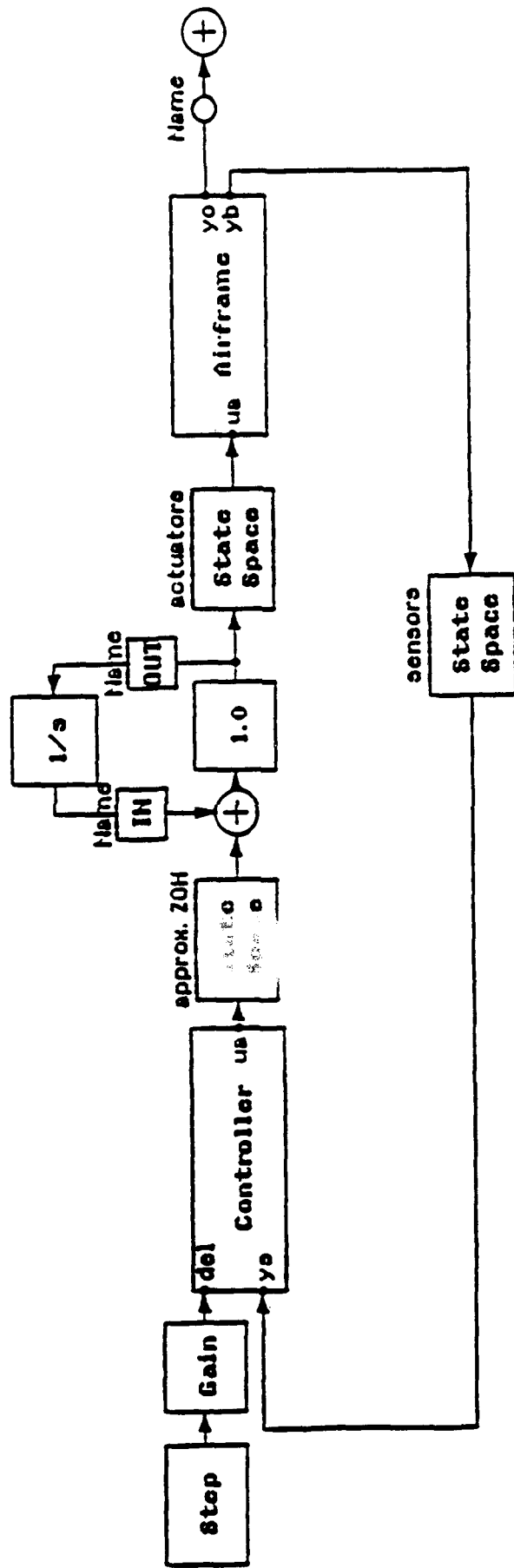


Figure 5.3 Block Diagram for Input Sensitivity Function

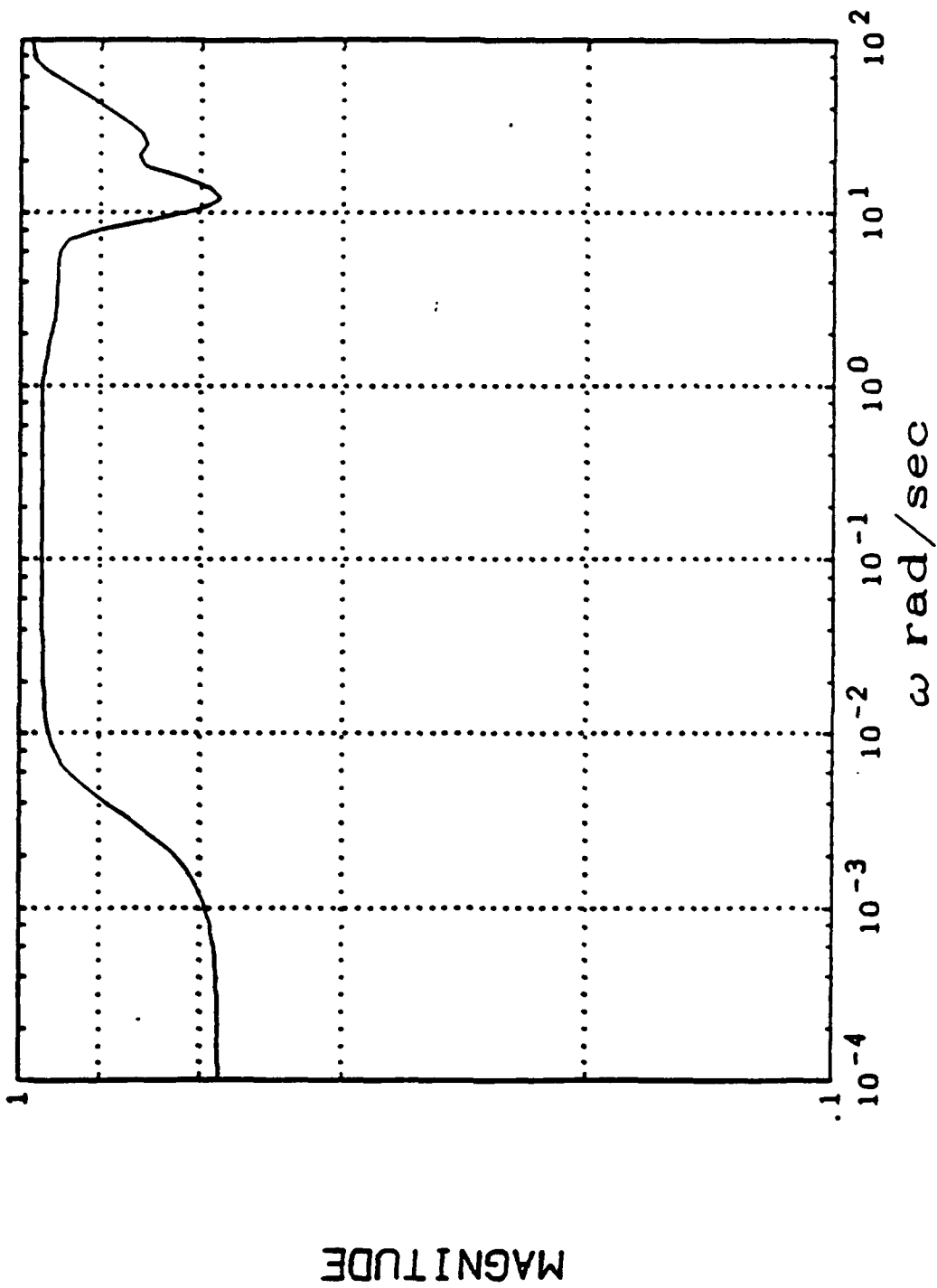


Figure 5.4 Input Sensitivity Function Singular Values

$$GM_{neg} = \min\left(\frac{1}{1+\alpha}, 1-\beta\right) = \min(0.10, 0.64) = 0.10 \quad (5.2)$$

The final gain margin estimate is then

$$GM = \pm 20 \log(\min(GM_{pos}, 1/GM_{neg})) = \pm 7.3 \text{ dB} \quad (5.3)$$

The phase margin estimates are,

$$PM_1 = \cos^{-1}\left(1 - \frac{\alpha^2}{2}\right) = 33.0^\circ \quad (5.4)$$

$$PM_2 = \cos^{-1}\left(1 - \frac{\beta^2}{2}\right) = 53.6^\circ \quad (5.5)$$

and the final phase margin estimate is,

$$PM = \pm \max(PM_1, PM_2) = \pm 53.6^\circ \quad (5.6)$$

In an attempt to reduce any conservatism inherent in these results, the computations were repeated using the Frobenius norm scaling technique. There was no significant improvement in either the gain margin or phase margin estimates. This result is undoubtedly due to the fact that all of the actuator inputs have units in degrees of surface deflection.

The above computations were repeated with the uncertainty inserted at the sensor outputs. Figure 5.5 shows a Model-C™ diagram with an uncertainty block inserted at the output of the sensors. Figure 5.6 shows a plot of the inverse of the maximum complimentary sensitivity function singular values (solid line) with the loops effectively broken at the output of the sensors. Figure 5.6 reveals that $\beta = 0.021$ at 0.001 rad/s.

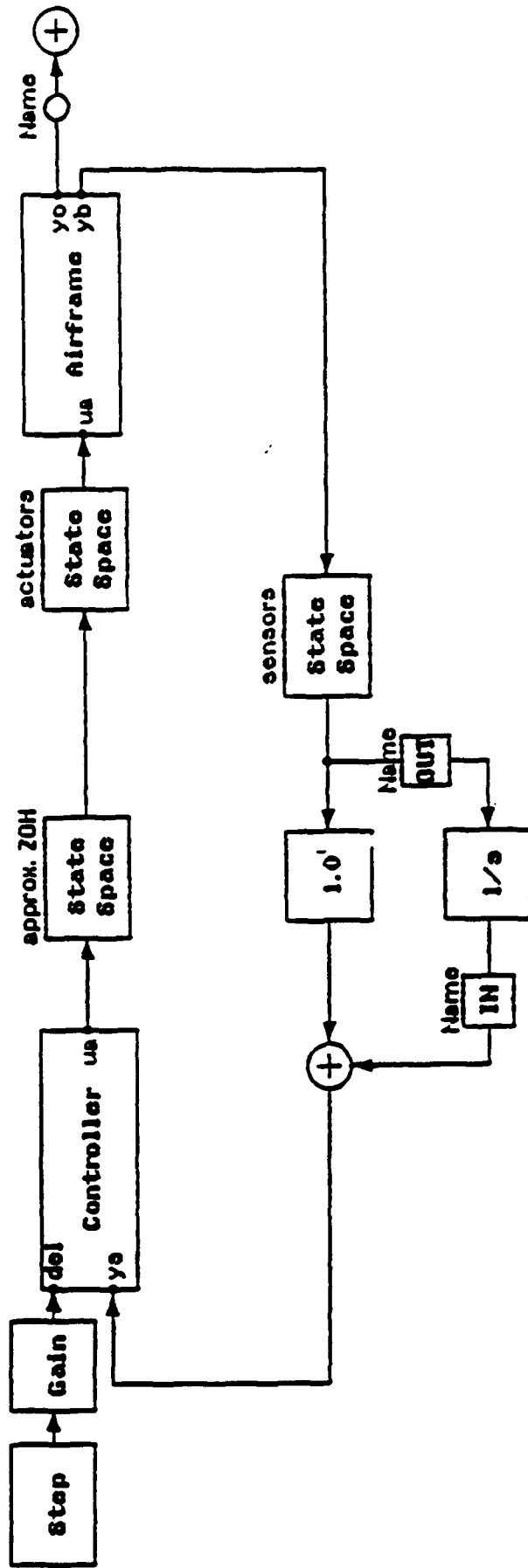


Figure 5.5 Block Diagram for Output Complimentary Sensitivity Function

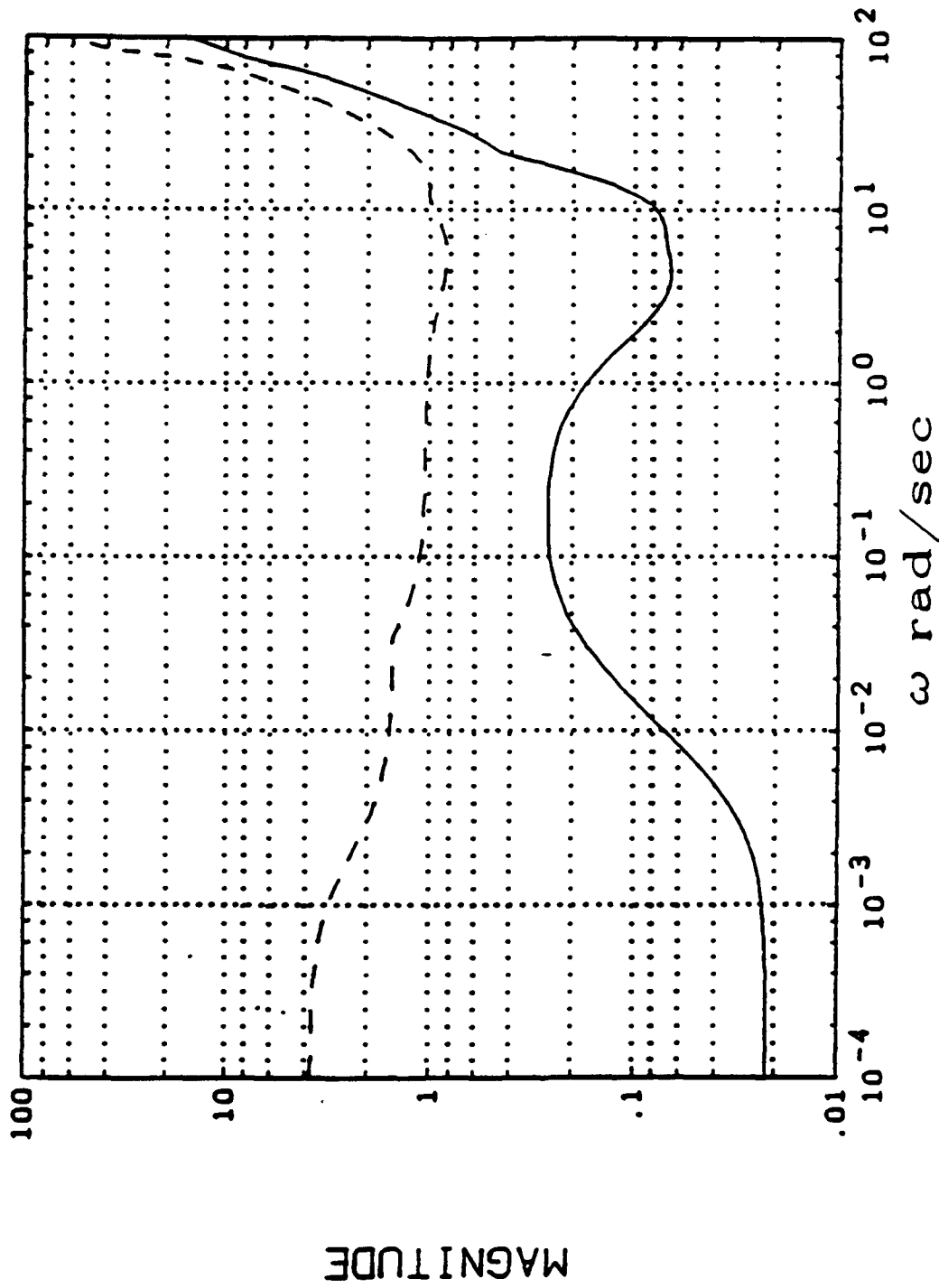


Figure 5.6 Output Complimentary Sensitivity Function Singular Values

To compute the stability margins using the sensor output sensitivity function, an uncertainty block was inserted as in Figure 5.7. The solid line in Figure 5.8 shows a plot of the inverse of the maximum sensitivity function singular values with the loops broken at the output of the sensors. The parameter $\alpha = 0.022$ at 0.001 rad/sec is defined in Figure 5.8.

The values of α and β seem unusually small when compared to $\alpha = 0.66$ at 8.0 rad/s obtained from the comparable X-29 study. In order to reduce the apparent conservatism, the computations were repeated with the Frobenius scaling method. The dashed lines in Figures 5.6 and 5.8 show the scaled versions of the singular value plots for the complimentary sensitivity and the sensitivity functions, respectively. The effect of scaling in this case is very dramatic! Figures 5.6 and 5.8 reveal values of $\beta = 0.83$ at 5.3 rad/s and $\alpha = 0.67$ at 24.7 rad/s, after scaling. The improvement after scaling results because the units of the feedback variables are very different. For example, the angular rate feedbacks are in units of rad/s while the accelerations are in ft/s². Using the parameters obtained after scaling, a gain margin of ± 9.6 dB and a phase margin of $\pm 49.2^\circ$ were obtained.

5.2.2. Open-loop Bandwidth

The measure of open-loop bandwidth was defined in Section 4.2.2 as the lesser of the frequencies at which the stability margin values of α and β were determined. From the Section 5.2.1 results, we find that an open-loop bandwidth of 5.3 rad/s was determined for both the input and output nodes of the control system. An open-loop bandwidth of 5.3 rad/s compares favorably with the Section 4.2.2 recommended values.

5.2.3. Departure Susceptibility

In order to compute the departure parameter metric, a structured uncertainty block was inserted into the Model-C™ diagram as shown in Figure 5.9. The block diagram consist of

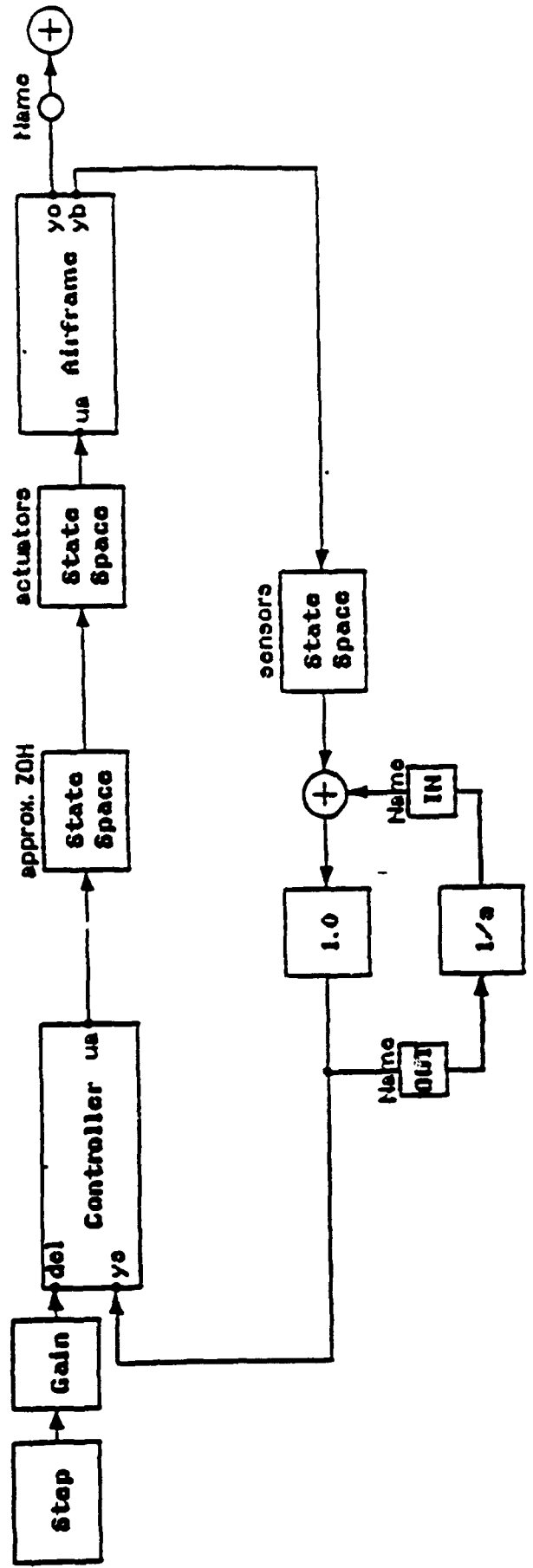


Figure 5.7 Block Diagram for Output Sensitivity Function

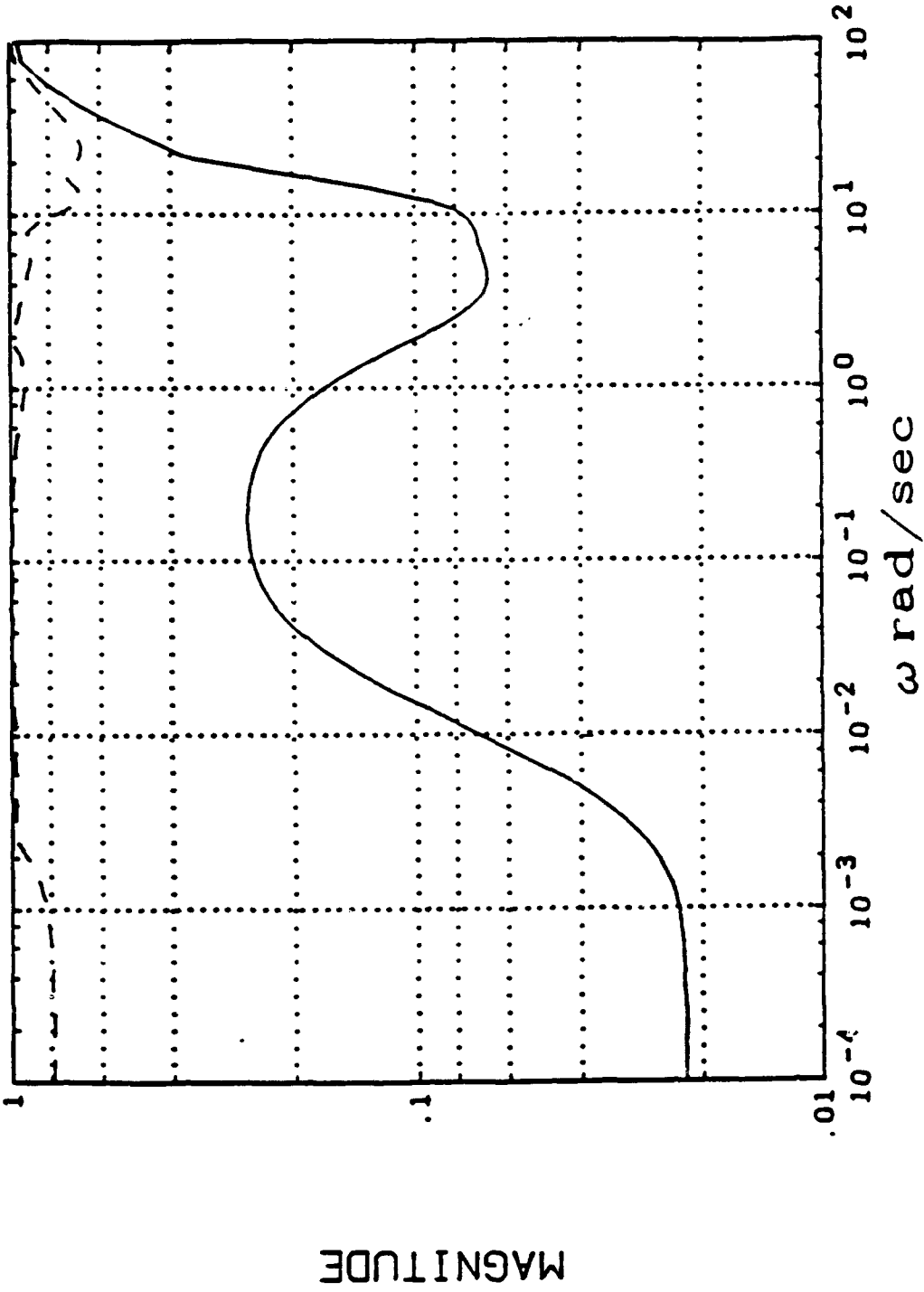


Figure 5.8 Output Sensitivity Function Singular Values

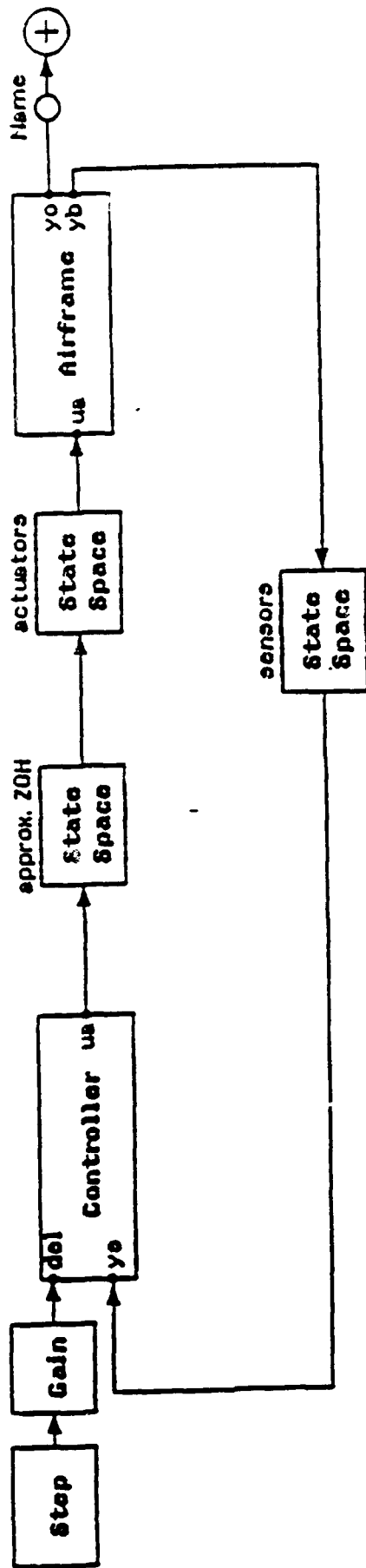


Figure 5.9(a) Block Diagram for Computing Departure Parameter

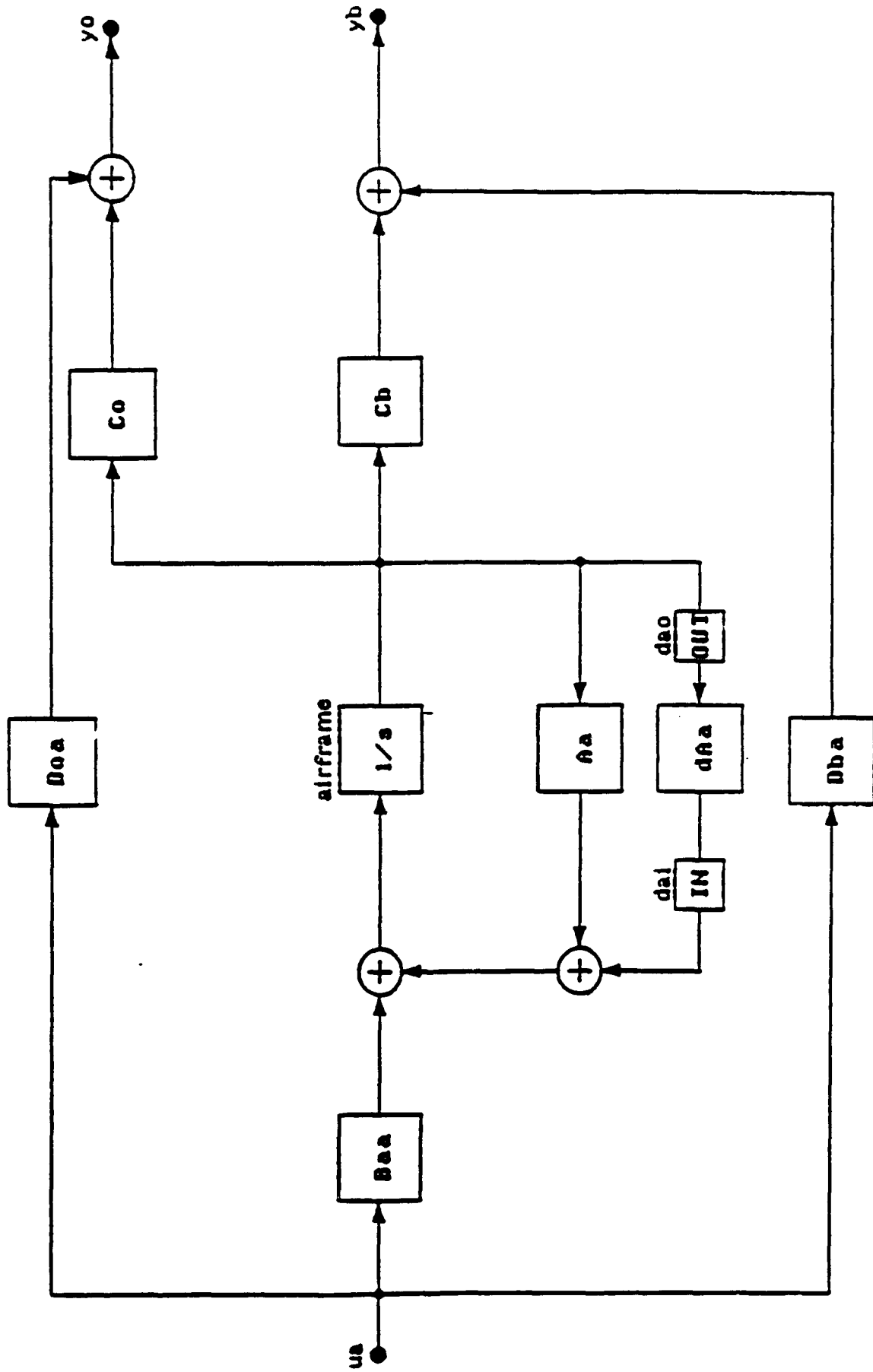


Figure 5.9(b) Airframe Block Diagram for Computing the Departure Parameter

two hierarchical block diagrams where one block diagram is actually represented a one block within the other diagram. Figure 5.9(a) is the overall system diagram consisting of all of the model subsystems: actuators, sensors, airframe, and control system. Figure 5.9(b) shows an expansion of the "Airframe" labeled block in Figure 5.9(a). The two uncertain stability derivatives are L_v and N_v and are assumed to be perturbed simultaneously. These two derivatives only effect the aircraft state matrix which is represented by the block labeled "Aa" in Figure 5.9(b). The uncertainty in L_v and N_v are represented by the block labeled "dAa". The uncertainties are normalized by their nominal values so that the resulting departure metric indicates a percentage of uncertainty rather than an absolute value. To compute the departure metric, the structured singular values are computed for the transfer function from the uncertainty input (labeled "dai") to the uncertainty output (labeled "dao").

Figure 5.10 shows the structured singular value plot for the departure metric. The solid line in Figure 5.10 is the structured singular value obtained using the Frobenius norm scaling technique while the dashed line shows that structured singular value approximation for real parameter variations. Because the perturbations in L_v and N_v are real, the value of the departure susceptibility metric is defined from the peak in the dashed line and is $DP = 1.1$ at 1.2 rad/s. As a result, the stability derivatives L_v and N_v can be perturbed by approximately 91% before an instability will occur.

As a comparison, the departure metric computations were repeated for the open-loop aircraft system. The open-loop computations were made by simply opening the control system loop in Figure 5.9(a) and repeating the structured singular value computation. The associated structured singular value plot is as shown in Figure 5.11. The dashed line is the real approximation of the structured singular value while the solid line is the complex, Frobenius norm approximation, given for reference. From this figure, we note that DP is at

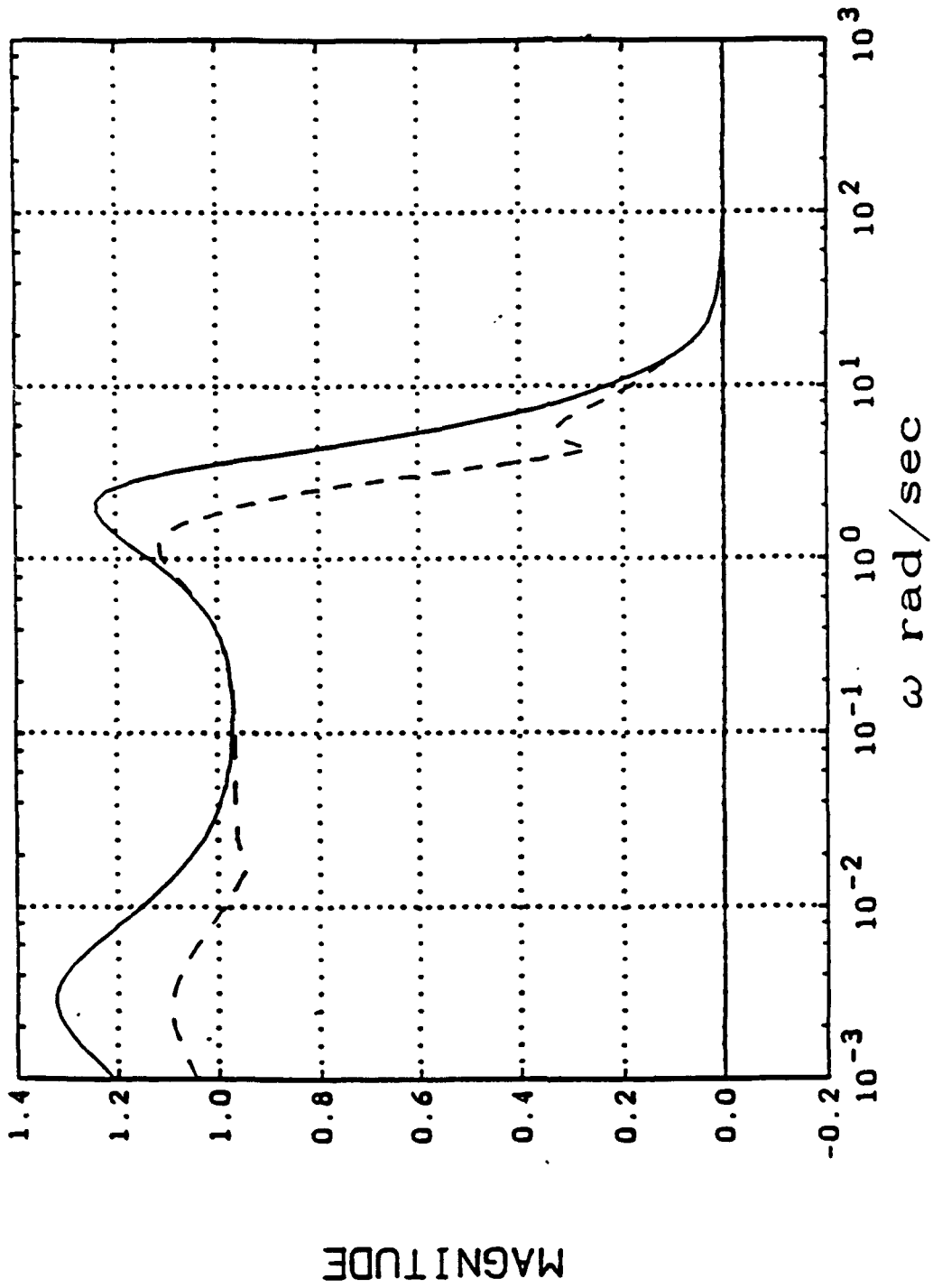


Figure 5.10 Closed-Loop Departure Parameter Structured Singular Values

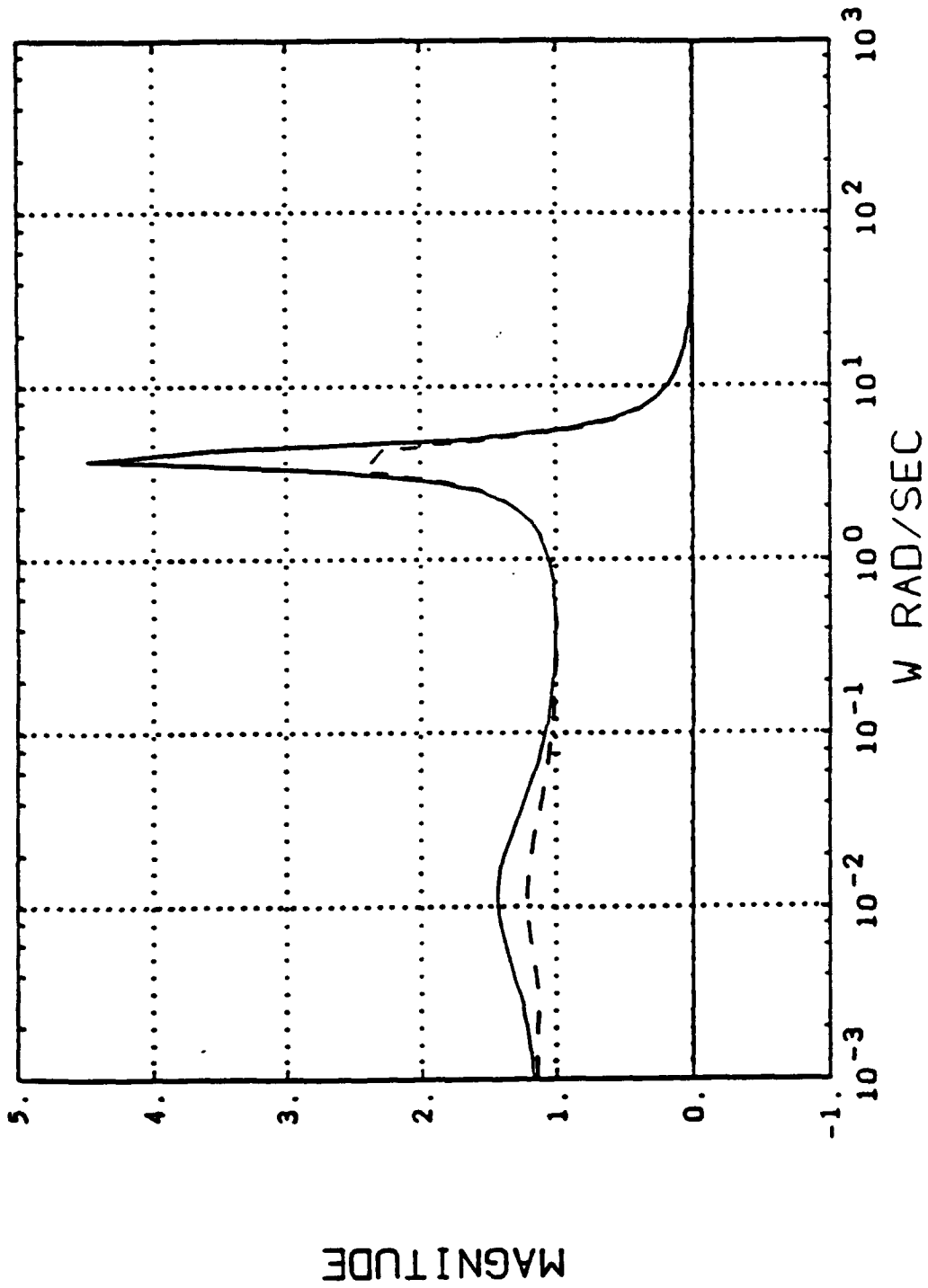


Figure 5.11 Open-Loop Departure Parameter Structured Singular Values

least 2.5 at 4.0 rad/s. Consequently, the open-loop airframe can tolerate only a 40% variation in L_v and N_v before instability occurs. These results indicate that the control system has decreased the sensitivity of the aircraft to uncertainty in L_v and N_v and, therefore, improved the departure characteristics as measured by the new departure susceptibility metric.

While the departure metric is relatable to the amount of uncertainty tolerable in the derivatives L_v and N_v , its most important value will be to assess the aircraft departure susceptibility throughout its flight envelope. The trim angle-of-attack for the flight condition considered in this report is approximately 2 degrees; hardly a "high" angle-of-attack flight condition where departure susceptibility measurement is most important. Departure susceptibility should be measured throughout the angle-of-attack operating limits and anticipated sideslip angles. The departure susceptibility metric could also be computed using linear models obtained by trimming at nonzero angular rates as well.

5.3. Nominal Performance Measures

The nominal performance measures are based on interpretations of the current military flying qualities specifications. These measures are multivariable generalizations of existing single-axis criteria. They will also be used to test robust performance (in Section 5.4) wherein the closed-loop system is perturbed using the standard uncertainty gain and phase variations.

5.3.1. Effective Order

The effective order of the longitudinal response of the F-16 aircraft was determined by computing the Hankel singular values of the pitch rate (deg/s) and vertical acceleration (g's) responses to longitudinal stick force (lb) input. Before computing the Hankel singular values, however, the 15

modes associated with the eigenvalues which were classified as longitudinal (from the mode classification study in Section 5.1.1) were extracted from the complete closed-loop model. The extraction was performed by transforming the complete closed-loop model into real, modal form and truncating all modes which were not classified as longitudinal.

One of the 15 longitudinal modes was previously shown to be unstable. This mode was also extracted from the closed-loop model because the Hankel singular values are not defined for an unstable system. (The unstable mode will be factored back into the model for equivalent system analysis in the next section).

For the longitudinal response, the five largest Hankel singular values are: 0.032, 0.018, 0.0078, 0.0029, and 0.0015. Counting the factored unstable mode as one state, an effective fourth-order response would be obtained if the third Hankel singular value was much larger than the fourth. In this case, the third Hankel singular value is 2.7 times the fourth. Bacon and Schmidt have considered a factor greater than 5.0 as a good relative indicator of effective order. [14]

The aircraft roll rate (rad/s) and sideslip (deg) response to lateral stick force (lb) and directional pedal force (lb) inputs were considered for the lateral-directional response effective order. After extracting the 21 lateral-directional states, the largest six Hankel singular values were: 0.42, 0.092, 0.041, 0.038, 0.014, and 0.010. The ratio of the fourth to the fifth Hankel singular value is 2.7. The value of 2.7 is still less than the recommended value of 5.0, but is much greater than unity.

5.3.2. *Equivalent System Error*

A third-order longitudinal equivalent system model was obtained using the balanced model reduction algorithm on the 14 state (15 state model without the unstable mode)

longitudinal model described in the preceding section. After the balanced model reduction, the unstable mode was factored back into the model so that a fourth-order equivalent system model was obtained. The transfer functions describing this fourth order model are given in Table 5.1. No attempt was made at this time to model the equivalent time delay found in the standard equivalent system representations shown in Tables 4.4 and 4.5.

A frequency response comparison of the low order equivalent system model and the complete (53 state) closed-loop model is shown in Figure 5.12. The dashed lines in Figure 5.12 depicted the response of the low-order equivalent system while the solid lines are the full-order system response.

The equivalent system error was then computed using the relation derived in Section 4.3.2. and repeated here,

$$\frac{\bar{\sigma}[G_{HOS}(j\omega) - G_{LOS}(j\omega)]}{\bar{\sigma}[G_{LOS}(j\omega)]} \leq e(\omega)$$

The left side of the above expression is shown as the solid line, while $e(\omega)$ on the right side is shown as the dashed line in Figure 5.13. Figure 5.13 shows that the equivalent system error stays below the recommended specification for all frequencies considered except a small range from about 30 to 90 rad/s. The error specification violation at high frequency is not considered serious and would probably not occur if an equivalent time delay was included in the analysis.

Note that effective order and equivalent system calculations can vary with different choices of input and output response units. The response units which seemed to minimize the error apparent in Figure 5.13 were selected for the effective order and equivalent system error studies. The

Table 5.1 Nominal Equivalent System Transfer Functions

Longitudinal

$$\frac{q(\text{deg/s})}{F_{lon}(\text{lb})} = \frac{-0.053 (s-0.005) (s + 0.63) (s-67.9)}{(s - 0.02) (s + 2.48) (s^2 + 2(.57)(8.73)s + 8.73^2)}$$

$$\frac{n_z(g's)}{F_{lon}(\text{lb})} = \frac{-0.0085 (s - 0.011) (s^2 + 2(.26)(13.51)s + 13.51^2)}{\Delta}$$

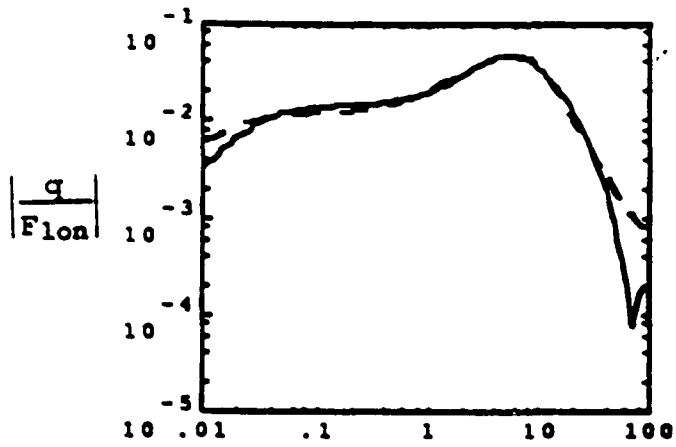
Lateral-Directional

$$\frac{p(\text{rad/s})}{F_{lat}(\text{lb})} = \frac{0.10 (s - 0.0017) (s^2 + 2(.68)(3.39)s + 3.39^2)}{(s + 0.0036) (s + 1.31) (s^2 + 2(.46)(3.66)s + 3.66^2)}$$

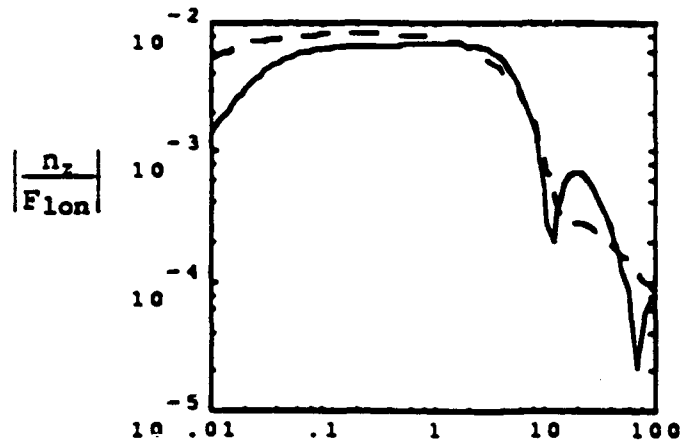
$$\frac{\beta(\text{deg})}{F_{lat}(\text{lb})} = \frac{-0.051 (s + 0.19) (s + 0.45) (s - 12.34)}{\Delta}$$

$$\frac{p(\text{rad/s})}{F_{ped}(\text{lb})} = \frac{0.021(s + 0.0024) (s - 3.12) (s - 5.26)}{\Delta}$$

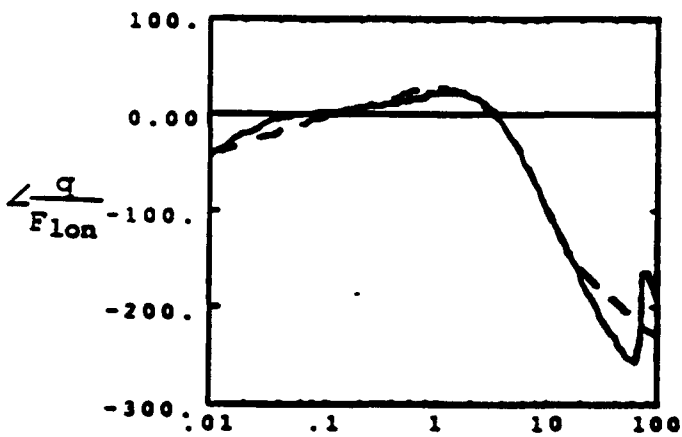
$$\frac{\beta(\text{deg})}{F_{ped}(\text{lb})} = \frac{0.066 (s + 0.0017) (s + 1.66) (s - 17.01)}{\Delta}$$



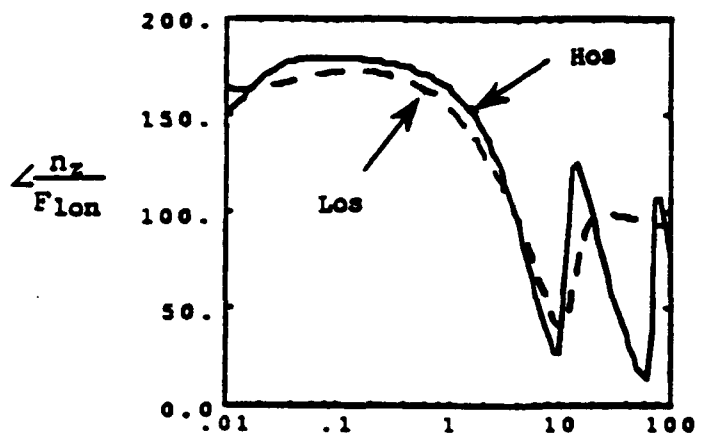
ω



ω



ω



ω

Figure 5.12 Nominal Longitudinal Equivalent System Comparison

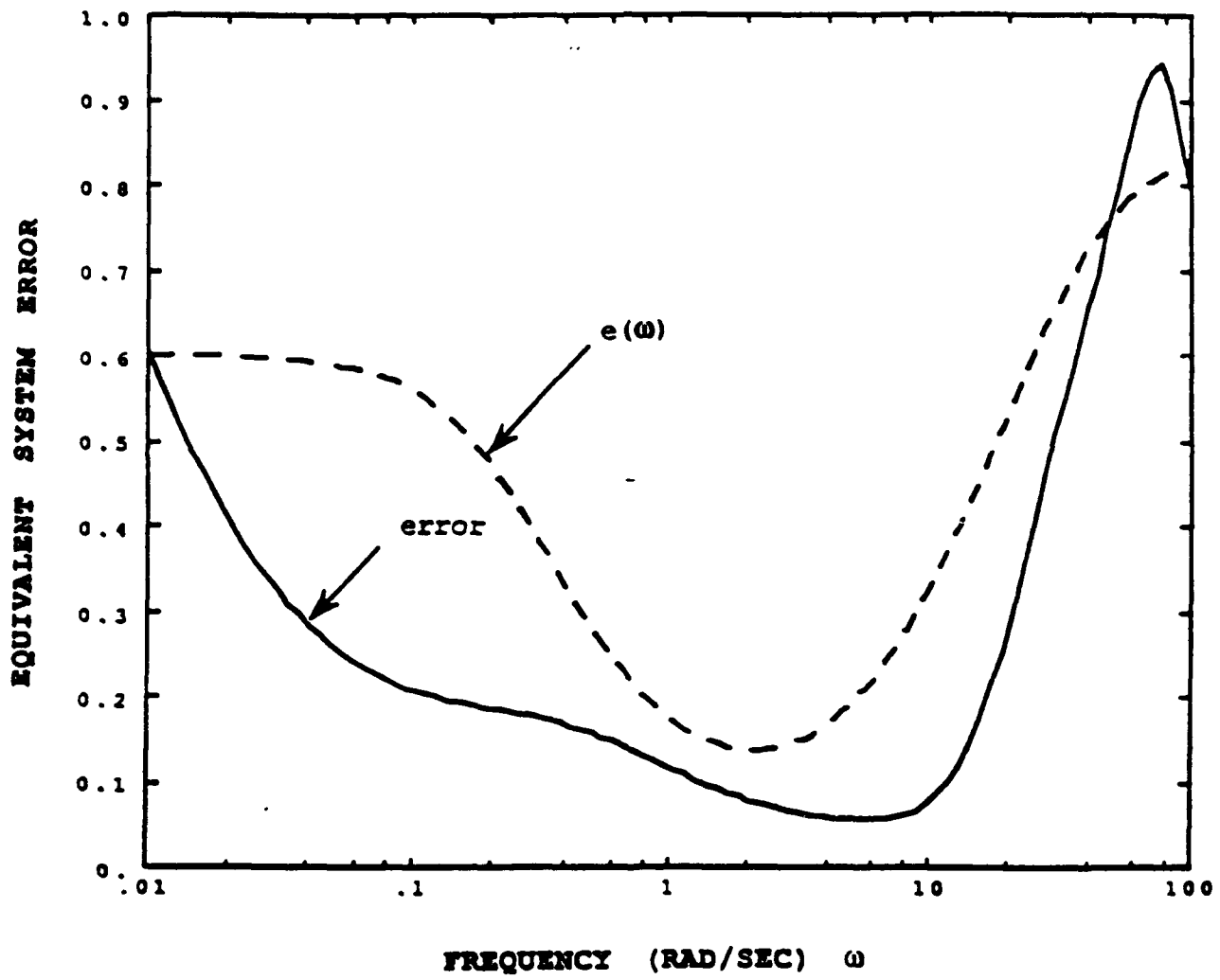


Figure 5.13 Nominal Longitudinal Equivalent System Error

response units selected were pitch rate (deg/s) and vertical acceleration (g's) to longitudinal stick force (lb) input.

A fourth-order lateral-directional equivalent system model was obtained via balanced model reduction of the 21 lateral-directional axis states. The input and output units were selected to minimize the equivalent system error. The units of aircraft roll rate (rad/s) and sideslip (deg) response to lateral stick force (lb) and directional pedal force (lb) inputs were selected. Note that roll rate was matched instead of the usual roll attitude signal (see Table 2.1) because the equivalent roll mode time constant seemed to be matched better. The resulting transfer functions for the lateral-directional equivalent system model are shown in Table 5.1. A frequency response comparison is made in Figure 5.14.

The equivalent system error is computed for the lateral-directional equivalent system model in Figure 5.15. The recommended error specification is violated at frequencies greater than about 0.5 rad/s with significant deviation occurring from about 6 to 40 rad/s. The peak in the error response curve is most likely due to the relatively large difference in this frequency range from the low-order and full-order lateral stick force to roll rate transfer function. Figure 5.14 shows that the full order lateral stick to roll rate response appears to be at least second order as opposed to the approximate first-order form obtained from the equivalent system match. It is probably not possible to reduce the response error without increasing the order of the equivalent system model or sacrificing the matching fidelity of the other responses.

5.3.3. Turbulence Response

The aircraft response to turbulence in the vertical and side velocity directions was determined by computing the 2-norm of the full-order closed-loop system. The output responses of interest are n_{zp} (g's) and n_{yp} (g's). The input

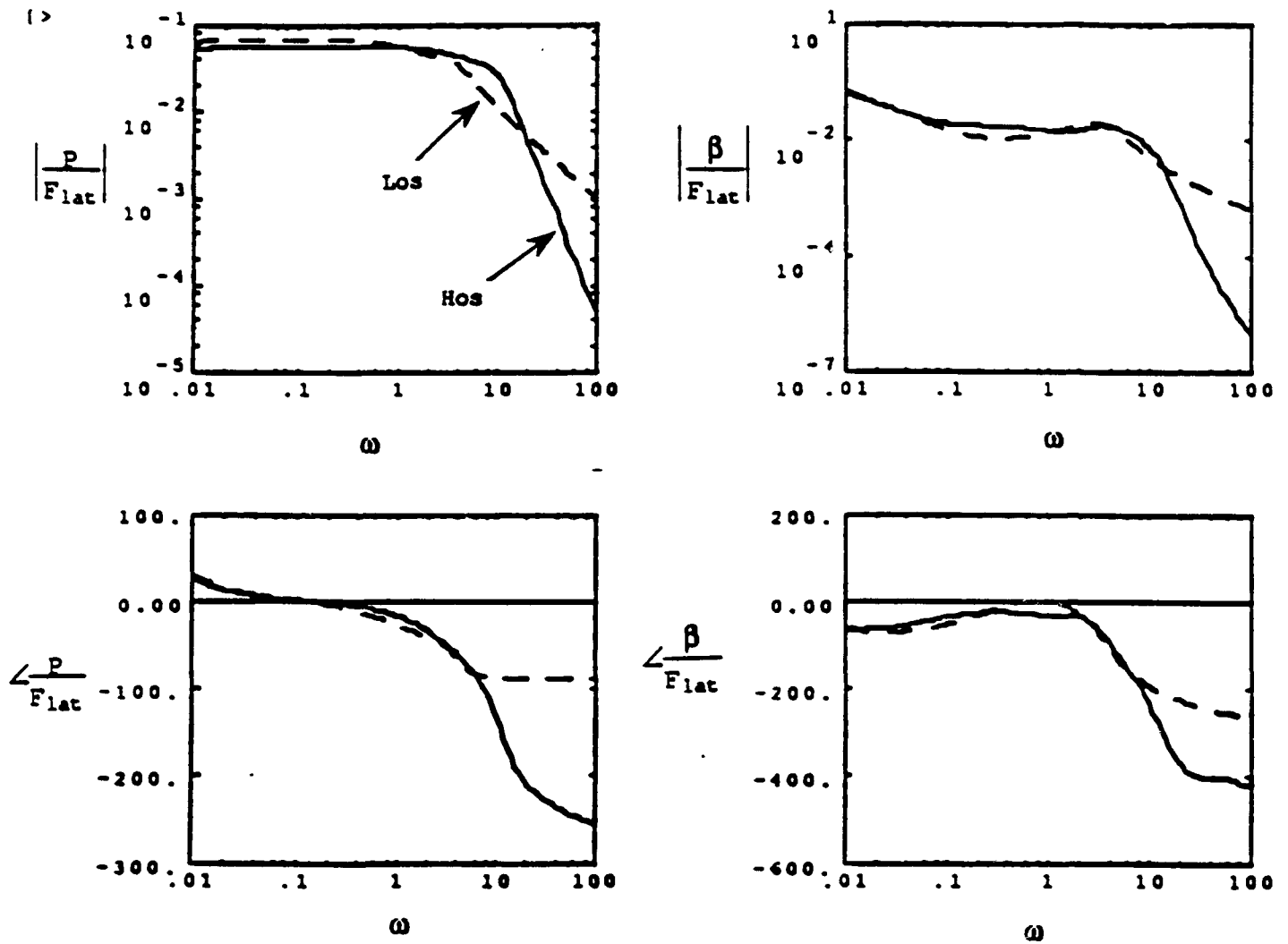


Figure 5.14 Nominal Lateral-Directional Equivalent System Comparison

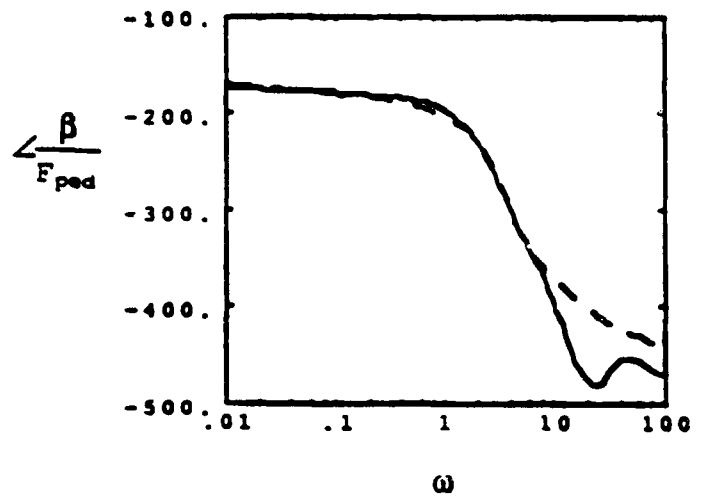
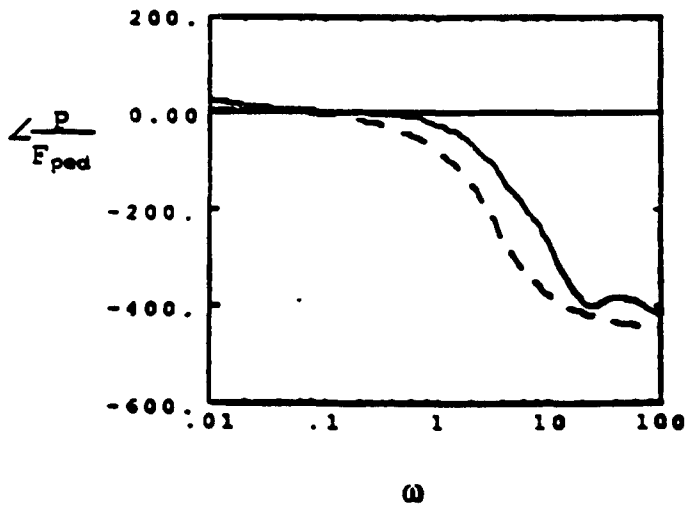
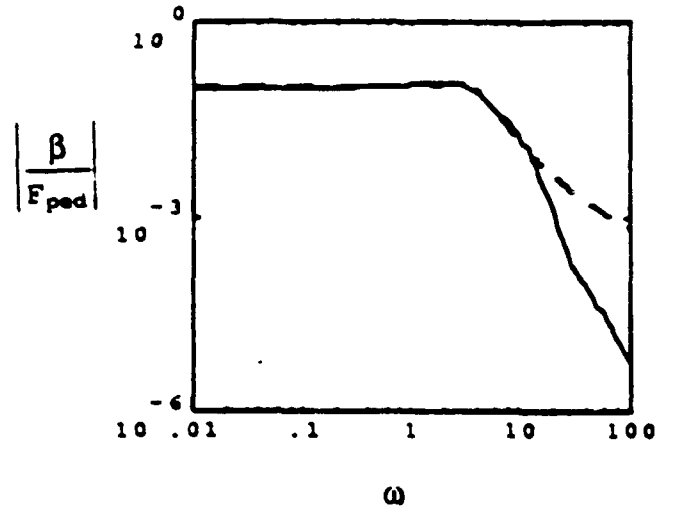
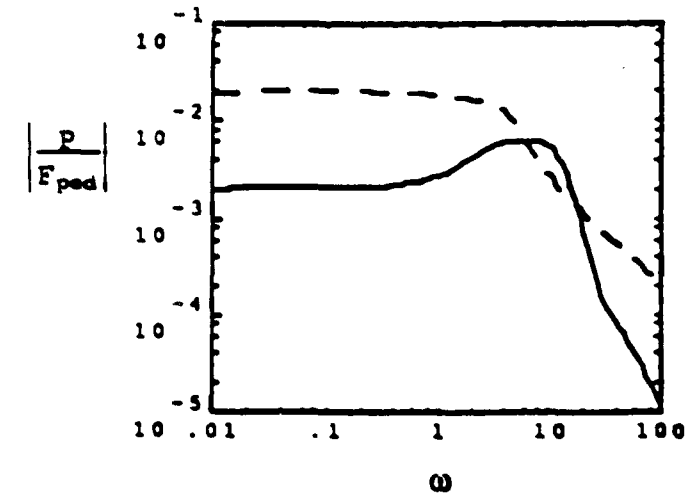


Figure 5.14 (con't)

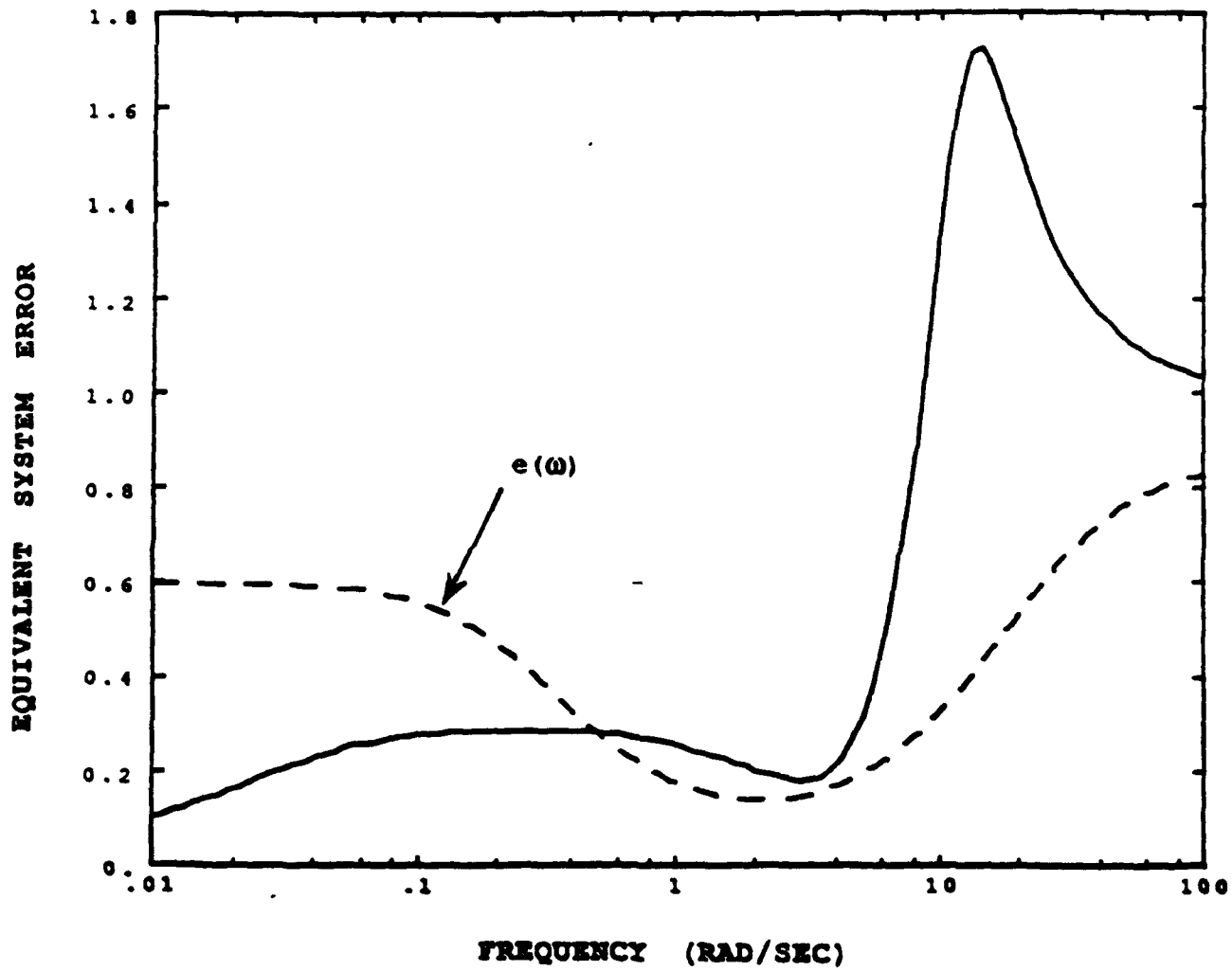


Figure 5.15 Nominal Lateral-Directional Equivalent System Error

consists of vertical velocity w_g (ft/sec) and side velocity v_g (ft/sec) turbulence. The Dryden turbulence model was used.

Because the closed-loop system is nominally unstable, the usual 2-norm is not defined. However, some indication of the turbulence response can be obtained by computing the 2-norm over a selected range of frequencies. The 2-norm for the F-16 model was computed from 0.1 to 1000 rad/sec using a simple trapezoidal integration approximation. The resulting 2-norm value was 0.023 (g's/ft/s). This value is greater than the expected value of 0.02. However, the expected value does not take into account contributions of the cross-axis components (lateral velocity turbulence influence on vertical acceleration, for example), which is included in the 2-norm calculation.

5.3.4. Response Decoupling

Aircraft response decoupling in a roll was measured by computing the maximum singular value of the transfer function from lateral stick force input (lb) to the cross-axis variables of interest: pitch rate (rad/sec), yaw rate (rad/sec), and side acceleration (g's). Before computing the matrix singular values, the airframe state equations are modified to reflect a body-axis roll rate of 128 deg/sec. The roll rate of 128 deg/sec was chosen from the MIL-STD-1797 requirements for roll control effectiveness wherein a Class IV, Category A, Flight Phase CO aircraft should be able to roll 360° in 2.8 seconds.

Figure 5.16 shows the maximum transfer function matrix singular values plotted for frequencies from 0.01 to 1000 rad/s. The singular value are shown to be large at low frequencies before peaking again near 10 rad/s. The second peak is near the bandwidth of the system and therefore defines the region of interest. The maximum value of the high frequency peak is 0.020 at a frequency of 9.5 rad/s. Unfortunately, there is no existing standard for comparison.

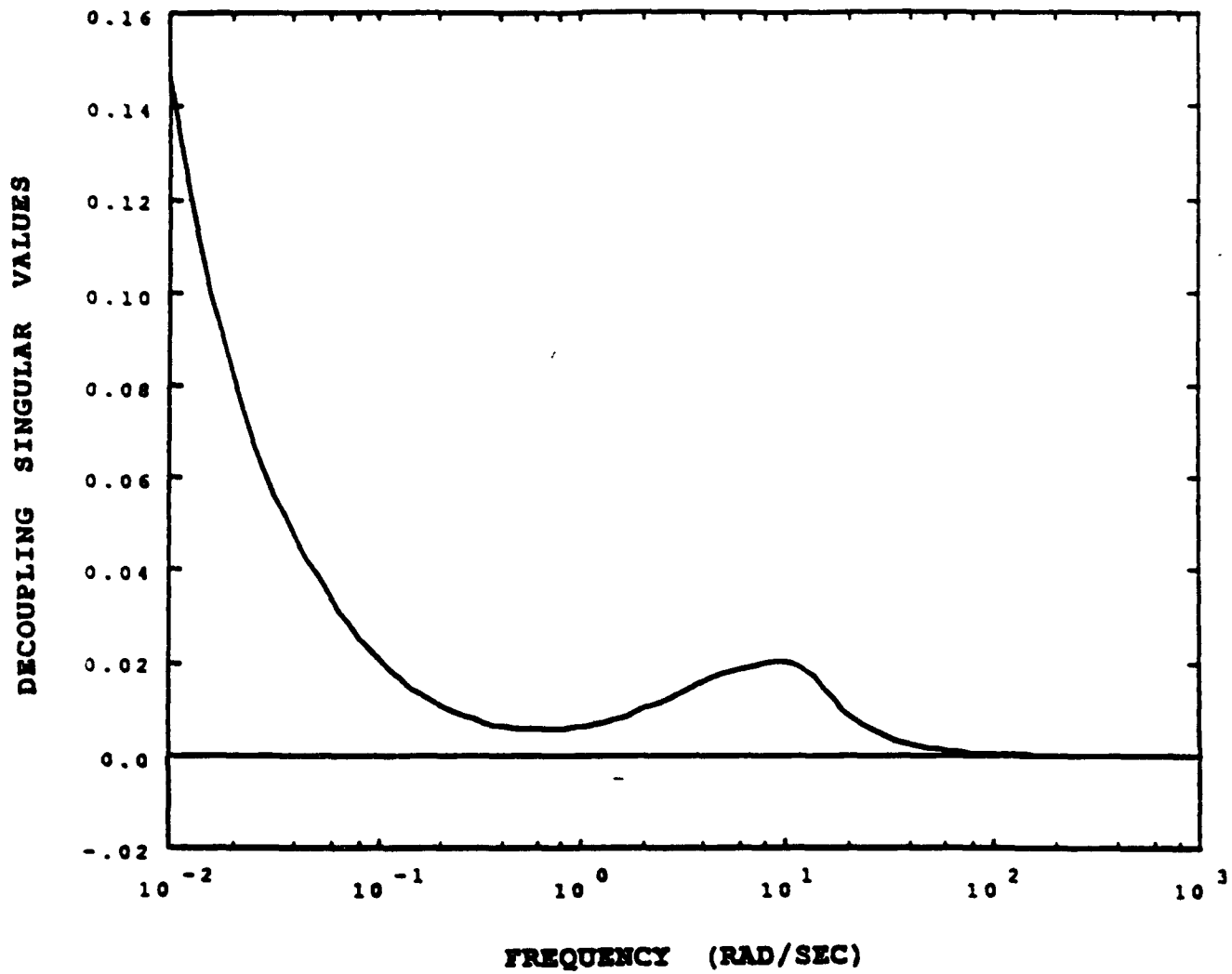


Figure 5.16. Nominal Response Decoupling

5.4. Robust Performance Measures

The robust performance measures are tested by perturbing the aircraft system dynamics and retesting the nominal performance measures established in the previous section. The standard uncertainty set, as defined in Section 4.4.1, consists of a gain and a phase uncertainty description.

For the gain uncertainty, the feedback gains are perturbed in the "worst case" direction, which is established using a real, structured singular value calculation. For this study, perturbations in the sensor output feedback signals are considered, although a similar study can be completed using the actuator input signals. Figure 5.17 shows the approximate structured singular value for real perturbations. The block diagram used to generate this curve is shown in Figure 5.5. The peak of the structured singular value curve occurs at the system bandwidth of 5.3 rad/s. At this frequency point, the permutation matrix which defines the worst case gain variations is $\Phi = \text{diag}(1, -1, 1, 1, 1, 1)$. The six feedback signals are (in order): roll rate (rad/s), pitch rate (rad/s), yaw rate (rad/s), angle-of-attack (rad), vertical acceleration (ft/s²), and side acceleration (ft/s²). The signs of the permutation matrix elements define the direction of the worst case uncertainty. A +1 indicates gain increase while a -1 indicates a gain decrease. As a result, the worst case gain uncertainty involves an increase in gain for all of the feedback signals except the pitch rate feedback gain, which should be reduced. Assuming a gain perturbation magnitude of ± 1.5 dB, the pitch rate feedback signal should be reduced by 0.84 while all other signals increased by a factor of 1.19.

Once the gain uncertainty set has been defined, the nominal aircraft dynamics are perturbed and the nominal performance measures are re-evaluated. For the F-16 model, however, very little performance degradation was noted in any of the performance measures. The multi-loop gain margin of \pm

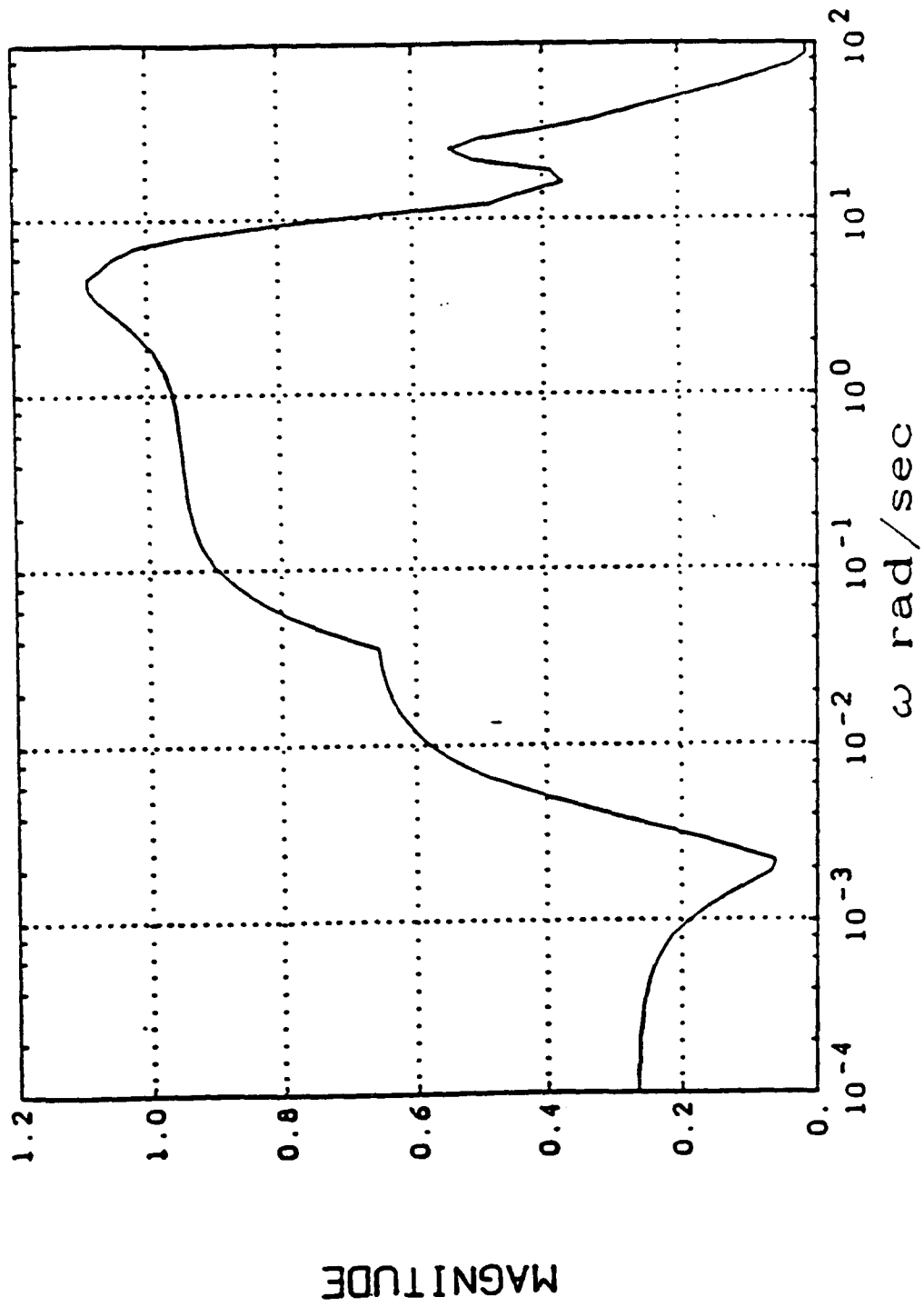


Figure 5.17 Worse case Output Structured Singular Values

9.6 dB computed for F-16 model provides evidence that the model will not be sensitive to gain variations. One might consider increasing the magnitude of the gain uncertainty; but it is expected that the multi-loop gain margin specification should be around ± 4.5 dB and robust performance measures based on a gain perturbation of greater than ± 1.5 dB may be too difficult to achieve. Therefore, data concerning the robust performance measures for gain variations of the F-16 model will not be presented.

The standard phase uncertainty set is defined in Section 4.4.1 as an equivalent first-order Pade' approximation of a pure time delay. The time delay is to be chosen using the following relation,

$$\tau = \frac{10\pi}{180\omega_{BW}} \quad (5.7)$$

With the system bandwidth previously found as $\omega_{BW} = 5.3$ rad/s, the computed time delay is $\tau = 0.033$ seconds. The remainder of this section presents the results of the robust performance measures for the standard phase uncertainty.

5.4.1. Robustness of Effective Order

The effective order of the phase perturbed system was computed in the same manner as in the nominal performance measure except that the Pade' time delay approximation has been included in the closed-loop F-16 aircraft model. In the longitudinal axis, the unstable root at +0.02 remains and the largest five Hankel singular values (without the unstable mode) are: 0.038, 0.022, 0.013, 0.0047, and 0.0029. The ratio of the third to the fourth Hankel singular value is 2.7, which was the same as the nominal case. Therefore, no degradation in effective order is noted in the longitudinal axis.

For the lateral-directional system, the six largest Hankel singular values were computed as: 0.63, 0.15, 0.081,

0.047, 0.020, and 0.013. The ratio of the fourth to the fifth Hankel singular value is 2.3. Recall that the nominal value was computed as 2.7. Thus, a small amount of degradation in effective order is caused by phase perturbation in the feedback loops.

5.4.2. Robustness of Equivalent System Error

A fourth-order longitudinal equivalent system was computed for the phase perturbed F-16 model. The transfer functions for the equivalent model are shown in Table 5.2 while a frequency response comparison of the full-order (which now has 59 states) and the fourth order equivalent model (dashed line) is shown in Figure 5.18.

The longitudinal equivalent system error is plotted in Figure 5.19 for the phase perturbed system. In comparison with the nominal equivalent system error, shown in Figure 5.13, one should see that the perturbed system error is larger at nearly all frequencies. However, the perturbed system error has nearly the same characteristics wherein it remains relatively small in the frequency range of 1 to 10 rad/s and relatively large outside of this range. In summary, it appears that the effective order of the perturbed system has not been degraded, but the relative error is certainly larger.

The lateral-directional equivalent system representation of the phase perturbed system is shown in transfer function form in Table 5.2 and the frequency response comparison is shown in Figure 5.20. The equivalent system error is plotted in Figure 5.21. In comparison with the nominal lateral-directional equivalent system error shown in Figure 5.15, we note that the perturbed error is much larger at all frequencies tested but, more importantly, the error is no longer relatively small in the 1 to 10 rad/s range. The increase in mid-frequency error may be a result of the degraded effective order noted in the previous section.

Table 5.2 Phase Perturbed Equivalent System Transfer Functions

Longitudinal

$$\frac{q(\text{deg/s})}{F_{lon}(\text{lb})} = \frac{-0.086(s + 0.0074)(s + 0.18)(s - 50.44)}{(s - 0.020)(s + 1.07)(s^2 + 2(.37)(10.81)s + 10.81^2)}$$

$$\frac{n_z(g)}{F_{lon}(\text{lb})} = \frac{-0.0077(s - 0.013)(s^2 + 2(.47)(13.64)s + 13.64^2)}{\Delta}$$

Lateral-Directional

$$\frac{p(\text{rad/s})}{F_{lat}(\text{lb})} = \frac{0.081(s - 0.0012)(s + 2.088)(s + 5.27)}{(s + 0.0042)(s + 1.02)(s^2 + 2(.40)(3.84)s + 3.84^2)}$$

$$\frac{\beta(\text{deg})}{F_{lat}(\text{lb})} = \frac{0.086(s + 0.060)(s - 1.86)(s - 8.77)}{\Delta}$$

$$\frac{p(\text{rad/s})}{F_{ped}(\text{lb})} = \frac{-0.077(s + 0.011)(s^2 - 2(.94)(1.10)s + 1.10^2)}{\Delta}$$

$$\frac{\beta(\text{deg})}{F_{ped}(\text{lb})} = \frac{0.050(s + 0.00078)(s + 2.77)(s - 22.59)}{\Delta}$$

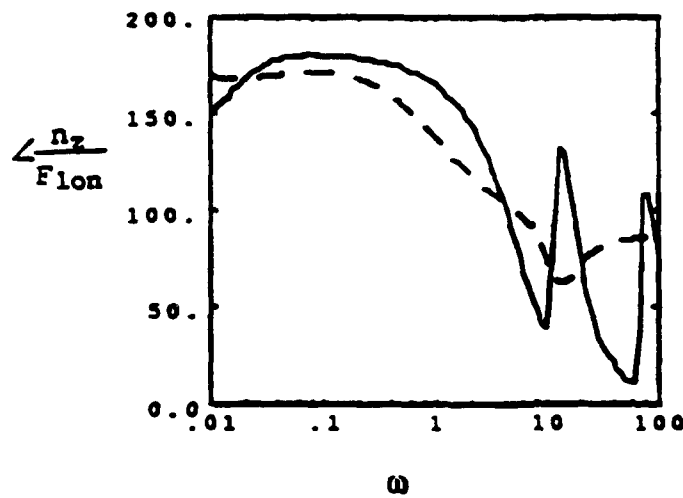
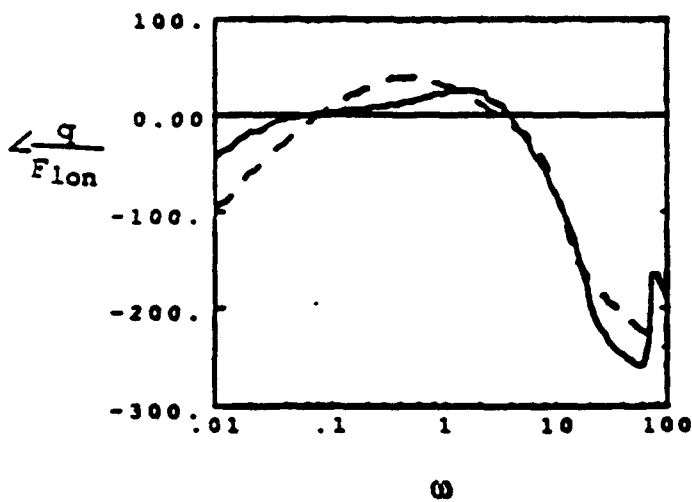
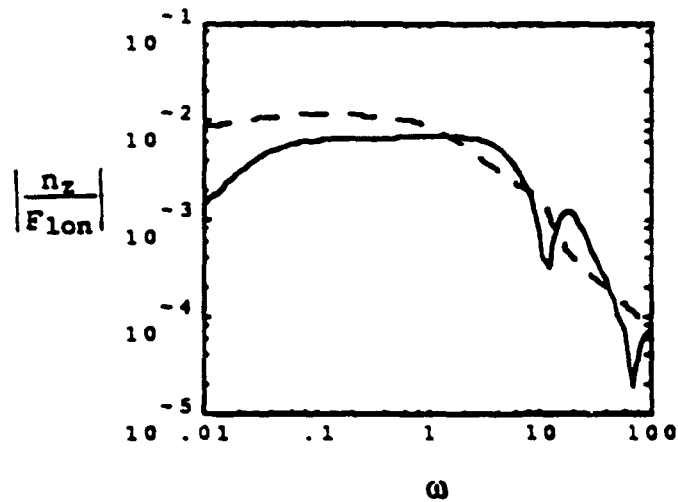
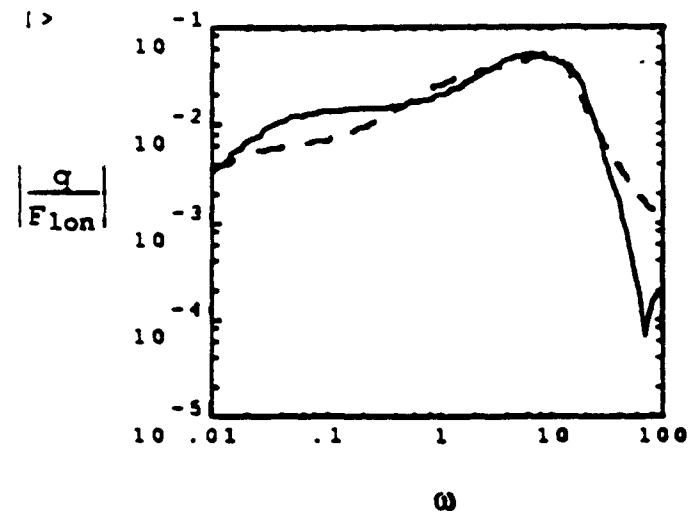


Figure 5.18 Phase Perturbed Longitudinal Equivalent System Comparison

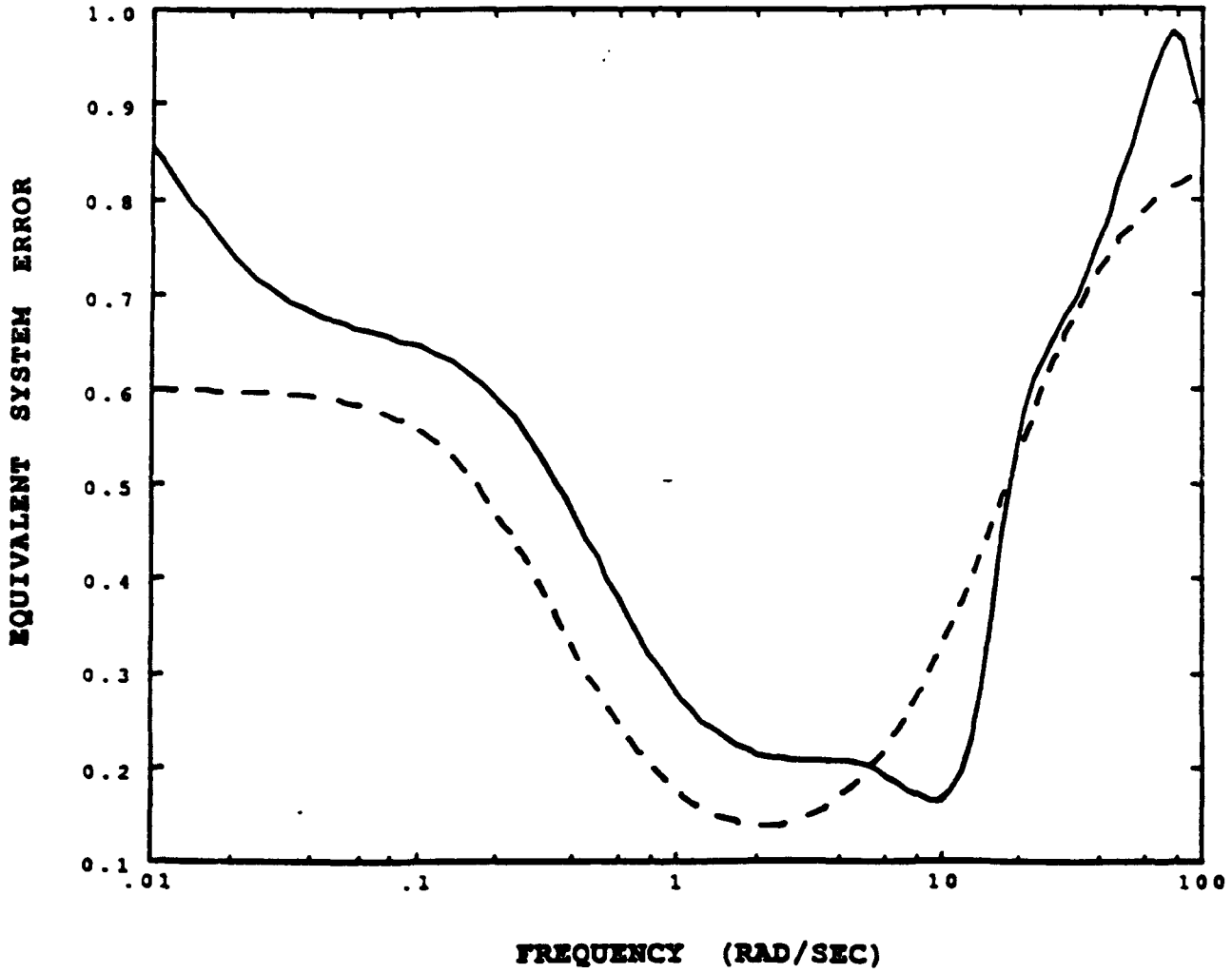


Figure 5.19 Phase Perturbed Longitudinal Equivalent System Error

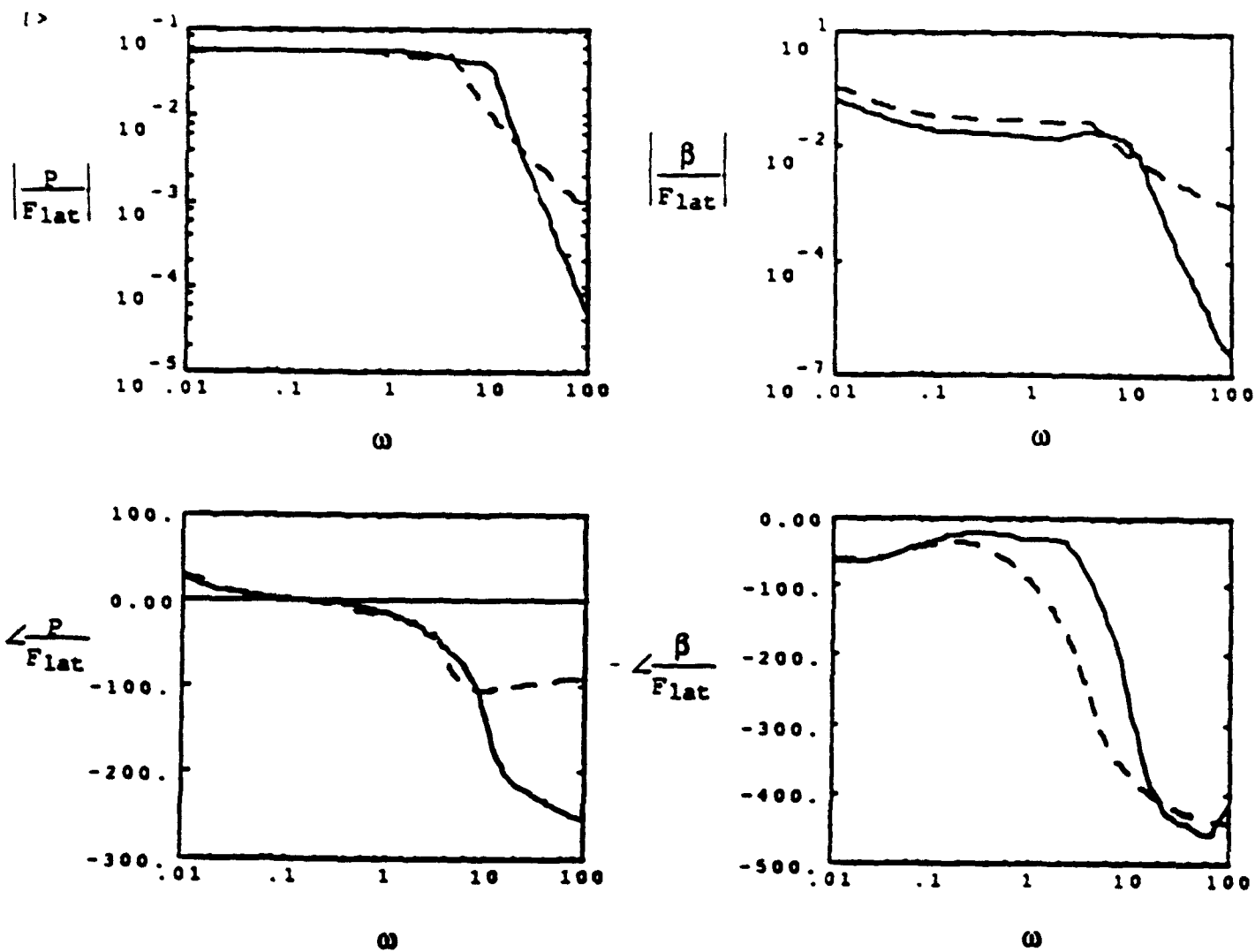


Figure 5.20 Phase Perturbed Lateral-Directional Equivalent System Comparison

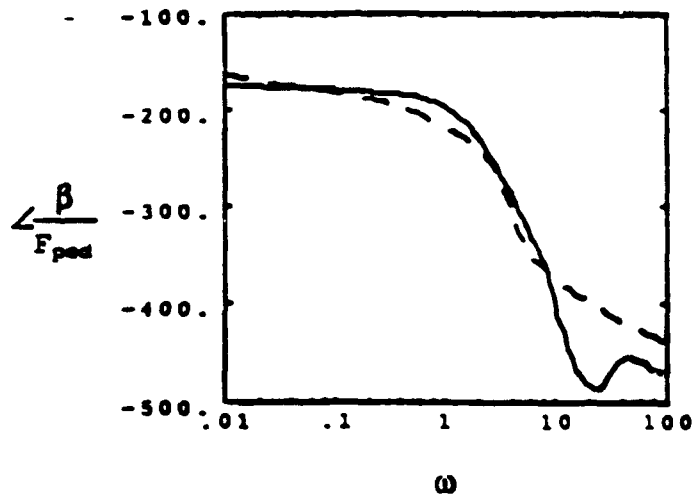
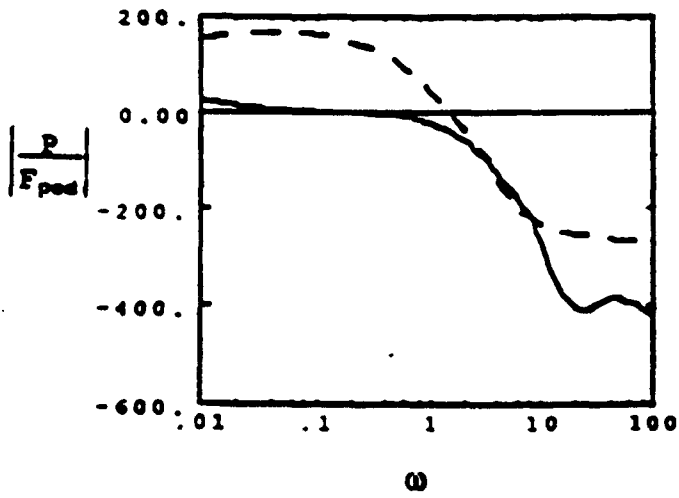
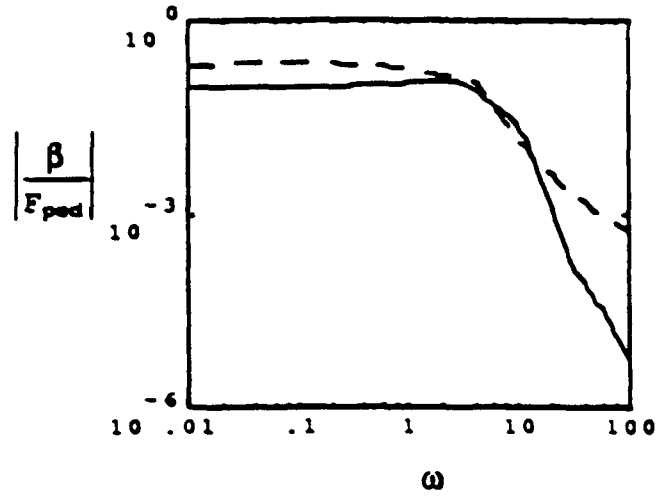
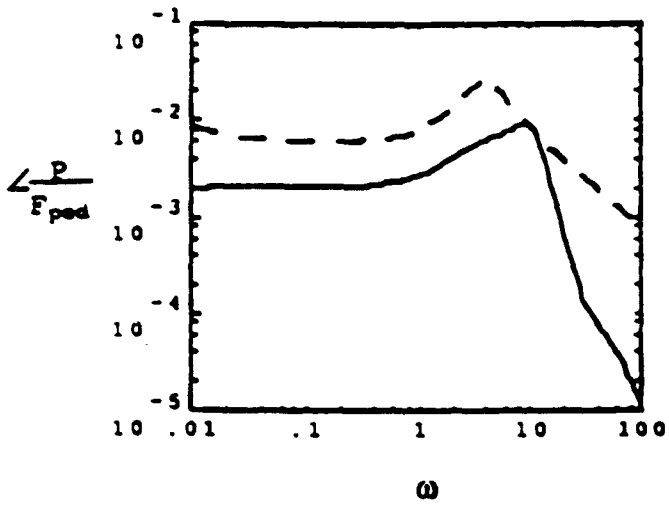


Figure 5.20 (con't)

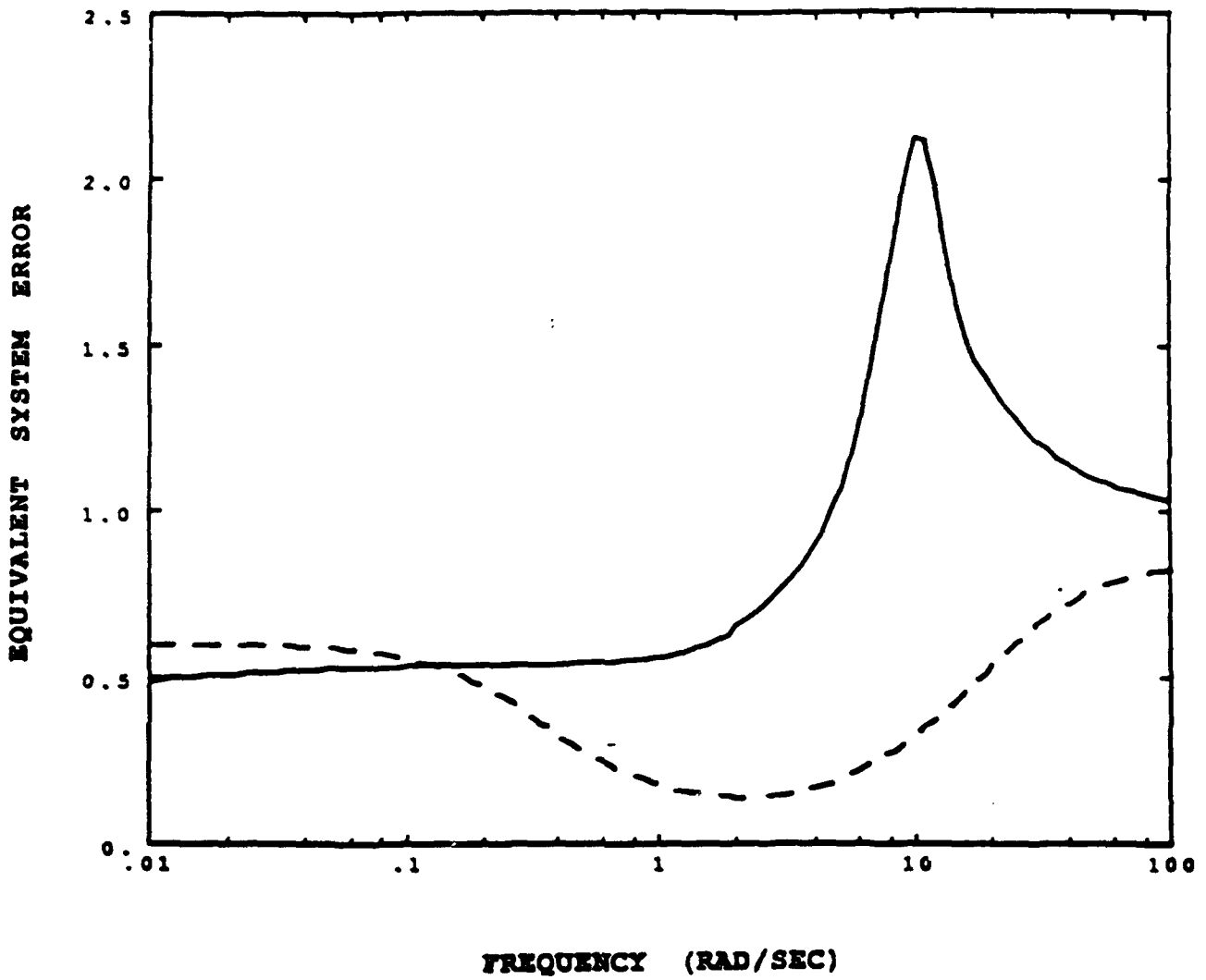


Figure 5.21 Phase Perturbed Lateral-Directional Equivalent System Error

It would appear that the robust performance measure of merit for equivalent system error should be posed as some multiple of the expected nominal measure, represented by $e(\omega)$. From the longitudinal axis results, it would seem appropriate to multiply the nominal measure by about a factor of 2.0 to define the robust performance measure. However, the lateral-directional axis equivalent system error would violate this robust performance measure.

5.4.3. Turbulence Response Robustness

The turbulence response robustness measure was computed in the identical manner as the nominal case except the phase perturbed F-16 model was used. The resulting 2-norm value was 0.023, which is the same as the nominal value.

5.4.4. Response Decoupling Robustness

A plot of the response decoupling metric is shown in Figure 5.22 for the F-16 phase perturbed model. The metric was computed in the same manner as in the nominal case, except that the phase perturbed-aircraft model was utilized. The figure reveals the same shape and characteristics as the nominal case, shown in Figure 5.16. The magnitude of the high-frequency peak has increased from a nominal value of $\nu = 0.020$ at 9.5 rad/s to a value of $\nu = 0.027$ at 9.5 rad/s for the phase perturbed model. The introduction of phase uncertainty has therefore lead to an apparent increase in aircraft roll coupling.

12

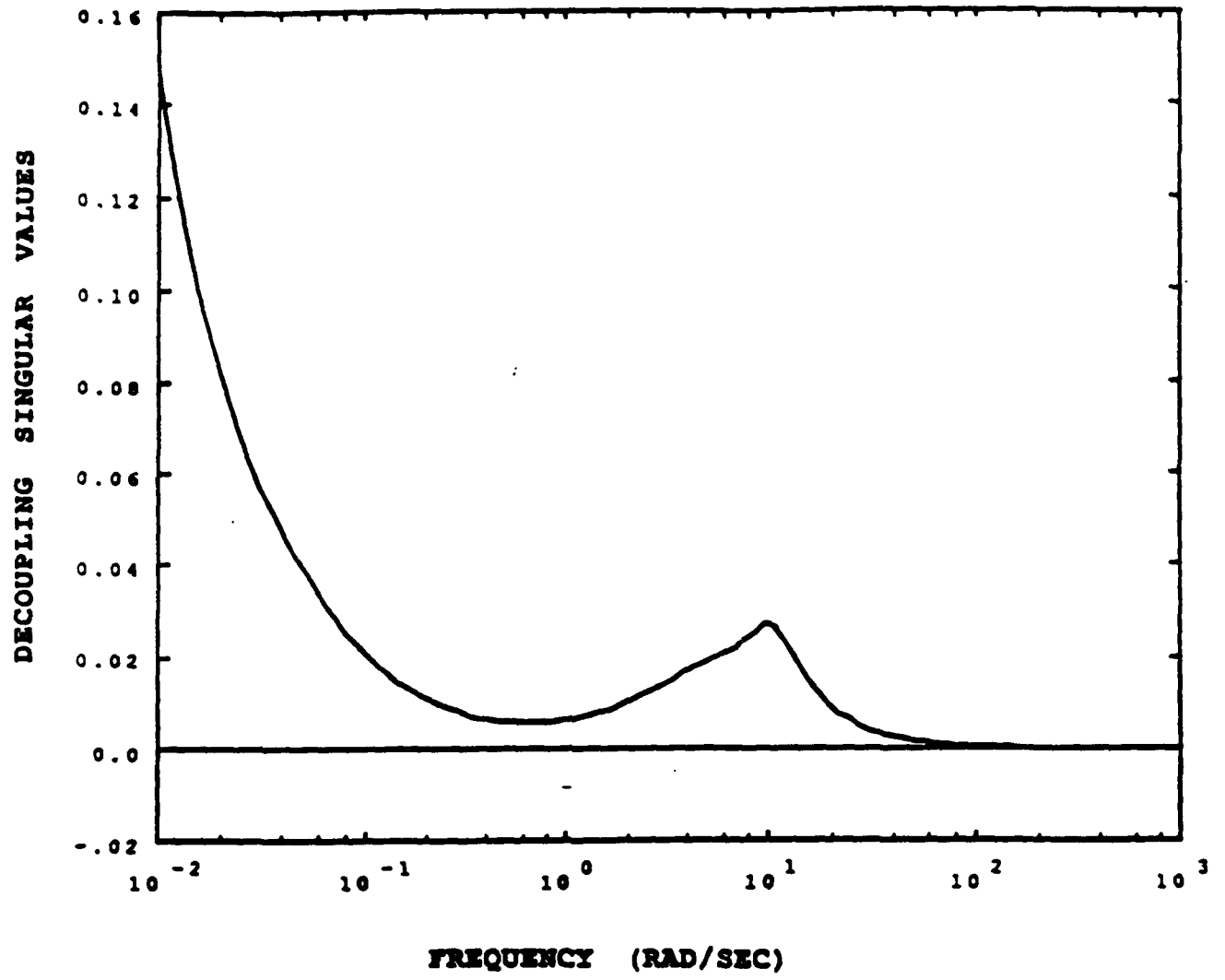


Figure 5.22 Phase Perturbed Response Decoupling

6. Conclusions

Eight new measures of merit, specifically designed to evaluate multivariable flight control systems, were proposed, developed, and tested in this report. These new measures represent an innovative application of recently developed multivariable control system evaluation techniques to the problem of adequate acceptance testing for complicated, multi-loop flight control systems.

This report provided a theoretical development of the measures of merit based on "modern" multivariable control analysis methods. The analysis techniques used to form the new criteria draw from recent control theory research in Hankel singular values, matrix singular values, and the so-called "structured" singular values. These methods were used to develop new measures of merit for: mode classification and nominal stability, multi-loop stability margins, open-loop bandwidth, departure susceptibility, effective response order, equivalent system error, turbulence response, and response decoupling.

The scientific and technical feasibility of the proposed new measures was demonstrated by application of the measures to a high fidelity linear model of the F-16 aircraft. The F-16 aircraft model was chosen to represent a high performance aircraft which is actually in production. Therefore, the linear model used in this evaluation cannot be viewed as a simple "academic" demonstration but as a realistic test which would likely be used in a commercial application. The results of this investigation, although limited in scope, provide an indication of the usefulness, computational methods, and numerical values expected from the new measures. It is hoped that this research will provide the foundation for a standardized form for multivariable flight control system evaluation results such that the performance of different designs and aircraft can be compared directly.

7. Recommendations for Phase II

Based on the Phase I results reported herein, the potential of a Phase II continuance to yield a product of importance to the government and application in industry is excellent. The F-16 results obtained in this research represent the initial formation of a "data base" of measure of merit results. The data base results can ultimately be used by the Air Force as a justification for flight control and flying qualities performance specifications for future multivariable aircraft flight control systems. The data base results could also potentially become a resource for airframe manufacturers and flight control design contractors for in-house evaluation of preliminary flight control designs.

To succeed with commercial application of this research (Phase III), there are three objectives that must be met in Phase II development. The first is to expand the applicability of the data base results in order instill confidence and broaden industry acceptance of the evaluation procedures. The data base requirements can be accomplished by continued testing of the measures in expanded regions of the F-16 aircraft flight envelope, nonlinear validation of the results using F-16 model simulations, and a comparison of results with a second aircraft.

The second objective is to prepare for a transfer of technology to the Air Force and commercial firms. Primarily, the transfer of technology must provide a method through which companies can compare their own designs to those represented in the data base. This need can be accomplished by providing a specialized software product which will simplify the computations required for the new measures of merit. In addition, the data base results which are determined during the data base expansion will be made available to commercial firms either in report or magnetic media form.

The third objective is to continue development of the measures defined in Phase I and to propose additional measures. After careful review of this report, Air Force personnel have identified a number of refinements to the currently studied measures of merit which promise to improve the usefulness of the measure results. Specifically, it has been noted that the effective order measure proposed in Phase I should be restated such that the ratios of several sequential Hankel singular values are computed. This new definition would measure an effective order of less than four, but would also insure that the true effective order is no larger than that predicted by the greatest computed ratio. Also, it has been suggested that a weighting filter should be added to the turbulence response measure definition so that the natural resonance of the human body is incorporated in the measure. Refinements to the current measures will compliment the continued theoretical research to develop additional measures, especially in the area of analytical performance robustness.

8. References

- [1] "Military Standard - Flying Qualities of Piloted Aircraft," MIL-STD-1797, March 1987.
- [2] "Military Specification - General Specification for Flight Control Systems," MIL-F-87242, March 1986.
- [3] "F-16 C/D Aero Data for Scheduled LEF," selected data from General Dynamics Corporation Report 16PR3179, March 1985.
- [4] "DFLCS Software Mechanization Document," General Dynamics Corporation. Report 16PR4044, Rev. D, Aug. 1985.
- [5] Doyle, J.C. and Stein, G., "Multivariable Feedback Design: Concepts for a Classical/Modern Synthesis," IEEE Transactions on Automatic Control, Vol. AC-26, No. 1, Feb. 1981, pp. 4-16.
- [6] Glover, K., "All Optimal Hankel-Norm Approximations of Linear Multivariable Systems and their L^∞ - Error Bounds," Int. J. Control, Vol. 39, No. 6, pp. 115-1193.
- [7] Maciejowski, J.M., Multivariable Feedback Design, Addison-Wesley Publishing Company, Inc., 1989.
- [8] Doyle, J.C., "Analysis of Feedback Systems with Structured Uncertainties," IEE Proceedings, Vol. 129, Pt. D, No. 6, Nov. 1982, pp. 242-249.
- [9] Doyle, J.C., "Performance and Robustness Analysis for Structured Uncertainty," 21st IEEE Conference on Decision and Control, Orlando, FL, Dec. 1982, pp. 629-636.
- [10] Doyle, J.C., "Structured Uncertainty in Control System Design," 24th IEEE Conference on Decision and Control, Ft. Lauderdale, FL, Dec. 1985, pp. 260-265.
- [11] Osborne, E.E., "On Pre-Conditioning of Matrices," *Journal of the Association for Computing Machinery*, Vol. 7, 1960, pp. 338-345.
- [12] Jones, R.D., "Structured Singular Value Concepts for Real Parameter Variations," AIAA Paper No. 87-2589, AIAA Guidance, Navigation, and Control Conference, Monterey, CA, Aug. 1987, pp. 1424-1432.

- [13] "Flying Qualities of Piloted V/STOL Aircraft," MIL-F-83300, Dec. 1970.
- [14] Roskam, J., Airplane Flight Dynamics and Automatic Flight Controls, Roskam Aviation and Engineering Corporation, 1979.
- [15] Bacon, B.J. and Schmidt, D.K., "Fundamental Approach to Equivalent System Analysis," *AIAA Journal of Guidance, Control, and Dynamics*, Vol. 11, No. 6, Nov.-Dec. 1988, pp. 527-534.
- [16] Smith, O.J.M., Feedback Control Systems, McGraw-Hill, New York, 1958.
- [17] Lehtomaki, N.A., Sandell, N.R., and Athans, M., "Robustness Results in Linear-Quadratic Gaussian Based Multivariable Control Designs," *IEEE Transactions on Automatic Control*, Vol. AC-26, No. 1, Feb. 1981, pp. 75-92.
- [18] Safonov, M.G., Laub, A.J., and Hartmann, G.L., "Feedback Properties of Multivariable Systems: The Role and Use of the Return Difference Matrix," *IEEE Transactions on Automatic Control*, Vol. AC-26, No. 1, Feb. 1981, pp. 47-65.
- [19] Yeh, H., Ridgely, D.B., and Banda, S.S., "Nonconservative Evaluation of Uniform Stability Margins of Multivariable Feedback Systems," *AIAA Journal of Guidance and Control*, Vol. 8, No. 2, March-April 1985, pp. 167-174.
- [20] Safonov, M.G., Chaing, R.Y., and Flashner, H., "H[∞] Robust Control Synthesis for a Large Space Structure," Proc. American Control Conference, Atlanta, GA, June 1988.
- [21] Paduano, J.D. and Downing, D.R., "Sensitivity Analysis of Digital Flight Control Systems Using Singular-Value Concepts," *AIAA Journal of Guidance, Control, and Dynamics*, Vol. 12, No. 3, May-June 1989, pp. 297-303.
- [22] Bowman, J.S., "Airplane Spinning," *Astronautics and Aeronautics*, Vol. 4, No. 3, March 1966.
- [23] Woodcock, R.J., "New MIL-F-8785 Requirements at High Angle of Attack," AFFDL/ASD Stall/Post-Stall/Spin Symposium, WPAFB, OH, Dec. 1971, pp. T-(1-12).
- [24] Weissman, R., Bowser, D.K., and Cord, T.J., "The Potential of Analytical Studies for the High Angle-of-

Attack Flight Regime," AFFDL/ASD Stall/Post-Stall/Spin Symposium, WPAFB, OH, Dec. 1971, pp. P-(1-23).

- [25] Bihrlle, W., "Influence of the Static and Dynamic Aerodynamic Characteristics of the Spinning Motion of Aircraft," *Journal of Aircraft*, Vol. 8, No. 10, Oct. 1971, pp. 764-768.
- [26] Weissman, R., "Preliminary Criteria for Predicting Departure Characteristics/Spin Susceptibility of Fighter-Type Aircraft," *Journal of Aircraft*, Vol. 10, No. 4, April 1973, pp. 214-219.
- [27] Porter, R.F. and Loomis, J.P., "Examination of an Aerodynamic Coupling Phenomenon," *Journal of Aircraft*, Vol. 2, No. 6, Nov.-Dec. 1965, pp. 553-556.
- [28] Hamel, P., "A System Analysis View of Aerodynamic Coupling," *Journal of Aircraft*, Vol. 7, No. 6, Nov.-Dec. 1970, pp. 567-569.
- [29] Stengel, R.F., "Effect of Combined Roll Rate and Sideslip Angle on Aircraft Flight Stability," *Journal of Aircraft*, Vol. 12, No. 8, Aug. 1975, pp. 683-685.
- [30] Stengel, R.F. and Berry, P.W., "Stability and Control of Maneuvering High-Performance Aircraft," NASA CR-2788 (summarized in AIAA Paper No. 76-1973), April 1977.
- [31] Pelikan, R.J., "F/A-18 High Angle of Attack Departure Resistant Criteria for Control Law Development," AIAA Paper No. 83-2126, AIAA Atmospheric Flight Mechanics Conference, Gatlinburg, TN, Aug. 1983.
- [32] Anderson M.R. and Alahverdi, O., "F-18/TF-18 Simulation High Angle-of-Attack Stability and Control Program," Naval Air Test Center Contract No. N00421-88-D-0227, NAS Patuxent River, MD, Feb. 1989.
- [33] Stengel, R.F., "Some Effects of Parameter Variations on the Lateral-Directional Stability of Aircraft," AIAA *Journal of Guidance, Control, and Dynamics*, Vol. 3, No. 2, March-April, 1980, pp. 124-131.
- [34] Johnston, D.E., "High AOA Lateral-Directional Design Guides and Criteria - A Piloted Simulation Assessment," Paper No. 251, Flying Qualities Workshop, AFWAL-TR-80-3067, May 1980.
- [35] Hoh, R.H., and Mitchell, D.G., "Proposed Revisions to MIL-F-83300 V/STOL Flying Qualities Specification," NADC-82146-60, Jan. 1986.

- [36] Hodgkinson, J. and LaManna, W.J., "Equivalent System Approaches to Handling Qualities Analysis and Design Problems of Augmented Aircraft," AIAA Paper No. 77-1122, Aug. 1977.
- [37] Moorhouse, D.J. and Kisslinger, R.L., "Lessons Learned in the Development of a Multivariable Control System," National Aerospace & Electronics Conference, Dayton, OH, May 1989.
- [38] Anderson, M.R., "Robustness Evaluation of a Flexible Aircraft Control System," AIAA Paper No. 90-3445, AIAA Guidance, Navigation & Control Conference, Portland, OR, Aug. 1990.
- [39] "Background Information and User Guide for MIL-F-9490D," The Boeing Company, AFFDL-TR-74-116, January 1975.
- [40] Schaechter, D.B., "Closed-Loop Control Performance Sensitivity to Parameter Variations," AIAA J. Guidance and Control, Vol. 6, No. 5, Sept.-Oct. 1983, pp. 399-402.
- [41] Anderson, M.R., "Linear Design Models for Robust Control Synthesis," AIAA Paper No. 89-3454, AIAA Guidance, Navigation, and Control Conference, Boston, MA, Aug. 1989.
- [42] Franklin, G.F., Powell, J.D., and Emami-Naeini, A., Feedback Control of Dynamic Systems, 2nd edition Addison-Wesley Publishing Company, 1991.